No. RITARS-14-H-RUT

Mobile Hybrid LiDAR & Infrared Sensing for Natural Gas Pipeline Monitoring

Compendium

Performance Period:

January 15, 2014 – June 30, 2016

Principal Investigator:

Jie Gong, Ph.D., CM-BIM

Assistant Professor

Center for Advanced Infrastructure and Transportation

Rutgers, The State University of New Jersey

Program Manager:

Caesar Singh, P.E.

Director, University Grants Programs

OST - Office of the Assistant Secretary for Research and Technology

U.S. Department of Transportation

Contents

APPENDIX A: Agendas and Summary Notes from Advisory Stakeholder Meetings

I. List of Stakeholders and their titles and affiliations

II. December 12, 2012 meeting

III. March 20, 2013 meeting

IV. March 20, 2014 meeting

Introductory TAC Meeting Minutes

Date: March 19, 2014 – 11AM EST (10AM CST)

RE: Introductory Technical Advisory Committee meeting

Attendance:

Caesar Singh – USDOT/RITA

James Merritt– UDOT Pipeline Safety

Jie Gong – Rutgers-CAIT

Trefor Williams – Rutgers-CAIT

Andrés Roda –Rutgers-CAIT

Sean Zhou –Rutgers-CAIT

Khalid Farrag – GTI

Monica Ferrer – GTI

Alicia Farag – GTI

Robert Marros – GTI

Serafino Catapano – National Grid

Steven Hope – NYSEG

Carrie Berard – NYSEG

George Ragula – PSEG

Agenda:

1. Roll call for conference call attendee
2. Overview of the Research Study
3. Discussions and Stakeholder Feedback

1. Roll Call

- 14 conference call attendee provided self-introduction

2. **Overview of the Research Study**
    - Dr. Gong and Dr. Farrag jointly presented an overview of the research study: Mobile Hybrid LiDAR and Infrared Sensing for Nature Gas Pipeline Monitoring

3. **Discussions and Stakeholder Feedback**
    - What is critical to measure?
        - The attendee on the call agreed that one of the most important components is the ability to identify which areas are inundated with water and areas of bank erosion, especially in rivers and creeks.
        - Erosion and inundation near cast iron pipes is particularly problematic.
    - What is the intended application of the developed tool?
        - This tool will be used to prioritize the deployment of inspection resources immediately after a natural disaster
    - How often must data be captures prior to the disaster in order to be useful? For example, streams change course in the spring time.
        - Dr. Gong suggested the following:
            - USGS maintains a database with biannual updates
            - Periodic update of asset database may be collected based on stakeholder need
            - There may be a need for targeted data collection in addition to annual data collection
    - What type of LiDAR survey is commercially available?
        - Dr. Gong suggested the following:
            - Aerial is available
            - UAV is close to commercial availability
            - Mobile is available but expensive
            - None of these deployment methods are fused with other sensing equipment

- The team solicited from owners/operators the most appropriate means of commercializing the proposed technology. Owners/operators suggested the following:
    - Utilities typically hire out contractors to collect data
    - Utilities will typically be on-site to observe and guide data collection activities
    - Post-processing is needed, and contractors typically offer
    - Getting data back in 1-3 days would be important
    - An independent perspective of site conditions is preferred
    - Output is typically post-processed data
    - They would also like to use contractors to perform the actual risk analysis.
- Owners/operators were asked to provide inputs concerning risk analysis. Owners/operators offered the following:
    - There is a need to better understand what the output would be. What is being offered as part of the technology package.
    - Can the model be used for both prediction and assessment?
        - Dr. Farrag suggested that risk can be reviewed both as proactive ranking of potential threats as well as post-event review of risk-potential sites
    - There is concern about confidence level without "data points"
        - Dr. Farrag suggested that the risk analysis is more absolute. For example the potential for pipe leaking may be interpreted from a number of potential risk factors, including material, construction technique, loading, outside influences and others.
    - One owner asked if the lidar would be used to pick up exposed pipe
    - Another owner asked what if they don't have depth measurements in their GIS? How will the soil erosion measurements be useful? How pipe would be located from 2D GIS data?
        - Dr. Farrag suggested that soil cover would be the critical measurement. As an example if the initial measurement indicated a

3-ft cover, and subsequent measurements indicated 3” cover, there would be a problem.

        - Dr. Gong indicated that thermography would play a role in identifying pipeline asset locations, as well as leak detection. This could provide some guidance.
    - An owner asked if, in the event of a flood would water level be modeled, and would the model be able to be re-run to indicate water subsidence?
    - One owner indicated that identifying areas of potential damage and prioritize these areas for inspection would be critical, but admitted that visual inspection of the pipeline assets would remain regardless
    - One owner asked at what point would technology be deployed
        - Dr. Gong indicated that various technologies would be deployed depending on site access. Initial deployment of aerial lidar would provide preliminary assessments of potential risk areas. Once access to mobile lidar could be granted, subsequent “sweeps” could be conducted to refine potential risk areas
    - The team solicited potential testing sites for the technology and for proof-of-concept
        - NYSEG indicated their outfit might be able to provide a site for testing
    - One operator suggested that future meetings should be face-to-face to provide more opportunity for interaction.

The meeting adjourned at 12:00PM EST.

TAC Conference Call Minutes

Technical Memoranda Q3-1

Date: September 29, 2014 – 10AM EST (9AM CST)

RE: 2nd Technical Advisory Committee conference call

Attendance:

Serafino Catapano – National Grid

Steven Hope – NYSEG

Carrie Berard – NYSEG

George Ragula – PSEG

Richard Trieste – ConED

Mary Holzmann – National Grid

Ralph E. Terrell – Teco Energy

Jie Gong – Rutgers-CAIT

Andrés Roda –Rutgers-CAIT

Sean Zhou –Rutgers-CAIT

Khalid Farrag – GTI

Alicia Farag – GTI

Robert Marros – GTI

Agenda:

4. Roll call for conference call attendee
5. Review survey results
6. Research update
7. Schedule a Face-to-Face TAC meeting

4. Roll Call

5. Review survey results

a. Alicia Farag gave a short presentation about the survey results

b. Survey results are attached at the end of this meeting minutes

6. Research Update

a. Jie Gong gave a short presentation on system integration

b. Khalid Farrag gave a short presentation on quantifying the risk posed by soil movement to pipelines

i. The TAC members provided some feedback on the size of pipeline to be considered and modeled
ii. One TAC member inquired about the source of some strain plots

7. Schedule a Face-to-Face TAC meeting
    a. The committee discussed the scheduling of a Face-to-Face meeting at Rutgers
    b. A tentative date during the week of November 10, 2014 is selected.

The meeting adjourned at 11:15AM EST.

Survey Results:

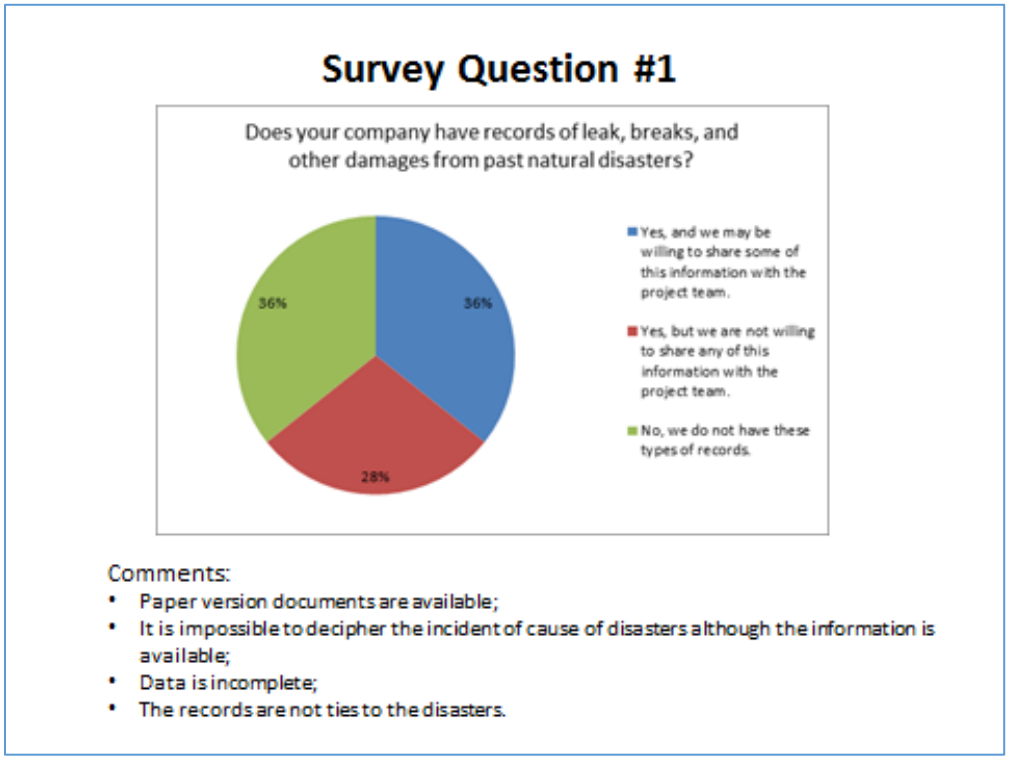

Comments:

- Paper version documents are available;
- It is impossible to decipher the incident of cause of disasters although the information is available;
- Data is incomplete;
- The records are not ties to the disasters.

Survey Question #2

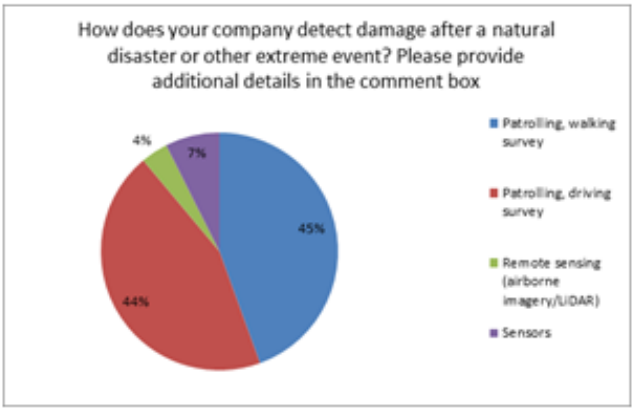

Comments:

- We do a fly over assessment but not with imagery technologies only video.
- The majority of these types of disasters are publicly reported to our company.
- Depends on how you define natural disaster. We have water sensors in the case of flooding.
- Local emergency management stations is primary mode since it ties in police and fire. News reports.

Survey Question #3

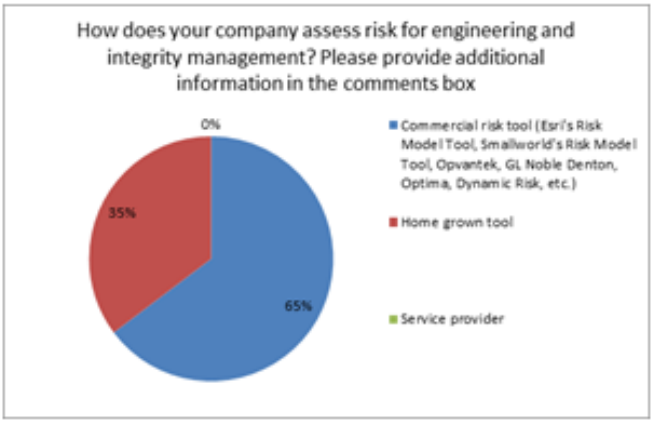

Comments on Commonly Used Tools:

- New Centruy SRA.
- Opvantek.
- Spatial Risk Analyst.
- Combination of the three.
- Overlay the flood zones on our facilities in GIS.
- APGA SHRIMP.

Survey Question #4

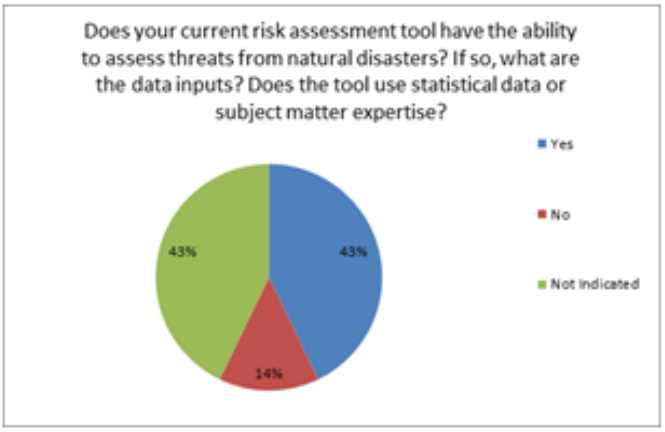

GeneralComments

- Both statistical and information can be entered a by subject mater expert.
- To a limited extent. A number of natural disaster threats are included in our TIMP and DIMP plans but very few of the threats are included in our assessment tool.
- Leak reports, and answering system data inquiries.
- It can use either. However it would mostly use leak data.

Survey Question #4 (Continued)

GeneralComments:
Leak data- historical data and sme.
No. Separate GIS files are kept of flood prone areas.
Yes. Rating for likelihood of failure, threat factor (degree of hazard) and impact factor (number of customers involved) is determined by subject matter experts.

Survey Question #5

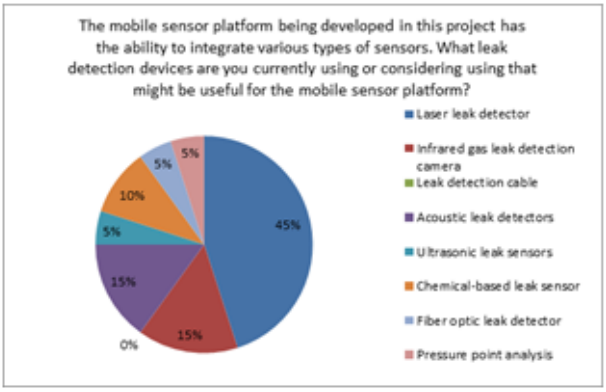

GeneralComments

- Currently use laser land base surveys, All others would be interest.
- We use ionization flame packs to analyze leaks during bar hole testing.
- Heath - DPIR. It's infrared but not a camera.
- We are looking to use Methane detectors in the buildings.
- OMD is used on mobile. Laser is used for walking.
- OMD and Flame ionization.

Survey Question #6

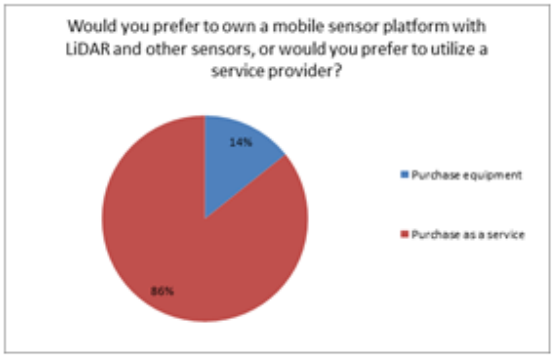

GeneralComments

- Service provider first but depending on upfront equipment costs and maintenance, the possibility to own equipment may be an option.
- Depend on the cost of the equipment, however, this happens so frequently my gut tells me that it would make more sense to purchase as a service.
- Typically own, but depends on the equipment and cost.
- It would largely depend on cost.
- Depends on cost and what final equipment package looks like, combined with level of expertise require to operate it.

Survey Question #7

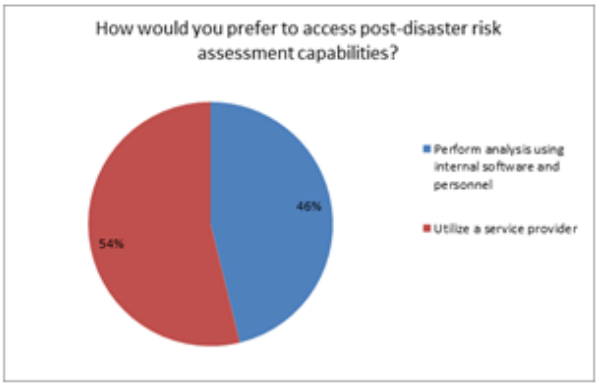

GeneralComments

- Utilize the service provider to analyze the initial inspection and then give the utility the ability to analyze difficult or trouble locations.
- Depend on the size and scope of the disaster.
- Would like results available for input in risk model.
- Depends on level of expertise needed to operate it and interpret results.

Survey Question #8

The project team is developing a commercialization and implementation plan as part of the project. Please provide your thoughts on strategies to ensure the technology is successfully commercialized and implemented.

GeneralComments

- As a service provider, the company needs to provide availability in the event of a disaster. Data from the surveys needs to be proven and repetitive in damage detection capabilities.
- 1) Limit the project scope to a subset of leak technologies to be incorporated within mobile sensor platform 2) Develop a test of the software output that can be shared 3) Conduct survey of disaster threats and include most significant in phase I model 4) Cost.
- Pipeline Magazine advertisement, newsletters, and trade booth shows at industry conferences.
- Natural disasters of a scale requiring such tools are rare and therefore the capability described would only make sense as a provided service...unless I don't understand (highly possible). Perhaps could be more widely applicable if appropriate to proactively identify washout risks (more frequent).

Survey Question #8

GeneralComments:

- Keep the I&D separate from the commercialized implementation. In my opinion GTI should only focus on the I&D.
- Would need to be able to handle disasters where access is difficult to get (aka downed bridges, buildings…).
- Would be helpful to have data available from multiple sources or technologies for better validation of approach.
- Ability to adapt to current system and available data. Cost of implementation.
- Need an actual count of customer impacted by the storm.
- When rolling out your product tries to keep in mind the majority of the publicly owned gas systems in the US are small systems (10,000 and less meters). So something that may be reasonably priced to a large gas system (MLGW) may not be to a smaller system.
- In a combination utility, electric will drive implementation since that is where the bulk of the budget lies.
- I would think a quick assessment after a natural disaster is critical therefore something that could cover a large area quickly without relying on roads that may be impassable would make the most sense (LiDAR).

Survey Question #9

Would your company be willing to enter into a retainer-type agreement to incentivize the service provider to maintain the equipment and expertise necessary to provide this service on an infrequent basis? Could regional agreements be put in place with other local utility companies to share the cost?

GeneralComments

- The company would need to negotiate a blanket contract for beginning on call and then as a service provider. There are possibilities that other utilities and government municipalities would be interested in sharing the cost.
- Would be willing to consider entering into a retainer type agreement based upon gaining a better understanding of the technology and a more comprehensive evaluation. Do like the idea of a regional agreement with other local utilities.
- If the technology is cost feasible, we may be interested.
- No, maybe regional.
- This would all depend on the overall buy in by the industry and would require a business case once the ongoing cost is determined.
- No.
- Possibly.

Survey Question #10

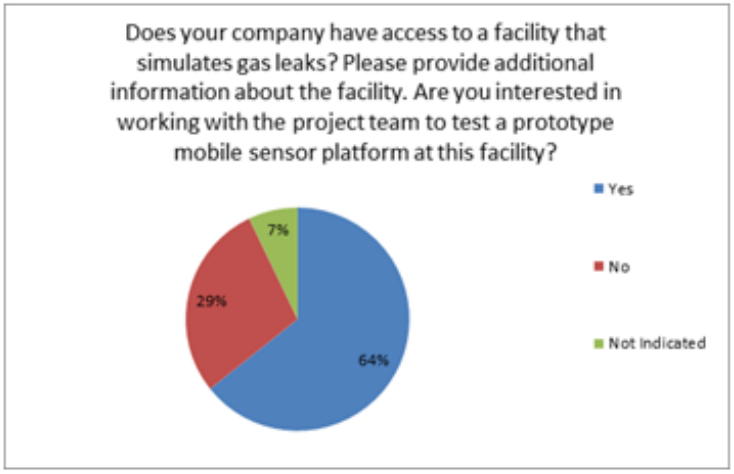

Date: November 13, 2014 – 10AM EST (10AM CST)

RE: 4th Technical Advisory Committee conference call

Attendance:

James Merritt – USDOT

Carrie A. Berard – NYSEG

George Ragular – PSE&G

Khalid Farrag – GTI

James Marean – GTI

Pradheep Kileti – National Grid

Jie Gong –Rutgers

Andres Roda – Rutgers

Sean Zhou –Rutgers-CAIT

1. Roll call for conference call attendee
2. Presentations

   Part I:

   Andres Roda briefly introduced the CAIT, and the projects CAIT has being working on.

   Part II:

   Prof. Jie Gong made two presentations, which covered the application of airborne LiDAR, mobile LiDAR, and Static LiDAR in post-disaster infrastructure assessment, the resolution, the range, the accessibility and the timeline of three techniques were discussed. At the second presentation, the application of thermography integrated with LiDAR technology was discussed, several examples including the field test using EyeCGAS camera was presented.

   Part III:

   Dr. Khalid Farrag introduced the research GTI has been working on regarding the pipeline analysis and assessment. The techniques in analyzing the pipeline displacement, pipeline deformation, soil movement were discussed.

3. Discussion during the meeting
    a) George Ragular from PSE&G suggested that Laser-based gas leak detection might be more applicable as the first screen device than infrared gas leak detection.
    b) George Ragular from PSE&G commented on the risk assessment module. The suggestions are: (1) detailed risk assessment might not be necessary for all the pipeline segments as in situations where cast iron gas lines are flooded, the gas operators will simply replace all of them. They will not go for detailed segment by segment risk assessment. (2) This further suggests the risk assessment should consider this type of situation. James Marean from GTI further suggested that a layered screening approach could be implemented first before conducting detailed risk assessment.
    c) James Merritt from USDOT PHSAMA commented on the remote sensing-based threat detection and risk analysis. The suggestions are: (1) The primary scope of the project is to provide remote sensing data and their derived information to gas operators and help them make decisions instead of making decisions for them. (2) From remote sensing data to strain-based design is interesting, but might go too far because that would fall more into making decisions for gas operators.

4. Mobile LiDAR System Demonstration
   The Rutgers team demonstrated the Mobile LiDAR System they have developed so far. The system has been integrated, though the team has noted that an additional lidar sensor will be added to the system for real-time point cloud visualization.

The meeting adjourned at 12:00AM EST.

Technical Advisory Meeting

When

- 10:30AM – 14:00PM, November 13, 2014

Meeting Agenda

10:30AM – 10:35AM	Welcome and Introduction
10:35AM – 12:10PM	Research Project Presentations
10:35AM – 10:40AM	Brief Introduction to CAIT and GTI
10:40AM – 11:10AM	Presentation I: Remote Sensing Technologies for Nature Gas Pipeline Integrity Inspection • Technology Evaluation • Technology Development
11:10AM – 11:40AM	Presentation II: Preliminary Results on Remote Sensing Data Integration and Processing • Results and Lessons Learned from Hurricane Sandy
11:40AM – 12:10PM	Presentation III: Preliminary Results on Post-Disaster Risk Assessment
12:10AM – 13:10PM	Lunch & Group Discussion
13:10PM – 14:00PM	1st Prototype Mapping System Demonstration (Weather Permits)
14:00PM	Meeting Adjourn

APPENDIX B: Advisory/Steering Committee Online Survey

Enter: Company, name, email

Introduction:

Rutgers University and GTI are developing a mobile sensor platform and a GIS-based risk model to identify high risk pipe segments after a natural disaster. LiDAR will be used to collect data before and after a disaster to determine changes in the environment that could impact pipe integrity (for example, soil erosion or shifted buildings). Other devices, such as infrared cameras and leak sensors, could also be incorporated into the mobile sensor platform. Detected changes in the environment will be extracted and overlaid in a GIS to assess the potential impact on a specific pipe segment. The GIS-based risk model will present users with results to identify high risk pipe segments and make decisions regarding the deployment of survey and mitigation resources. The purpose of this survey is to gather information to allow the project team to gather information that will assist in the design and development of the technology as well as commercialization and implementation. Please provide complete and detailed information to the questions below.

1. Does your company have records of leak, breaks, and other damages from past natural disasters? If so, would you be willing to share some of this data with the project team?

   [Yes] (If yes, the team will further contact for data or to identify contact person]
   [No records are available for this threat]

2. How does your company assess risk [**Before**] a natural disaster or other extreme event?

   [Statistical Data] (Please specify source(s)]
   [Subject Matter Experts, SME]

3. How does your company measure damage **[After]** a natural disaster or other extreme event?
   a) Patrolling/ Foot on ground inspection
   b) Remote sensing (airborne imagery/LiDAR)
   c) Smart wireless sensor network
   d) Others? Please specify

4. How does your company assess risk **[After]** a natural disaster or other extreme event?
    a) Use GIS-based pipeline risk analysis program (e.g., Spatial Risk Analyst, Esri-ArcGIS DIMP Risk Calculator Model, Opvantek Optimain, GL Noble Denton Uptime) [Other, please specify ……]
    b) Own spreadsheet forms , based on Experts' judgment
    c) Other? Please specify
5. The mobile sensor platform being developed in this project has the ability to integrate various types of sensors. What leak detection devices are you currently using or considering using that might be useful for the mobile sensor platform?
    a) Chemical-based leak sensor
    b) Fiber optic leak detector
    c) Lasers
    d) Infrared gas leak detection camera
    e) Leak detection cable
    f) Acoustic leak detectors
    g) Ultrasonic leak sensors
    h) Pressure point analysis
    i) Others, please specify
6. Would you prefer to own a mobile sensor platform with LiDAR and other sensors, or would you prefer to utilize a service provider?
    [Own]
    [Utilize a provider]
7. How would your organization like to develop post-disaster risk analysis capabilities?
    a. Own a GIS software if they don't have one
    b. Incorporate the natural disaster module into existing GIS system
    c. Have a stand-alone GIS software for natural disaster areas
    d. Use service provide
    e. Others, please specify

8. The project team is developing a commercialization and implementation plan as part of the project. Please provide your thoughts on strategies to ensure the technology is successfully commercialized and implemented.
   Would your company be willing to enter into a retainer-type agreement to incentivize the service provider to maintain the equipment and expertise necessary to provide this service on an infrequent basis?

   Could regional agreements be put in place with other local utility companies to minimize the cost?

9. Does your company have access to a facility that simulates gas leaks? Please provide additional information about the facility. Are you interested in working with the project team to test a prototype mobile sensor platform at this facility?

A Screenshot of the Online Survey

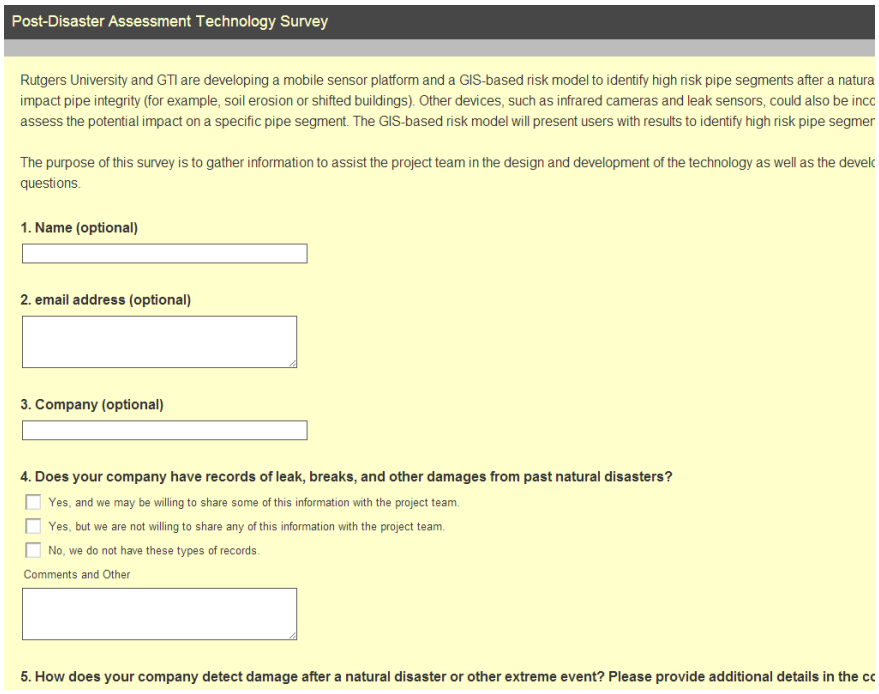

Post-Disaster Assessment Technology Survey

Rutgers University and GTI are developing a mobile sensor platform and a GIS-based risk model to identify high risk pipe segments after a natura
impact pipe integrity (for example, soil erosion or shifted buildings). Other devices, such as infrared cameras and leak sensors, could also be incc
assess the potential impact on a specific pipe segment. The GIS-based risk model will present users with results to identify high risk pipe segmer

The purpose of this survey is to gather information to assist the project team in the design and development of the technology as well as the develc
questions.

1. Name (optional)

2. email address (optional)

3. Company (optional)

4. Does your company have records of leak, breaks, and other damages from past natural disasters?

- [ ] Yes, and we may be willing to share some of this information with the project team.
- [ ] Yes, but we are not willing to share any of this information with the project team.
- [ ] No, we do not have these types of records.

Comments and Other

5. How does your company detect damage after a natural disaster or other extreme event? Please provide additional details in the cc

APPENDIX C: Publications and Presentations

I. Publications

Farrag, K. and Gong, J. (2015) "Risk Analysis of Natural Gas Distribution Lines Subjected to Natural Forces" Submitted to 2016 Transportation Research Board meeting.

Zhou, Z., Gong, J., Roda, A., Farrag, K. (2015) "A Multi-Resolution Change Analysis Framework for Post-Disaster Natural Gas Pipeline Risk Assessment" Submitted to 2016 Transportation Research Board meeting.

II. Presentations

TRB Workshop 160 - Sensing Technologies for Transportation Applications – Jan 10, 2016

Multi-Source Remote Sensing Data Fusion for Post-Disaster Assessment of Natural Gas Pipeline Systems

Presenter: Jie Gong

Session 428 – Hazardous Materials Transportation Research – Jan 11, 2016

Risk Analysis of Natural Gas Distribution Lines Subjected to Natural Forces

Presenter: Khalid Farrag

Session 859 – Advances in Geospatial Technology Applications in Transportation – Jan 13, 2016

Multiresolution Change Analysis Framework for Post-Disaster Natural Gas Pipeline Risk Assessment

Presenter: Zixiang Zhou

APPENDIX D: Workshop, Demonstrations, and Responses

Mini-Workshop on Remote Sensing Technologies for Post-Disaster Risk Assessment of Natural Gas Pipeline Systems

The U.S. Department of Transportation's Pipeline and Hazardous Materials Safety Administration (PHMSA) requires operators of gas distribution pipelines to develop and implement a Distribution Integrity Management Program (DIMP) to identify and reduce pipeline risks. Specific regulations require evaluations of the effect of natural forces (e.g., landslides, erosion, flooding, earthquakes, and other environmental hazards) that could potentially influence the integrity of the pipeline. ***This workshop will look at the role of remote sensing technologies in post-disaster risk assessment of natural gas pipeline systems. In the workshop, we will share research findings from a project that is*** directed at exploring the integration of several remote-sensing technologies and developing dedicated data processing and decision support tools that would allow pipeline operators to monitor changes in the built environment (structures, terrain, etc.) adjacent to pipelines after a natural disaster and to allow operators to assess the potential for increased risk of failure. System demos will be conducted at the workshop. Part of the workshop will also be dedicated to discuss future technological and regulatory needs in building and maintaining resilient natural gas pipeline infrastructure systems.

When: 9:00AM-1:00PM, June 22, 2016

Where: Auditorium of CAIT Building, Rutgers University Busch Campus, 100 Brett Road, Piscataway, NJ, 08854

Workshop Organizers:

- Jie Gong, Ph.D., Assistant Professor
  Center for Advanced Infrastructure and Transportation

Department of Civil and Environmental Engineering
Rutgers, The State University of New Jersey

- Andrés Roda, P.E., Research Manager
  Center for Advanced Infrastructure and Transportation
  Rutgers, The State University of New Jersey
- Khalid Farrag, Ph.D., P.E.
  Gas Technology Institute

Workshop Schedule

Mini-Workshop on Remote Sensing Technologies for Post-Disaster Risk Assessment of Natural Gas Pipeline Systems	
9:00 AM - 9:20AM	**Coffee and Introductions**
9:20AM – 9:30AM	**Welcome**
9:30AM – 10:00AM	**Session 1: Introduction to Remote Sensing Technologies**
	• Introduction to Research Project: Mobile Hybrid LiDAR & Infrared Sensing for Natural Gas Pipeline Monitoring • Remote Sensing Technologies
10:00AM – 10:30AM	**Session 2: Integration of Remote Sensing, GIS Technologies, and Risk Modeling for Post Disaster Damage Assessment**
	• Damage Assessment Framework • Algorithms and Software Implementation
10:30AM – 10:45AM	Break
10:45AM – 11:45PM	**Session 3: System and Software Demonstration**
	• Technologies o Mobile LiDAR (outside CAIT)

	○ Infrared Thermography ○ Drone • Visualization and Software ○ Online LiDAR Data Visualization ○ Spatially Resolved Infrared Thermography ○ Damage Assessment Workflow ○ Microsoft Hololens
11:45AM – 12:15PM	**Session 4: Structured discussions on future**
12:15PM – 1:00PM	**Working Lunch**

Attendee List

NAME	Company	Note
Andrew Sykes	Pepco	Confirmed, but did not attend due to outage break caused by a thunderstorm
Carrie Berard	NYSEG	
Colleen Richwall	Taylor Wiseman & Taylor	
George Ragula	PSE&G	
Jim Tarleton	New Jersey Natural Gas	
Kamil Fryzowski	PSE&G	
Maria Diaz	New Jersey Natural Gas	
Mobeen Khan	New Jersey Natural Gas	
Paula James	Atlantic City Electric	Confirmed, but did not attend due to outage break caused by a thunderstorm
Phillip Galka	NJBPU	Confirmed, but did not attend due to outage break caused by a thunderstorm
Steve Hope	NYSEG	
Rick Trieste	ConEdison	
Mary Holzmann	Natiional Grid	
Ed. Kunz	American Aerospace	
Khalid Farrag*	Gas Technology Institute	Call in
Ali Alavi*	A & M Structural Solution	Call in
Caesar Singh*	USDOT	Did not attend due to last minute conflict

Vasanth Ganesan*	USDOT	Did not attend due to last minute conflict
Jie Gong	Rutgers CAIT	
Andres Roda	Rutgers CAIT	
Patrick Szary	Rutgers CAIT	
Brian Tobin	Rutgers CAIT	
Yi Yu	Rutgers CAIT	
Xuan Hu	Rutgers CAIT	
Zixiang Zhou	Rutgers CAIT	
Mengyang Guo	Rutgers CAIT	

Workshop Summary:

The workshop was a very successful event. The workshop attendees were particularly interested in the demonstration part. There were great questions and discussions regarding the role of remote sensing, in particular the lidar technology, in assessing the integrity of natural gas pipeline systems. Some particular interesting future research needs that were brought up by the workshop attendees include the ability of using remote sensing to determine the accessibility of critical valves after major disasters and the role of remote sensing in locating buried assets after major topological changes as the results of disaster impacts. Some workshop attendees are interested in deploying our systems in monitoring the threat posed by flood to natural gas pipeline systems that are close to rivers and lakes. Further discussion are ongoing with these companies.

APPENDIX E - Market Analysis of Leak Survey Sensors Used by the Natural gas Utilities

Objective

The objective of this work, part (a), of Task-7 is to provide an analysis of the current market of natural gas leak detection and survey devices, based on the performance of the various methane detection technologies that can be employed in walking and driveby for leak survey of natural gas pipelines. Part (b) of Task 7 involves an analysis of the various risk assessment software used by the natural gas utilities and it will be presented in a following report. A thorough literature review was conducted for determining the essential variables as they relate to specific equipment and site conditions for the evaluation of current and emerging leak survey technologies. A total of six leak detection approaches were reviewed. Vendor specifications and literature review of these technologies were collated and evaluated.

Introduction

Various new and existing methane leak survey technologies are being developed and enhanced by research and development organizations and manufacturers. The framework for the leak detection and classification procedures is presented in the GPTC guide (1).

The ability to maximize the effectiveness of the leak survey process is critically important for distribution and transmission gas pipelines which are subject to the requirements of the Department of Transportation CFR codes §192.723 and the pipeline integrity management regulations.

With methane detection sensitivities approaching levels at or below 1 ppm (part per million) and increasing specificity to target pipeline sources of methane, there currently exists significant interest by operators in determining which leak detection approaches provide the optimal capability in identifying pipeline leaks.

Numerous leak survey devices currently exist in the market, each operating on different underlying detection technologies. These devices range from man-portable walking survey instruments such as the Flame-Ionization Detector (FID), the Portable Methane Detector (PMD), the Remote Methane Leak Detector (RMLD) and Infrared Spectroscopy (DP-IR); to bulkier devices more suitable for drive-by leak surveys such as the Optical 18 Methane Detector (OMD), and the Picarro sensor based on Cavity Ring-Down Spectroscopy (CRDS). Note that the FID and DP-IR technologies are employed in both walking and drive-by surveys.

Each of these devices and technologies, summarized in Table 1, are likely to entail a different set of essential variables for consideration and require specific test and assessment methods

Table 2 - Summary of Currently Available Methane Leak Detectors

Device	Technology	Manufacture/Supplier	Survey Type
Flame-Ionization Detector [FID]	Hydrogen fuel to power a small flame in a detector cell.	Several; e.g., Heath Consultants and Photovac	Walking and Drive-by
Optical Methane Detector [OMD]	Methane absorption bands in broadband light source	Heath Consultants, Inc.	Drive-by
Remote Methane Leak Detector [RMLD]	Tunable Diode Laser Absorption Spectroscopy / Wavelength Modulation Spectroscopy	Heath Consultants, Inc.	Walking
Portable Methane Detector [PMD]	Filtered Infrared Spectroscopy	Sensit Technologies Inc.	Walking
Infrared [DP-IR]	Infrared-Controlled Interference Polarization Spectroscopy	Heath Consultants, Inc.	Walking and Drive-by
Picarro Sensor	Cavity Ring-Down Spectroscopy (CRDS)	Picarro Inc.	Drive-by, stationary

1. Flame-Ionization Detectors (FID)

The flame ionization detector (FID) is currently the most widely-used technology for walking leak-detection surveys and it has been available since the 1960s. Although a considerable portion of the gas system is currently patrolled with mobile surveys, the majority of the system, especially service lines, is checked on foot and the FID technology still account for a sizeable portion of this market segment today. Due to the maturity level of this technology, a number of vendors manufacture FID units for use in methane leak-detection. Figure 1 show examples of these devices.

(a) Portable flame Ionization Detector [FID], by Photovac

(b) DP 4 device [FID], by Heath Consultants Inc.

Figure 1. Examples of Portable Flame Ionization Detectors

The FID device utilizes an internal gas cylinder containing a calibrated H2/N2 mixture. This gas, flowing at a metered rate, is mixed with a sample of atmospheric gas and ignited. By applying a voltage across the flame, it is possible to detect ions generated in the combustion process. The electrical current response is proportional to the organic concentration of the gas mixture. Hydrocarbon molecules exhibit a molar response factor equal to the number of carbon atoms contained. A positive detection is not necessarily specific to methane detection and ambiguity exists between a high methane concentration and a lower concentration of heavier hydrocarbons.

While the FID is very accurate, it has several shortcomings, particularly associated with the maintenance and the need for hydrogen gas. The reference calibrated gas mixture must be replenished in the device. In addition, the unit is not intrinsically safe. It is a routine precaution that operators ignite the flame (startup the unit) in a noncombustible atmosphere prior to approaching and seeking potential methane leak sources 2). FID instruments has been mounted to mobile platforms to perform drive-by leak surveys.

Several vendors of this technology include Heath Consultants Inc. (2), Southern Cross (3), and Photovac (4).

The key device parameters include the following:

- Fuel & Calibration gas concentrations (Hydrocarbon impurities),
- Mixture feed rate to flame (sample pump),
- Sample pump and external tubing.

The site-specific parameters include the following:

- Ignite fuel (hot wire) in non-combustible atmosphere,
- Needs to be inside leak plume,
- Inaccurate above 1% methane by volume (10,000 ppm),
- False positives can include sewer gas, car exhaust, gasoline, and atmospheric contaminants,
- Special procedures are required for high altitude (>3,000 feet above sea level).

General Comments on the devices:

- 40-50 years old tech, most widely utilized in natural gas leak detection method,
- Suitable for walking and drive-by surveys,
- Total hydrocarbon detector,

- 1 – 10,000 ppm (up to 1% gas) detection range,
- High accuracy.
- Instrument weight is about 7 lbs.

Advantages:

- Cheap, rugged with highly linear response range from 1-10,000 ppm range (i.e., up to 1% gas by volume),

Disadvantages:

- Significant maintenance cost,
- Less specificity, it can't distinguish between different organic substances such as CO or CO2.
- Substantial device calibration and maintenance requirements (6), including 5-15 min. warm up time required post-ignition, lubricating O-ring on stem of cylinder valve once per week and replacing inlet filter prior to each use, and refueling and recharging.

2. Optical Methane Detector (OMD)

The OMD was developed by the Gas Research Institute (GRI), Carnegie-Melon Research Institute and Westinghouse Science & Technology Center, prior to being commercialized by its current vendor Heath Consultants. The device is shown on a survey vehicle in Figure 1.

The OMD performs an optical detection of methane based upon this molecule's absorption spectrum. A spectrally broad photodiode, mounted on one side of the vehicle's front bumper, directs a beam of infrared light at an optical detector, mounted at the other end of the bumper. Methane present within the path between the light source and detector will act as a filter, absorbing IR photons only from the discrete quantized, and spectrally narrow, frequency regions corresponding to molecular excitation energies. The difference between emitted and received spectral content thus represents the integration of numerous methane absorption events along the light path. Careful instrument calibration permits accurate detections of line averaged methane concentrations down to the 1 ppm level.

Figure 2. Optical Methane Detector (OMD) mounted on survey vehicle, by Heath Consultants Inc.

The Vendor specified measurement accuracies of ±10% can be obtained for methane concentrations in the range of 1 ppm – 100 ppm, and ±20% in the range of 100 ppm – 200 ppm.

Vendor: Heath Consultants, Inc.

Operating principle:

- Absorption spectroscopy, utilize broad spectral source,
- Filter photodiode to detect narrow spectral region containing substantial methane absorption features.

The key device parameters include:

- Device is mounted on vehicles, Sensitivity 1 ppm – 200 ppm, 10% accuracy,
- Weight (external system 17 lbs.; power box 6 lbs.; internal display 3 lbs.; cables 4 lbs.).
- -22oF to 122oF operating temperatures General Comments:
- Specific to methane,
- Similar to RMLD but double-ended.

3. Portable Methane Detector (PMD)

The Portable Methane Detector (PMD) (Figure 3) was envisioned as walking survey instrument that combines both the high sensitivity capability of an FID with the high concentration (up to 100% methane) detection capabilities of a catalytic combustible gas indicator (CGI). The PMD draws a gas sample into an internal chamber much like an FID but instead of combusting the gas, employs an optical analysis

technique referred to as filtered infrared spectroscopy. The development of this technology, from concept through construction and testing of field prototypes was largely funded by GRI and OTD. There exist reports from extensive field testing comparing performance of prototype PMDs to FID readings in extensive field tests under a range of conditions. A total of four independent gas utilities participated in the field tests which concluded the PMD prototypes produced measurements consistent with FID instrument readings in virtually all scenarios. In one particular test, a failure of the PMD prototype to locate a weak methane leak (ppm level readings observed on the FID) was attributed to the presence of frost on the ground. Overall, independent evaluations determined this device to indeed be a viable alternative to FID in walking leak surveys. The above findings are summarized from the final OTD report (7).

Figure 3. The Portable Methane Detector (PMD), by Sensit Technologies

The PMD provides FID levels of accuracy and sensitivity, greatly enhancing specificity to methane detection, and extends the detection limit range to 100% methane atmospheres. Prior to the PMD, very high methane concentrations measurements in the field required CGI detectors.

Vendors: Sensit Technologies (8):

Operating principle:

- Filtered Infrared Spectroscopy.

Key Device Parameters:

- Fast sensing , high sensitivity 1 ppm, and +/- 10% accuracy,
- Detection range 0-100% gas (covers ranges of both FID & CGI devices),
- Lower Explosive Limit (LEL) and tick style leak detecting mode
- Data logging with event capture, GPS and Bluetooth options,
- Weight 6.1 lbs., size 10” x 4.1” x 5.5”, 7 hr. operation,

- Continuous operation with Li-ion battery,
- No moving parts,
- Self-zeroing function, minimal calibration required (Smart-Cal). Site Specific Parameters:
- Operating conditions: -4oF to 122oF,
- Suitable for vehicle mounting or walking surveys,
- Commercial unit available for walking surveys.

Site Specific Parameters:

- Operating conditions: -4oF to 122oF,
- Suitable for vehicle mounting or walking surveys,
- commercial unit available for walking surveys.

4. Remote Methane Leak Detector (RMLD)

The RMLD is an optical-detection based methane leak detector (Figure 4). Like the OMD, this device operates on the principle of looking for a signature spectral filtering of an emitted optical signal. Unlike the OMD, it employs a tunable laser source to emit coherent energy at a single frequency. The ability to modulate this frequency on and off resonance with a methane spectral line lends this approach its Tunable Laser Absorption Spectroscopy nomenclature. In addition, the device is single-ended. Both the detector and source are housed in a single hand-held head unit with an umbilical connection to a separate portable electronics box (2).

Figure 4 - Remote Methane Leak Detector (RMLD), by Heath Consultants Inc.

A substantial advantage of this device over most other leak detectors presented in this report is its ability to obtain methane measurements from outside methane plumes. This effectively removes the operator and detector from a potentially dangerous environment and allows for detection at greater distances from the device, useful for examining system components that are difficult to access directly. While this improves operator safety, remote detection comes at a price. The first penalty is the requirement for an object to be located behind the plume, in the direct line of sight between the operator and the methane concentration to be detected.

Vendors: Heath Consultants, Inc.

- Key Device Parameters:
- Sensitivity 5–10,000 ppm,
- Typically 100 ft. maximum range to topologic target, with actual range dependent on scattering media (e.g. < 1 m for clear standing water vs. > 50 m for brick),
- 5 second startup/self-test,
- Can routinely measure absorption levels of 10-5 relative to the off-resonance baseline

Site Specific Parameters:

- Transmits and captures reflected light,
- Absence of surface behind or obstacle in-front of leak plume will prevent detection,
- Max. 100 ft. standoff distance,
- Ground based surveys have benefit of immediately marking leak location,
- Wind speeds 0-50 mph,
- Operation limited to -20 to +120oF.

General Comments:

- Developed by PSI and DOE/NYSEARCH,
- Open path version of the OMD,
- Background levels of ~2ppm integrate over path volume measured,
- Suitable for walking and driving surveys.

5. Infrared Spectroscopy (DP-IR)

Figure 5 shows the Heath's Detecto Pak-Infrared (DP-IR) unit. As per the vendor's user manual, the DP-IR utilizes the Infrared Controlled Interference Polarization Spectrometry method for

methane gas detection (9). This technique entails applying a narrow band-pass periodic optical filter, matched to absorption spectra of gas being detected.

Figure 5 - Infrared Controlled Interference Polarization Spectrometer DP-IR, Heath Consultants Inc.

The instrument is intended to replace the current surveying equipment that relies on traditional Flame Ionization detection methods and eliminates the need for expensive gas cylinders and refill systems resulting in reduced instrument maintenance costs. No independent field condition tests were available in the public domain for this device. Vendors: Heath Consultants, Inc. (10). Key Device Parameters:

- Methane specificity, fast measurements,
- 1 ppm sensitivity, auto-ranges up through 100% methane,
- Accuracy greater of either ±0.5% or ±10% of reading,
- No moving parts,
- Ease of operation,
- Low maintenance (filter replacements),
- 8-hour Li-Ion battery life (32oF),
- Intrinsically safe, Safety Class 1 Division 1 Group D T31 ,
- About 5 minutes warm-up time,
- Internal calibration cell, self-test and zero functions,
- Digital methane detection and tick sound modes for tracking back to source of leak,

- Internal data logging and Bluetooth connectivity.

Site Specific Parameters:

- Operates in wide temperature range (0 to 122oF),
- Commercial unit available for walking surveys.

6. Cavity Ring-Down Spectroscopy (CRDS)

One of the new of detectors on the market today is the Picarro Surveyor for Natural Gas Leaks (Figure 6). This detector technology utilizes a highly sensitive optical detection scheme known as Cavity Ring-Down Spectroscopy (CRDS) and it is marketed toward gas utilities for the purpose of conducting fast mobile surveys. As per most of these optical detection methodologies, detections are highly specific to the target gas species being sought, and for this case to carbon-12 and carbon-12 constituents of methane. An advantage of this particular technology is its ability to fingerprint isotopic ratios of methane. This allows for discrimination of trace pipeline methane leaks from higher background levels attributed to landfills.

Figure 6 - CRDS analyzer and mobile kit, by Picarro

The vendor-specified high sensitivity levels and detection speeds are attained by utilizing a high quality optical cavity. Thus a 200-mm (8 inch) long cavity can yield effective optical path-lengths of many kilometers (11). A telecom grade coherent laser source is required to be tuned over the optical absorption feature of the targeted gas species of interest. The gas sample is

continuously drawn into the optical cavity, illuminated by the laser source and the level of optical leakage from the cavity monitored. Once a maximum intensity buildup is observed, the laser source is turned off and the time required to deplete the stored energy is measured. This decay time is referred to as the cavity ring-down time and is related to the optical loss of the gas molecules and the cavity mirrors. Vendors: Picarro Inc.

Key Device Parameters:

- Wavelength (~1.6 μm for methane),
- Intra-cavity gas temperature and gas pressure,
- Cavity sample exchange rate (about 1 second, impacts time between measurements at different locations),
- Speed of vehicle up to 40 mph, as claimed by the vendor.

Site Essential Variables:

- Requires vehicle to drive through the gas plume to measure concentration of gas drawn inside the cavity,
- Requires incorporating wind speed and direction,
- Based on communication with the manufacturer, fingerprinting using isotope ratios uses 1 ppb precision from 3 ppm up to 16 ppm methane concentrations, isotopic ratio measurements get noisy outside this range.
- The system is not suitable for concentrations above 20-45 ppm as per vendor,

General Comments:

- High sensitivity (1ppb)/high speed (1 Hz) methane leak detection technology,
- Picarro Surveyor (vehicle mounted for fugitive emissions leak detection),
- Suitable for driving or stationary surveys. Not suitable to walking surveys,
- Detect and fingerprint methane emissions.

References Cited in Document

1. Gas Piping Technology Committee [GPTC], GPTC Guide for Gas Transmission and Distribution Piping Systems, Appendix G-192-11: Gas Leakage Control Guidelines for Natural Gas Systems, American Gas Association, 2008.

2. Detecto-Pak 4® User's Manual, Heath Consultants, 2013, http://www.heathus.com/.

3. Flame Pack 400, Souther Cross, 2013, http://www.southerncrosscorp.com/.

4. Photovac MicroFID II Portable Flame Ionization Detector, 2013, http://products.inficon.com/.

5. OMD™ User's Manual, Heath Consultants Inc., 2006, http://www.heathus.com.

6. RMLD Remote Methane Leak Detector,Heath Consultants Inc., 2010, http://www.heathus.com/.

7. Portable Methane Detector, R&D: Refinements, Configuration, and Field Tests; final report, Gas Technology Institute, April 2007.

8. Sensit® PMD Portable Methane Detector, Sensit Technologird, 2012, http://www.gasleaksensors.com/.

9. DP-IR™ Detecto-Pak-Infrared User's Manual, Heath Consultants Inc., 2007, http://www.heathus.com/.

10.DP-IR A New Look in Leak Survey, Heath Consultants Inc., 2011, http://www.hetek.com/.

11.Picarro Methane & Hydrogen Sulfide Analyzer, Picarro Inc., 2013, http://www.picarro.com/

APPENDIX F- Current Risk Analysis Market for the Natural Gas Industry

There are several risk analysis packages that are widely used in the natural gas risk analysis market. These packages include New Centruy SRA - Spatial Risk Analyst, Opvantek, and APGA SHRIMP.

Spatial Risk Analyst

Spatial Risk Analyst is a workflow-driven application that allows pipeline operators to quickly and objectively measure risk along a pipeline. It leverages customized risk algorithms and an improved user interface to facilitate risk assessment and mitigation.

Opvantek

Opvantek is a comprehensive decision-support solution that enables gas operators to meet recently enacted federal Distribution Integrity requirements by enabling automated system-wide risk assessment and support for the prioritization of cost effective mitigation strategies. In essence, it integrates with relational and spatial (GIS) systems to collect and assimilate information associated with a gas operator's distribution network.

APGA SHRIMP

SHRIMP is an online tool that operators of natural gas distribution systems use to create a complete, written DIMP plan customized for the specific needs of their system.

Common Risk Assessment Approaches

Scenario-based risk assessment is a commonly supported paradigm in these software packages. In scenario-based risk assessment, the commonly used techniques are HAZOP technique, Fault Tree Analysis, Index Models, Muhlbauer's risk assessment methodology, and Consequence model. The following provides a short overview of each of these techniques.

HAZOP Technique

A HAZOP analysis typically involves a detailed examination of pipeline system components to determine the outcome if a specific component does not function as it is designed to (within its normal parameters). Each parameter (e.g., pressure or flow rate) is examined to identify potential changes in the system that is based on changes in the component parameter.

Fault Tree Analysis

In the fault tree analysis, the sequence of events is traced backwards from a failure. This technique uses most probable or most severe pipeline failure scenarios. Based on these scenarios, resulting damages are estimated and mitigation responses and prevention strategies are developed. In the Fault tree analysis, factors such as natural disasters, human activity, and other externally induced caused can be included.

Index Models

The Index Models use customized algorithms such as Muhlbauer's risk assessment methodology, Consequence Modeling, and the PipeView Risk model. In the Muhlbauer's risk assessment methodology,

it is believed that data on pipeline failures are still insufficient to perform a thorough risk assessment using purely statistical concepts, and an assessment using probabilistic theory is not required because the probabilities used in these approaches are questionable. Instead, it argues that risk is defined by answering three questions:

- What can go wrong (every possible failure must be identified)?
- How likely is it to go wrong?
- What are the consequences?

In this approach, numerical values are assigned to conditions on the pipeline system that contribute to risk. The score, which reflects the importance of an item relative to other items, is determined from a combination of statistical failure data and operator experience. The other example is Consequence Model (C-FER Model). The C-FER model examines isometric thermal radiation distances to determine a burn radius and a 1 percent fatality radius from a natural gas pipeline break. An assumption of this model is that risk can be expressed as the product of failure probability and failure consequences, and reliability is the complement of failure probability.

Appendix G: Final Paper for Submission

Journal papers:

1. Zhou, Z. and Gong, J. (2016) “Multi-Level Post Hurricane Damage Assessment of Residential Buildings using Pre- and Post- Airborne Lidar Data” To be submitted to International Journal of Remote Sensing and Photogrammetry. (attached)
2. Hu, X., Gong, J., and Wu, Z. (2016) “Data Efficiency of LiDAR Technologies for Supporting Post-Sandy Damage Assessment” to be submitted to ASCE Journal of Computing in Civil Engineering. (attached)
3. Hu, X., Gong, J., and Zhou, Z. (2016) “LiDAR assisted Transportation Routing Decision Making to Improve Critical Asset Accessibility during Major Natural Disasters” to be submitted to International Journal of Disaster Risk Reduction. (attached)
4. Gong, J., Zhou, Z., Hu, X., Farrag, K., and Roda, A. “A Framework for Natural Gas Pipeline Damage Assessment with Multi-Sourced Remotely Sensed Data” to be submitted to ASCE Journal of Infrastructure Systems. (in preparation)

Conference papers:

5. Gong, J., Guo, M., Zhou, Z., Lin, N., and Kennedy, A. “Fusion of Geo-Tagged Post-Storm Damage Photos with Mobile LiDAR Data for Storm Surge Height Measurement” to be submitted to 2017 International Workshop on Computing in Civil Engineering. (attached)

MULTI-LEVEL POST HURRICANE DAMAGE ASSESSMENT OF RESIDENTIAL BUILDINGS USING PRE AND POST AIRBORNE LIDAR DATA

Zixiang Zhou[1]and Jie Gong[2*]

[1] Graduate Research Assistant, Dept. of Civil & Environmental Engineering, Rutgers, the State University of New Jersey, E-Mail: zx_zhou@hotmail.com

[2] Corresponding Author, Assistant Professor, Dept. of Civil & Environmental Engineering, Rutgers, the State University of New Jersey, Phone: 848-445-2881, E-Mail: jiegong.cee@rutgers.edu

ABSTRACT

The timelines of the building damage assessment has become a critical concern in modern age of post-disaster assessment. Conventional approaches are labor intensive and time consuming. Meanwhile, the accessibility of damaged area restricts the investigators and engineers to a great extent. In this study, a multi-level airborne LiDAR-based damage assessment approach is proposed. The input data is classified at first, then the building clusters are extracted using a density-based algorithm. A novel cluster matching algorithm is proposed to robustly cluster clusters corresponding to same building together. Multiple features, including 1) roof area, volume, 2) roof orientation, and 3) roof shape, are computed as indicators of building damage condition. A hierarchical determination process is then employed to identify the damage category and damage level of each building. The result of experiment suggests that this approach is able to: 1) recognize building objects; 2) extract damage features; 3) identify damage category due to multiple damage patterns.

INTRODUCTION

In the past decades, natural disasters have posed severe impacts to public safety. Billions of dollars of financial losses and thousands of injuries and death have been reported during the main catastrophes such as the 2008 earthquake at Wenchuan, China, 2010 earthquake at Haiti, 2011 tsunami at Japan and 2012 hurricane at New Jersey, US. The limitation of accessibility of impact regions is one of the most challenging issues for rapid rescue and recovery. Conventional approaches rely on visual inspection, which are labor intensive and time consuming. Recent years, the fast growing remote sensing technologies have provided alternative solutions to this problem. Satellite imagery, unmanned aerial vehicle imagery and airborne LiDAR have been used in post-disaster assessment in many cases (Tralli, D. M., et al 2005, Li, M., et al 2008, Tsai, F., et al., 2010, Van Aardt, J. A., et al 2011).

Generally, there are two types of post-disaster assessment routines, 1) using pre-event and post-event data, and 2) using post-event data only. For the regions with pre-event data, it is easier to conduct the damage assessment by comparing the pre-event data to the post-event data. Bovolo, F., et al (2012 November) used the high resolution SAR images to detect the building changes, and airborne LiDAR data is used for the same purpose in (Murakami, H., et al 1999).

Although change detection is obtainable from the comparison between multi-temporal data, there are still limitations for current approaches. For image based approach, most of them are pixel-by-pixel based, and the change detection is implemented on a 2D basis (Huang, X., et al 2014). Since the building change also occurs at height direction for certain scenarios, the stereo imagery is used to introduce the height information (Tian, J., et al 2014, Zeng, C., et al 2014). However, due to the low quality of DSMs from satellite images and erroneousness in detecting small size objects, a quantitative change damage assessment is still a challenge. Turner, D., et al (2012) and Sui, H., et al (2014) use a UAV based platform to conduct the change detection. Their approach employs numerous high resolution images and reconstructs the scene through a Structure from Motion algorithm. This approach has higher resolution and higher accuracy due to 3D spatial data is available, although, the image based reconstructed model typically needs to be scaled to real size and geo-registered. Meanwhile, the reconstruction of dense 3D model from high resolution images is a computationally expensive procedure, which makes it difficult for a large region reconstruction and damage assessment.

One advantage of airborne LiDAR based methods is that accurate spatial data is available. In addition, as for most airborne laser scanning (ALS) system, the data is integrated with a navigation system, which simplifies the geo-registration of multi-temporal LiDAR data. Although ALS based system has abovementioned advantages, current methods still have following limitations. For most of the researches, the change detection is conducted on a global basis. This means they detect whether a building is changed or not, however, they are unable to tell to what extent the change is. In addition, most of current change detection approaches focus on changes caused by urban development, rather than disaster damage. Due to the different change patterns between man-made change and disaster-caused change, the approach works for man-made induced scenario might not work for disaster induced scenario well.

To address these issues, a novel multi-level post-disaster building damage assessment approach is proposed in this paper. This approach extracts building objects from both pre-event and post-event data, then the objects belonging to same building from multiple-temporal data sets are matched using a novel cluster matching algorithm. The damage level determination is then conducted using multiple indicators on a hierarchical basis. This process leverages the area and volume of building roof, roof orientation and roof shape to determine whether a building is damaged. And multiple damage patterns are obtained based on the extracted features and damage indicators.

RELATED WORKS

Numerous of studies have been conducted on building extraction, change detection and damage assessment using airborne LiDAR during the past decades. For the purpose of object recognition and building extraction, the surface smoothness, distance between points, and the height information of the point cloud are mainly used as features. A review of state-of-art techniques regarding to building extraction is conducted by Tomljenovic, I., et al (2015). Filin, S., & Pfeifer, N. (2006) proposed a segmentation algorithm based on neighborhood slope. Meng, X., et al (2009) used a morphological based filter to extract building objects from airborne LiDAR point cloud. When non-ground points are classified, the building objects are extracted according to the geometric features. Zhang, J., et al (2013) proposed a support vector machine (SVM) based classifying algorithm for object-based point cloud analysis. In their research, the point cloud is first clustered using region growing based segmentation, and the geometric features of each cluster are calculated. Finally, a SVM is used to classify the cluster into different

objects. The planar feature of the points is used to segment building objects in the work of (Lari, Z., & Habib, A. 2014). In their work, the PCA is used to obtain the geometry feature of the neighbor points. Once the features are computed, a clustering algorithm is used to segment the planar objects.

Regarding to LiDAR-based building change detection, two different change patterns are considered. One pattern is man-made building change, which implies building change due to development of urban environment. Another is disaster-induced change. For man-made change, Murakami, H., et al (1999) used the DSM generated from airborne LiDAR data to detect the building changes. To improve the algorithm performance, an orthoimage is employed for the removal of errors and noise. Vögtle, T., & Steinle, E. (2004) proposed a method leveraging airborne LiDAR data for building change detection. The raw data is first segmented into multiple objects including ground object, building object, vegetation object and other objects. This is achieved through a region growing algorithm. The building change is then conducted via comparing the DSMs from multi-temporal data sets. A change detection of dense urban area using airborne LiDAR data is carried out by (Vu, T. T., et al 2004, September). In their research, two different flight data are registered and gridded. Then the comparison is conducted on the grid basis. The test shows a high automation during the entire procedure. An object based building change detection algorithm is proposed in (Pang, S., et al 2014). Similarly, the DSM data is used, but the change point is detected through a connected component analysis. This approach finds the changed objects if the smoothness between consecutive points is larger than a threshold. The damage type is then categorized into newly built, taller, demolished and lower. Teo, T. A., & Shih, T. Y. (2013) developed a framework for building change detection and change type determination. The proposed method first generates DSM data, and then various objects are segmented. This classifies the vegetation points, building points, and other objects. The change detection is carried out upon these objects so that the building-to-building and building-to-vegetation/ground change is determined.

For disaster-induced change, Labiak, R. C., et al (2011, May) presented an approach for building change detection and quantification. A height model is generated by subtracting a digital terrain model from the original point cloud. Within the processed data, line-based change detection is conducted, which detects change points using a slope threshold. The change degree at each direction is calculated through the slope between consecutive points by fixing the change

at other dimension. Kashani, A. G., & Graettinger, A. J (2015) proposed a land-based platform uses both terrestrial and mobile LiDAR to evaluate the wind-induced roof damage. Although this approach is able to determine the damage condition of building roof, it is restricted by the accessibility of impact area right after the disaster attack. Elberink, S. O., et al (2011) uses an airborne-based platform for building collapse detection. The building objects are extracted using a surface growing algorithm. A supervised learning approach is conducted levering multiple features including number of points per segment, mean height above DTM, unsegment to segment ratio, and planarity to inference the damage condition. Yonglin, S., et al (2010, June) also uses an airborne-based system to detect inclined buildings after earthquake attack. But their work mainly focuses on symmetric and partial symmetric roofs. Khoshelham, K., & Oude Elberink, S. J. (2012, May) investigated the dimensionality reduction in data training and classification of airborne LiDAR data. The result of experiment shows that the proposed approach is capable of identifying buildings between damage and intact. However, this is not sufficient because the damage severity plays critical role in post-disaster rescue and assessment.

METHODOLOGY

This paper presents a multi-level damage detection pipeline as shown in Figure 1. The pipeline first classifies the input data to extract the building objects. Then a clustering algorithm is applied to extract individual building clusters. A novel cluster matching algorithm is proposed then to match the clusters corresponding to the same building. Afterwards, four geometric attributes are computed, including the area and volume of roof, the roof orientation, and roof shape distribution. A multi-level damage detection process is then conducted, this classifies the damage into multiple damage patterns and also extracts the intact buildings. A detail discussion of each step is provided in following sections.

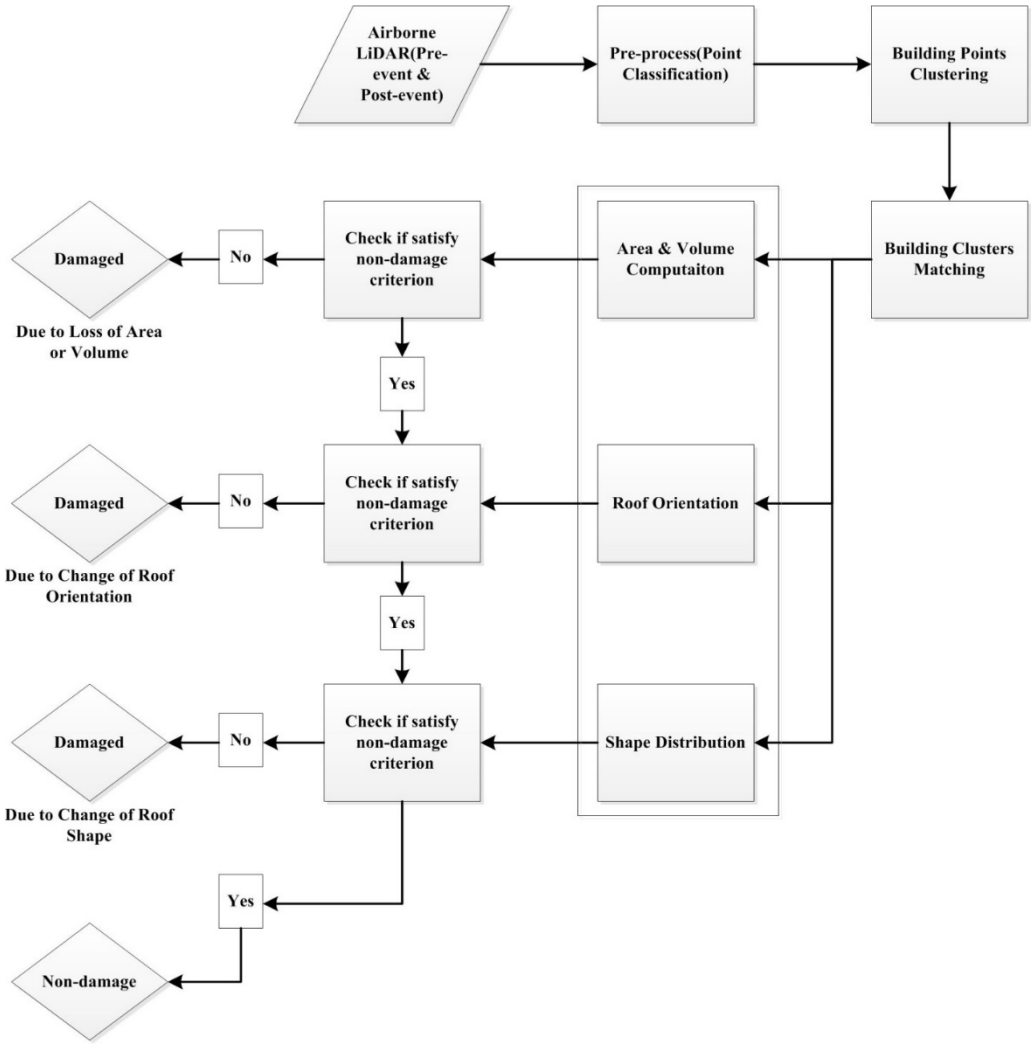

Figure 1. Proposed Framework

1. Data Pre-Processing

The first step of proposed approach is pre-processing the raw input data. This means a classification procedure that classifies the point cloud into different categories is conducted. What are interested afterward are the building objects. A good classification is obtainable for pre-disaster scenario, however, it is difficult to segment the building points out from non-building points especially for post-disaster scenario. Because the damaged building components might be very close to vegetation or ground. In addition, a building might splits into multiple parts subject to natural disasters, which poses challenges to points clustering procedure. However, since the scope of this research is rapid building damage assessment, the mis-clustering of building objects for post-disaster scenario does not affect the determination of

damage condition. This is because a building is most likely damaged if the roof part reaches close to ground. And a building is determined to be damaged if the roof splits. Numerous researches have been studied to filter the airborne LiDAR data such as (Meng, X et al., 2009, Zhang, K et al., 2003, Chen, Q et al., 2007, Hodgson, M et al., 2005, Meng, X, 2005). All of these approaches can be employed for the purpose of ground points filtering and vegetation removing. Since these are beyond the scope of this paper, the interested readers are referred to the above-cited papers for detailed discussion of the algorithmic conduction.

2. Building Points Clustering

Within the output of data pre-processing, which is the point cloud of building objects, a building clustering process is then implemented for the purpose of building model extraction. Since a cluster is a set of point cloud in which the distance between any pair of neighbor points $\{\boldsymbol{p_i}, \boldsymbol{p_j} | \boldsymbol{p_i} \in \boldsymbol{P}, \boldsymbol{p_j} \in \boldsymbol{P}\}$ is less than a threshold. On the contrary, the distance between any pair of points $\{\boldsymbol{p_i}, \boldsymbol{q_j} | \boldsymbol{p_i} \in \boldsymbol{P}, \boldsymbol{q_j} \in \boldsymbol{Q}\}$ is larger than the threshold if they belong to different clusters. Although this concept is intuitive, it still has challenges in clustering building objects if the point cloud is in low density. Since the average distance between any pair of neighbor points increases with the decrease of point density, multiple clusters might be grouped as one if the cluster-to-cluster distance (red dashed line in Figure 2 (a)) is similar or smaller to the distance between point pairs inside a same cluster (red solid line in Figure 2 (a)). The example in Figure 2 (a) shows such scenario that these two data clusters are grouped as one large cluster. To address this, a density-based (Ester, M et al., 1996, August) concept is adopted. In their paper, the algorithm starts from arbitrary point and clusters all the density-reachable points of this starting point. A modification of the algorithm is proposed in this research. Instead of starting from a point and finding all the density-reachable points of this point, the proposed algorithm simply finds all the points with *K* neighbor points within radius of ε as core points. Then a Euclidean-distance based clustering is employed to cluster these core points. In this step, the core points are grouped as one cluster if the distance between arbitrary pair of neighbor points is smaller than ε. And those clusters with number of points less than a threshold *n* are removed because these clusters are most likely to be vegetation or noise points. The next step is checking whether the rest points belong to any clusters. To do this, every non-core points is visited and the neighbor points are found. If a neighbor point with distance smaller than ε is found and this neighbor point is a core

point, cluster this visited non-core point to the cluster of this core neighbor point. A pseudo code of the proposed algorithm is presented in Table 1.

Table 1. Pseudo Code of Proposed Building Clustering Algorithm

Input parameters are: number of neighbor points *K*, search radius ε, minimum number of core points for each cluster *n*

----------Find the Core Points----------

FOR (each point ($\boldsymbol{p}_i \in \boldsymbol{P}, i = 1,2, \dots, n$)){
  find the neighbor points ($\boldsymbol{p}_k^i \in \boldsymbol{P}, k = 0,1,..,l$) within radius of ε;
    IF ($l > K$){ label $\boldsymbol{p}_i$ as core point; }
    ELSE { label $\boldsymbol{p}_i$ as non-core point; } }

The original data is grouped into core points ($\boldsymbol{c}_i \in \boldsymbol{C}$) and non-core points ($\boldsymbol{c}_j^* \in \boldsymbol{C}^*$)

----------Cluster the Core Points----------

Create a Kd-tree for core points $\boldsymbol{C}$
FOR(each point ($\boldsymbol{c}_i \in \boldsymbol{C}$)}{
  IF ($\boldsymbol{c}_i$ has not been visited) {
    create a new cluster $\boldsymbol{C}(I)$ and put $\boldsymbol{c}_i$ to this cluster;
    set $\boldsymbol{C}(I)$.number(0) = 0, $\boldsymbol{C}(I)$.number(1) = 1, and $i = 1$;
    WHILE ($\boldsymbol{C}(I)$.number(i) $\neq$ $\boldsymbol{C}(I)$.number($i-1$)) {
      FOR (each point $\boldsymbol{c}_j^+ \in \boldsymbol{C}(I)$) {
        IF ($\boldsymbol{c}_j^+$ has not been visited) {
          search the neighbor points ($\boldsymbol{c}_k^{j+} \in \boldsymbol{C}$) within radius of ε;
          IF ($\boldsymbol{c}_k^{j+}$ has not been visited) { put it to the cluster $\boldsymbol{C}(I)$, i++;}
        }
      }
    }
  } I++;
  IF ($\boldsymbol{C}(I)$.number < *n*){ remove $\boldsymbol{C}(I)$;}

12 *ELSE* { keep $\boldsymbol{C}(I)$; }

}

----------Cluster the Non-Core Points----------

1 *FOR* (each point ($\boldsymbol{c}_j^* \in \boldsymbol{C}^*$){

2 find its neighbor points ($\boldsymbol{c}_k^{j*} \in \boldsymbol{C}$) within radius of ε;

3 *IF* (found $\boldsymbol{c}_k^{j*}$ and $\boldsymbol{c}_k^{j*} \in \boldsymbol{C}(I)$) {

4 put $\boldsymbol{c}_j^*$ to cluster $\boldsymbol{C}(I)$; }

}

3. Building Clusters Matching

Since the damaged buildings are identified through comparison between pre- and post-event data, the building matching is needed when the building clusters are obtained. A matching clusters means a pair of pre- and post-event clusters that corresponding to the same building. Intuitively, this is obtained by computing the distance between centroid points of each pre-event cluster to post-event clusters, and the matching clusters are the pair with shortest between-centroid distance. This is a feasible approach, although, it still fails to match all the clusters that correspond to the same building if that building splits during the disaster. An illustration of this is shown in Figure 2 (b). If the blue region is the pre-event cluster, and the other regions are post-event clusters. The shortest between-centroid distance will match the white region to the blue region. However, it is noticed that both green, black and white regions are the same building but splited due to collapse or damage, these should be matched to the blue region as well. One alternative solution to this is searching the clusters with centroids inside the search sphere. However, due to the irregularity of building roof shape, a robust searching radius is hard to determine, therefore the yellow region might be matched if the searching radius is chosen large.

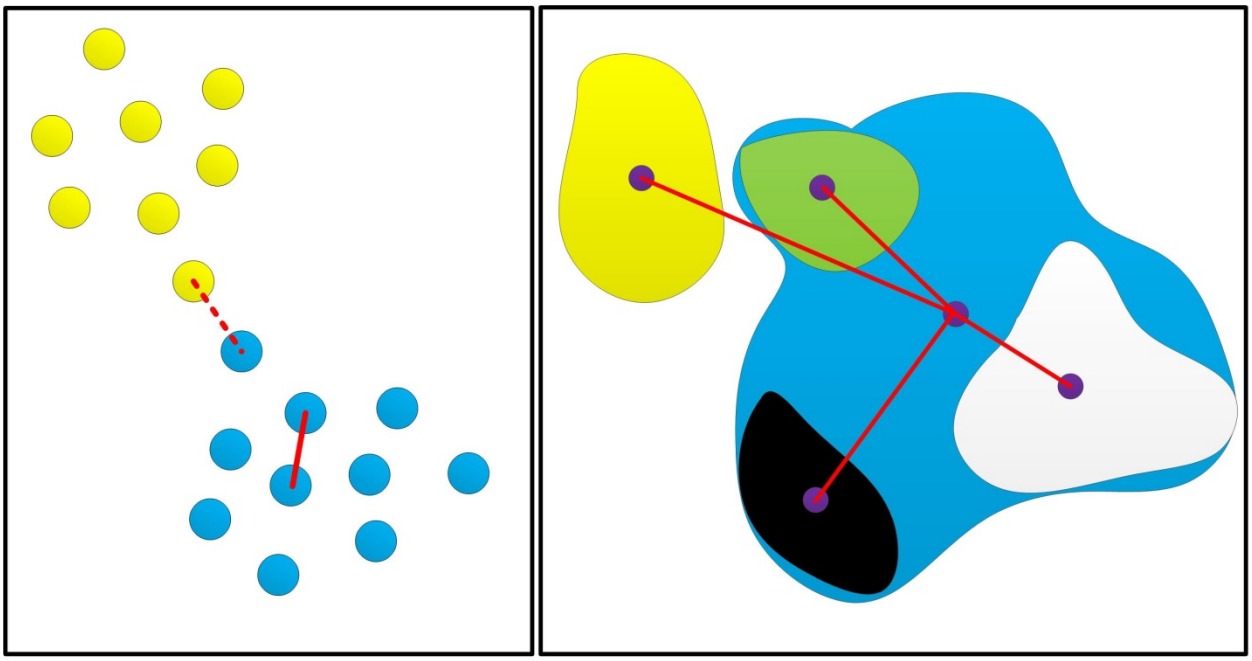

(a) (b)

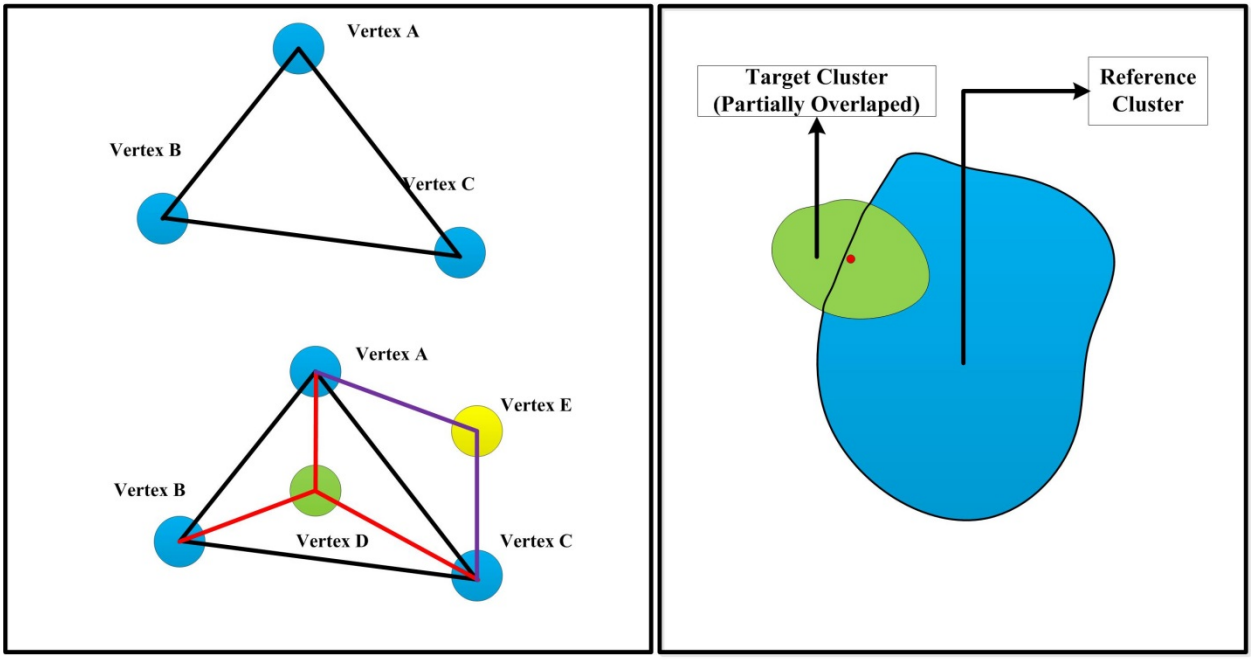

(c) (d)

Graphical illustration: (a) clustering based on distance between points tends to merge different clusters together; (b) One reference cluster might correspond to multiple target clusters; (c) Added point will not increase the triangle area if it is inside the triangle, otherwise the area will be increased; (d) The proposed matching algorithm will match the partially overlapped clutsers

Figure 2. Graphical Illustration of Clustering and Matching Algorithm

To overcome this, a novel cluster matching approach is proposed in this paper. Denote the pre-event cluster as reference cluster, and the post-event clusters as target clusters. To find the target clusters with centroids inside the region of reference cluster, triangulation of the reference cluster $\boldsymbol{C}^r$ is performed (Lee, D. T., & Schachter, B. J. 1980) at first to compute its area A^r. A detailed discussion on computing the area of point cloud is presented in section 4. Then for each target cluster $\boldsymbol{C}_i^t$ close to $\boldsymbol{C}^r$, add its centroid $\boldsymbol{c}_i^t$ to $\boldsymbol{C}^r$ and construct the Delaunay triangles and compute the new area A_i. If $A_i = A_r$, this centroid point $\boldsymbol{c}_t^i$ is inside the region of cluster $\boldsymbol{C}^r$, and match this cluster $\boldsymbol{C}_i^t$ to $\boldsymbol{C}^r$, otherwise, do not match it. This is because if the added point is inside one of the Delaunay triangle, it will not increase the area of that triangle, but only meshes that triangle into three small triangles (vertex D in Figure 2 (c)). On contrary, an added point will increase the area of Delaunay triangle by adding a new triangle to it, if this point is outside the range of this Delaunay triangle (vertex E in Figure 2 (c)).

This algorithm is robust in finding all the in-region centroid points of target clusters. However, it is noticed that clusters partially overlap the region of reference cluster might be matched, if their centroid points are located near the boundary of reference cluster region. For example, in Figure 2 (d), the centroid point of green region is inside the region of blue cluster but very close to its boundary. As result half of the target region is outside the reference region. It is controversial to either match this target cluster or not since this cluster could be either a part of the same cluster or not. However, it is considered as a matching cluster in this paper and indicating building damage for the following reason:

1) If this cluster is a part of the same building, this indicates that the building is damaged because it splits. And therefore this cluster is matched;
2) If this cluster is not a part of the same building, but vegetation or part of other building, which also indicates that the building is damaged. Unlike the possible damage pattern discussed above, the damage of this building is caused by physical collision between buildings.

4. Area and Volume Computing

In this research, the area of a building is represented by the area of the footprint of its roof. Therefore, the point cloud in 3-D spatial coordinate is projected onto horizontal plane by assigning the Z-coordinate a constant value. Computing the area of a point cloud is a challenging

problem. The convex hull (Graham, R. L. 1972) is an effective algorithm for computing the area of a point sets with a convex shape, but it tends to enlarge the area of a point set if the shape is concave. For this reason, the area of a point set is computed as the summation of Delaunay triangles of this point set. Since Delaunay triangulation meshes the point set so that no point is inside any of the triangles, the triangulation covers the entire region of point set, and therefore the empty region is filled if the point set is in concave shape. In Figure 3 (a), the triangles enclosed by green lines are those that fill the empty region. Apparently, these triangles increase the summation of the area largely, and need be removed from computing the area. For each Delaunay triangle DT_i, denote its three vertexes and three edges as $\{\boldsymbol{V}_i^A, \boldsymbol{V}_i^B, \boldsymbol{V}_i^C, \boldsymbol{L}_i^{AB}, \boldsymbol{L}_i^{AC}, \boldsymbol{L}_i^{BC}, i = 1,2, \dots, m\}$, where $\boldsymbol{V}$ stands for vertex and $\boldsymbol{L}$ stands for edge. Label the triangle as unwanted triangle, $\mathcal{L}(DT_i) = 0$, if the length of one of its three edges is larger than a threshold L_0, otherwise, label it as a wanted triangle $\mathcal{L}(DT_i) = 1$. Looping through every triangle and repeating this procedure give a refined Delaunay triangulation of the point set $\boldsymbol{P}$ (Figure 3 (b)). Then the area of this point set is computed as Eqn (1),

$$A = \sum_{i=1}^{m} [\mathcal{L}(DT_i)\, A_i] \qquad (1)$$

where A_i is the area of triangle i.

For the purpose of matching building clusters, the area of reference cluster added with the centroid point of target cluster need be computed. However, the abovementioned approach is not applicable because it removes all the triangles with edges longer than a threshold. And if the added point is outside the region of reference, it will not increase the total area because all the triangles sharing this point are removed if this point is far away to the reference cluster. To address this, a modification to abovementioned approach is made. For this scenario, the triangles with edges longer than a threshold are still labeled as unwanted $\mathcal{L}(DT_i) = 0$, but those triangles sharing the added centroid point are labeled as wanted $\mathcal{L}(DT_i) = 1$ no matter how long their edges are. As shown in Figure 3 (c), this will ensure that the area increased if the added point is outside the region of reference cluster.

For volume computing, one intuitive solution is multiplying the height of each triangle to its area. Since the spatial geometry needs be considered for the purpose of volume computing, the point cloud is no longer projected onto horizontal plane, and therefore the triangles are constructed in 3-D coordinate system. In many cases, it is hard to estimate the height of a building solely from the roof data because the anisotropy of the ground slopes. However, since

the eaves are mostly horizontal, these can be employed as base level in estimating the roof height. For each matching building clusters, the base level height is chosen as the height of the lowest eave. For simplicity, the height of each 3-D Delaunay triangle, h_i, is computed from the base level to the height of its geometric center, and the area of each 3-D triangle is still computed as its projected area, A_i. The volume of roof is therefore computed as the Eqn (2).

$$V = \sum_{i=1}^{m} [\mathcal{L}(DT_i) A_i h_i] \qquad (2)$$

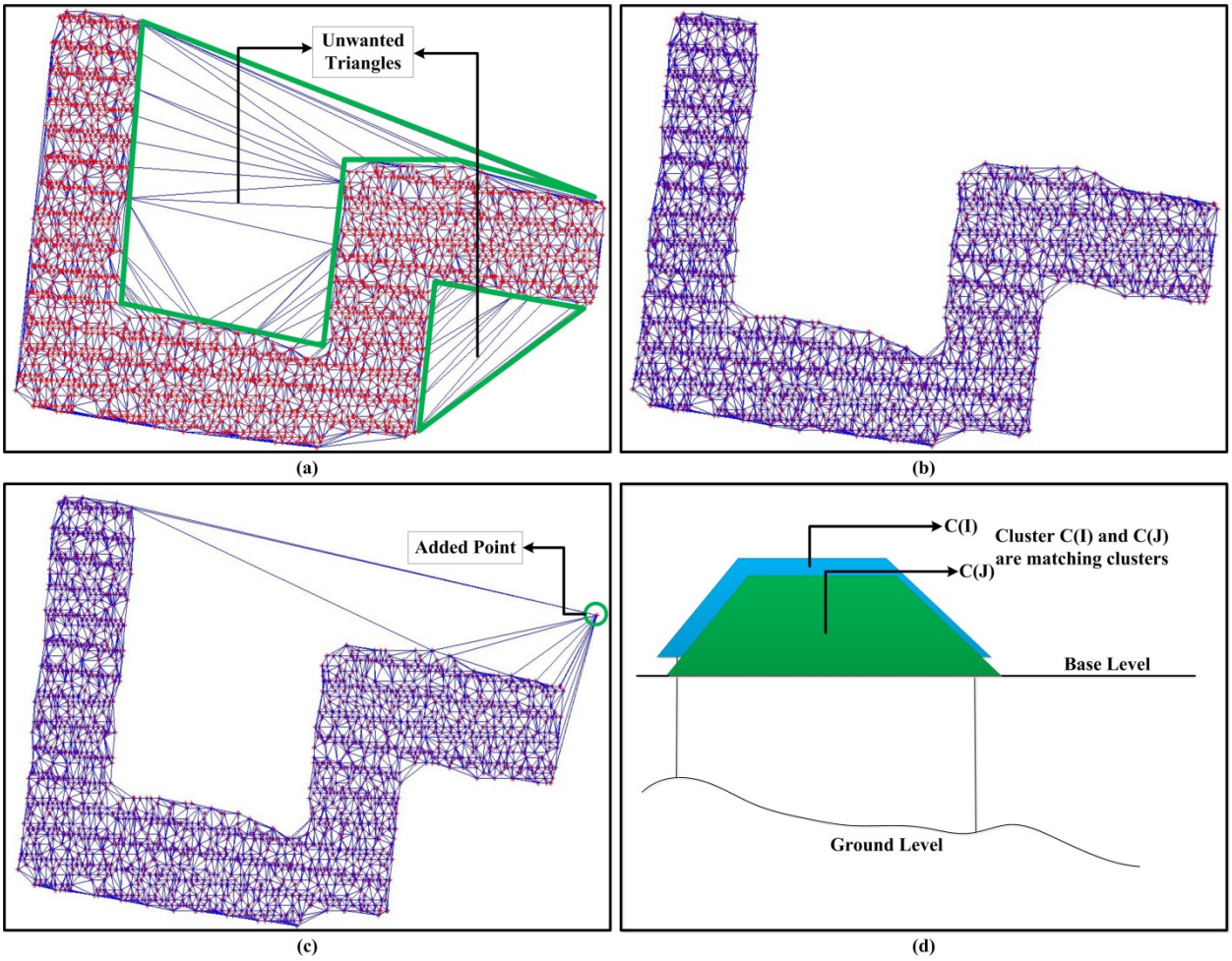

Graphical illustration to Area and Volume Computing: (a) Original Delaunay triangulations with all the wanted triangles and unwanted triangles; (b) Refined Delaunay triangulations with all the unwanted triangles removed; (c) Refined Delaunay triangulations for cluster matching with all the wanted triangles and triangles sharing the added point; (d) Estimation of base level among matching clusters

Figure 3. Graphical Illustration of Area and Volume Computing

5. Similarity Measurement of Cloud Orientations

Although the area and volume of building roof play an important role in damage identification, they are insufficient for the case when the building splits into parts or inclined or

rotated but keeps the footprint area and roof volume unchanged. In these scenarios, the orientation of building roof changes, and this can be utilized as an indicator of damage. To identify whether a building is damaged due to splitting, roof inclination or roof rotation, the similarity of its principal components (PCA) is used. Since PCA reduces the dimensionality of data into a set of linearly uncorrelated components, and each eigenvector of the covariance matrix corresponds to a direction with maximum data variation. Denote each point as $\boldsymbol{p}_i = \{p_i^x, p_i^y, p_i^z\}$, and the mean value among *x*, *y*, and *z* directions as $\bar{\boldsymbol{p}} = \{\bar{p}^x, \bar{p}^y, \bar{p}^z\}$. Then its covariance matrix is computed as Eqn (3).

$$COV_{ij} = \frac{1}{N}\sum_{k=1}^{N}\left[(\boldsymbol{p}_i - \bar{\boldsymbol{p}}) \cdot (\boldsymbol{p}_j - \bar{\boldsymbol{p}})\right] \qquad (3)$$

Denotes its eigenvalues as $\lambda_1 > \lambda_2 > \lambda_3$, and the corresponding eigenvectors as $\boldsymbol{V}_1, \boldsymbol{V}_2, \boldsymbol{V}_3$ then V_1 corresponds to the component with maximum data variation, and V_3 corresponds to that with minimum data variation, and $\{\boldsymbol{V}_1, \boldsymbol{V}_2, \boldsymbol{V}_3\}$ is an orthogonal space of the original data space. Since for most buildings, the dimension of roofs at horizontal directions are larger than that at vertical direction, $\boldsymbol{V}_3$ is therefore assumed as the axis pointing at vertical direction, and $\boldsymbol{V}_1$, $\boldsymbol{V}_2$ are the vectors at the horizontal plane. If the orientation of buildings keep unchanged, the similarity between the principal components is large, otherwise it is small (Figure 4). The similarity is herein expressed by the absolute value of the inner product of two corresponding eigenvectors (Eqn (4)). If the eigenvectors are normalized, the similarity ranges from {0,1}.

$$S_i = \langle \boldsymbol{V}_i^r, \boldsymbol{V}_i^t \rangle, \quad i = 1,2,3 \qquad (4)$$

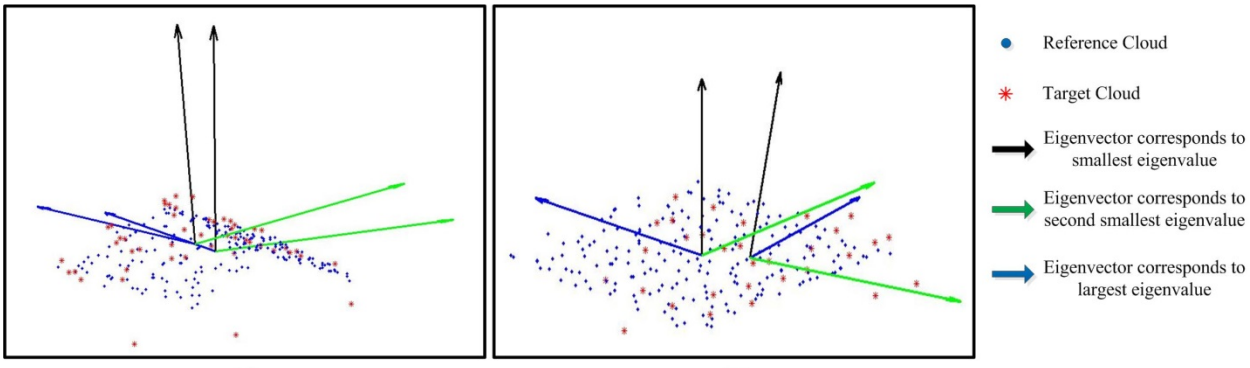

Similarity Measurement of Shape Orientation: (a) Eigenvectors of similar point clouds; (b) Eigenvectors of dissimilar point clouds

Figure 4. Similarity Measurement of Cloud Orientations

Since all the eigenvectors are normalized, the similarity computed in Eqn (4) is equivalent to the cosine angle of the corresponding pair of eigenvectors (Eqn (5)). Intuitively, the change of roof orientation can be represented by the rotation angle, $\theta_i^{r,t}$, between corresponding eigenvectors.

$$\cos\theta_i^{r,t} = \frac{\langle \boldsymbol{V}_i^r, \boldsymbol{V}_i^t \rangle}{\|\boldsymbol{V}_i^r\| \|\boldsymbol{V}_i^t\|} = \langle \boldsymbol{V}_i^r, \boldsymbol{V}_i^t \rangle = S_i \qquad (5)$$

6. Similarity Measurement of Shape Distribution

In addition to the orientation, shape distribution proposed by (Osada, R et al., 2002) is also used for the purpose of damage identification. In Osada's paper, the shape signature of a point cloud is represented as a probability distribution of specified geometric properties. In this paper, the following geometric properties are selected:

1) the distance between arbitrary pair of points in point cloud, denoted as D_{pt2pt};
2) the square root of the area of the triangle between three arbitrary points in point cloud, denoted as A_{tri};
3) the cubic root of the volume of the tetrahedron between four arbitrary points in point cloud, denoted as V_{tetra}.

For each point cluster, 1000 point sets are randomly selected to construct the corresponding distribution histogram. For the simplicity of computation, the bin width of each histogram is predefined to ensure that each histogram covers at least 100 bins. χ^2 Statistics is used herein to compute the similarity between histograms, where χ^2 Statistics is expressed as Eqn (6).

$$\chi^2 = \sum_{i=1}^{n} \frac{(h_i - g_i)^2}{h_i + g_i} \qquad (6)$$

where h_i and g_i are two different histograms. And *n* is the maximum number of bins of two histograms.

Since the variety of the building roof shape, it is difficult to identify damage buildings by simply comparing the χ^2 statistics to a threshold, but need to compare the χ^2 statistics with ground truth. Due to the lack of ground truth data set, it is hypothesized in this research that the similarity between the histograms of the same reference data is equivalent to the ground truth. For each iteration, randomly select 1000 sets of points from reference cluster $\boldsymbol{C}_r$ and construct the corresponding histograms. Due to random selection, the selected point set at iteration *i* is

different from that at iteration j. This makes the selected point clouds slightly different among iterations, and therefore could be used to compute the ground truth χ_g^2 statistics. The pseudo code of computing ground truth χ_g^2 is given in Table 2.

Table 2. Pseudo Code of Proposed Ground Truth $\boldsymbol{\chi_g^2}$ Computation

1	*FOR* (reference cluster $\boldsymbol{C}_i^r$) {
2	*FOR* (iteration j) {
3	randomly select 2 sets of points $\{\boldsymbol{p}_{i,1}, \boldsymbol{p}_{i,2}, j = 1,2, \dots, 1000\}$, each point set contains four randomly selected points $\boldsymbol{p}_{j,1}\{\boldsymbol{p}_{j,1}^1, \boldsymbol{p}_{j,1}^2, \boldsymbol{p}_{j,1}^3, \boldsymbol{p}_{j,1}^4\}$, $\boldsymbol{p}_{j,2}\{\boldsymbol{p}_{j,2}^1, \boldsymbol{p}_{j,2}^2, \boldsymbol{p}_{j,2}^3, \boldsymbol{p}_{j,2}^4\}$;
4	construct the histogram $h_{D_{pt2pt},1}$ using $\{\boldsymbol{p}_{j,1}^1, \boldsymbol{p}_{j,1}^2\}$ and $h_{D_{pt2pt},2}$ using $\{\boldsymbol{p}_{j,2}^1, \boldsymbol{p}_{j,2}^2\}$;
5	construct the histogram $h_{A_{tri},1}$ using $\{\boldsymbol{p}_{j,1}^1, \boldsymbol{p}_{j,1}^2, \boldsymbol{p}_{j,1}^3\}$ and $h_{A_{tri},2}$ using $\{\boldsymbol{p}_{j,2}^1, \boldsymbol{p}_{j,2}^2, \boldsymbol{p}_{j,2}^3\}$;
6	construct the histogram $h_{V_{tetra},1}$ using $\{\boldsymbol{p}_{j,1}^1, \boldsymbol{p}_{j,1}^2, \boldsymbol{p}_{j,1}^3, \boldsymbol{p}_{j,1}^4\}$ and $h_{V_{tetra},2}$ using $\{\boldsymbol{p}_{j,2}^1, \boldsymbol{p}_{j,2}^2, \boldsymbol{p}_{j,2}^3, \boldsymbol{p}_{j,2}^4\}$;
7	compute the statistics $\chi_{j,D_{pt2pt}}^2$ of $h_{D_{pt2pt},1}$ and $h_{D_{pt2pt},2}$;
8	compute the statistics $\chi_{j,A_{tri}}^2$ of $h_{A_{tri},1}$ and $h_{A_{tri},2}$;
9	compute the statistics $\chi_{j,V_{tetra}}^2$ of $h_{V_{tetra},1}$ and $h_{V_{tetra},2}$;
	}
10	find the maximum $\chi_{j,D_{pt2pt}}^2$, $\chi_{j,A_{tri}}^2$, and $\chi_{j,V_{tetra}}^2$ as ground truth of $\boldsymbol{C}_i^r$;
	}

7. Damage Category Determination

Within the damage indicators computed above, a multi-level damage determination process is conducted. For the area and volume, the ratio of target (post-event) clusters to reference (pre-event) cluster is computed as $r_A = A^t/A^r$ and $r_V = V^t/V^r$. These ratios are then grouped to multiple categories. The map from each ratio value to corresponding category is presented in Table 3.

Table 3. Categories of Ratios and Similarity

Area ratio, r_A	Volume ratio, r_V	Category

$r_A \in [1.1, +\infty)$	$r_V \in [1.1, +\infty)$	0
$r_A \in [0.9, 1.1)$	$r_V \in [0.9, 1.1)$	1
$r_A \in [0.8, 0.9)$	$r_V \in [0.8, 0.9)$	2
$r_A \in [0.7, 0.8)$	$r_V \in [0.7, 0.8)$	3
$r_A \in [0.6, 0.7)$	$r_V \in [0.6, 0.7)$	4
$r_A \in [0.5, 0.6)$	$r_V \in [0.5, 0.6)$	5
$r_A \in [0.4, 0.5)$	$r_V \in [0.4, 0.5)$	6
$r_A \in [0.3, 0.4)$	$r_V \in [0.3, 0.4)$	7
$r_A \in [0.2, 0.3)$	$r_V \in [0.2, 0.3)$	8
$r_A \in [0.1, 0.2)$	$r_V \in [0.1, 0.2)$	9
$r_A \in [0.0, 0.1)$	$r_V \in [0.0, 0.1)$	10

For area ratio, only the building with level 1 category is considered as intact candidate, while the building with level 2 to 10 are treated as damaged due to area loss, and the buildings with level 0 is assumed to be damaged due to collision with other buildings or mismatching of vegetation. For volume ratio, the buildings with level 0 to 3 are treated as intact candidate. This is because the airborne LiDAR data might contain some wall points, and therefore the volume will increase, resulting the change of volume change.

The building damage is also identified from the change of roof orientation. In this paper, the change categories are grouped based on the angles of corresponding eigenvectors and defined as follow, a graphical illustration of each scenario is given in Figure 5:

1) the roof rotates around eigenvector $\boldsymbol{V}_i$ if only one of $\theta_i^{r,t}$ is less than a threshold value θ_0 and other two angles are larger than θ_0. This can be divided into two subcases:
   a. if $\boldsymbol{V}_i$ corresponds to λ_3, the roof remains horizontal and rotates around vertical direction;
   b. if $\boldsymbol{V}_i$ corresponds to λ_1 or λ_2, the roof rotates around the horizontal plane.
2) the roof rotates around three eigenvectors if all the $\theta_i^{r,t}$ are larger than threshold θ_0.
3) the roof remains the same orientation if all the $\theta_i^{r,t}$ are smaller than θ_0.

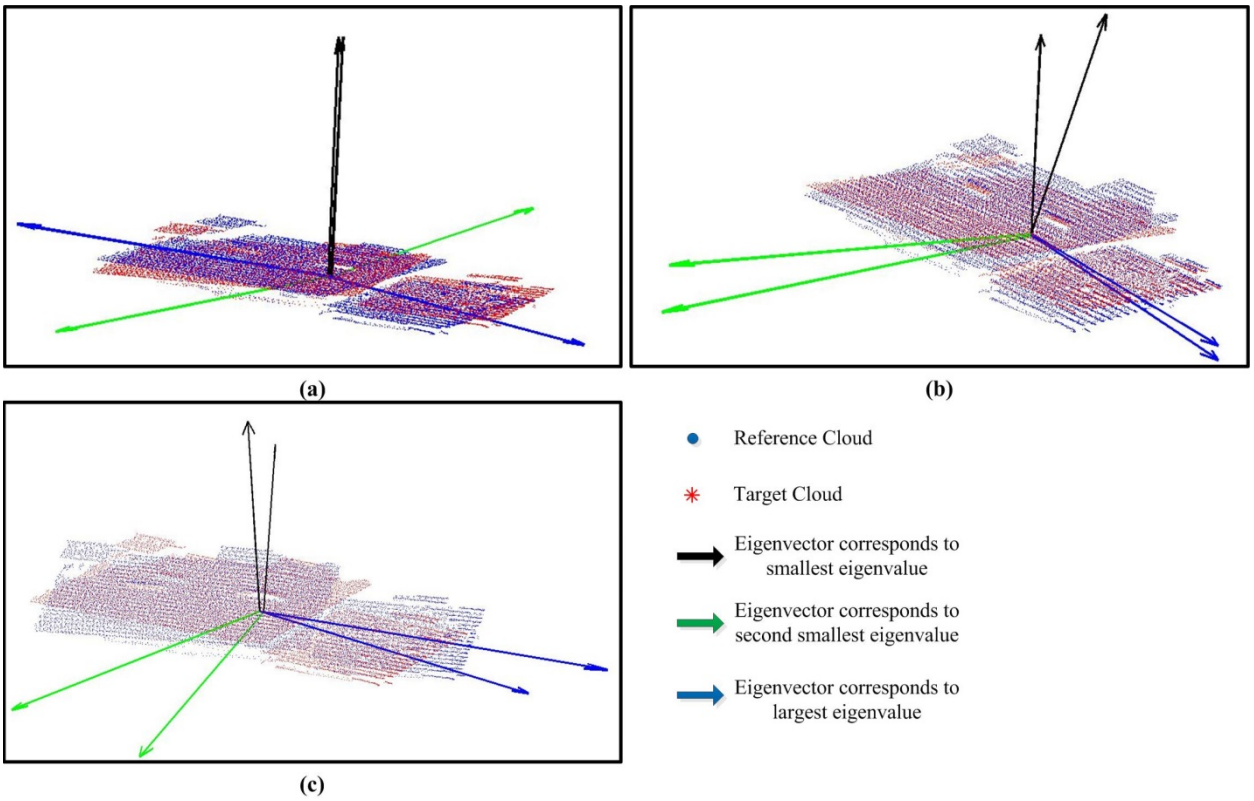

Graphical Illustration of Damage Determination from Shape Orientation: (a) Rotation about Vertical Axis; (b) Rotation about Major Axis; (c) Rotation about Three Axis

Figure 5. Damage due to Change of Roof Orientation

In addition, the χ^2 value between histograms is capable of identifying building damage condition. For each matching clusters, if $\chi_l^2 < \chi_{g,l}^2$, set $\chi_l^2 = \chi_{g,l}^2$, where $l \in \{D_{pt2pt}, A_{tri}, V_{tetra}\}$, and subscript g stands for ground truth. Then denote two vectors $\boldsymbol{X} = \{\chi_l^2\}, \boldsymbol{X}_g = \{\chi_{g,l}^2\}$ for each matching clusters, and denote $r_l^{\chi^2}$ as the ratio of χ_l^2 to $\chi_{g,l}^2$. If the clusters are perfectly matched, $r_l^{\chi^2} = 1$, otherwise, $r_l^{\chi^2} > 1$. Considering the noise and vegetation points might be clustered as building points, which will increase the χ_l^2 slightly, a buffer value ξ is introduced to address this issue. Therefore, a building is determined as damaged if the maximum ratio of $r_l^{\chi^2}$ is larger than the threshold, $1 + \xi$, otherwise, the building is determined as non-damaged.

By defining three indicator functions

$$\mathcal{I}(r_A, r_V) = \begin{cases} 1 & \text{if } r_A \in [0.9, 1.1),\ r_V \in [0.7, +\infty) \\ 0 & \text{otherwise} \end{cases}$$

$$\mathcal{J}(\theta_l^{r,t}) = \begin{cases} 1 & \text{if } max\{\theta_l^{r,t}\} < \theta_0 \\ 0 & \text{otherwise} \end{cases}$$

$$\mathcal{K}(r_l^{\chi^2}) = \begin{cases} 1 & \text{if } max\left\{r_l^{\chi^2}\right\} < 1 + \xi \\ 0 & \text{otherwise} \end{cases}$$

and defining the following damage categories: DC_0 as non-damage, DC_1 as damage due to loss of area or volume, DC_2 as damage due to change of roof orientation, DC_3 as damage due to change of roof shape. The building damage condition is determined by following rules:

1) if $\mathcal{I}(r_A, r_V) = 1$, $\mathcal{J}\left(\theta_l^{r,t}\right) = 1$, and $\mathcal{K}\left(r_l^{\chi^2}\right) = 1$, the building is determined as DC_0.
2) if $\mathcal{I}(r_A, r_V) = 0$, $\mathcal{J}\left(\theta_l^{r,t}\right) = 1$ and $\mathcal{K}\left(r_l^{\chi^2}\right) = 1$, the building is determined as DC_1.
3) if $\mathcal{I}(r_A, r_V) = 1$, $\mathcal{J}\left(\theta_l^{r,t}\right) = 0$ and $\mathcal{K}\left(r_l^{\chi^2}\right) = 1$, the building is determined as DC_2.
4) if $\mathcal{I}(r_A, r_V) = 1$, $\mathcal{J}\left(\theta_l^{r,t}\right) = 1$ and $\mathcal{K}\left(r_l^{\chi^2}\right) = 0$, the building is determined asDC_3.
5) if $\mathcal{I}(r_A, r_V) = 0$, $\mathcal{J}\left(\theta_l^{r,t}\right) = 0$ and $\mathcal{K}\left(r_l^{\chi^2}\right) = 1$, the building damage is determined as DC_1.
6) if $\mathcal{I}(r_A, r_V) = 0$, $\mathcal{J}\left(\theta_l^{r,t}\right) = 1$ and $\mathcal{K}\left(r_l^{\chi^2}\right) = 0$, the building damage is determined as DC_1.
7) if $\mathcal{I}(r_A, r_V) = 1$, $\mathcal{J}\left(\theta_l^{r,t}\right) = 0$ and $\mathcal{K}\left(r_l^{\chi^2}\right) = 0$, the building damage is determined as DC_2.
8) if $\mathcal{I}(r_A, r_V) = 0$, $\mathcal{J}\left(\theta_l^{r,t}\right) = 0$ and $\mathcal{K}\left(r_l^{\chi^2}\right) = 0$, the building damage is determined as DC_1.

These eight rules imply an order of priority among the damage indicators as $\text{Area/Volume} > \text{Orientation} > \text{Shape}$. This is based on the assumption that the density of point cloud and outliers affect the accuracy of orientation and shape more severe than area and volume. As shown in Figure 6, the footprint of Delaunay triangles are very similar between high density point cloud (Figure 6 (a)) and low density point cloud with outliers (Figure 6 (b)). While the orientation of point cloud changes with the change of point density and the occurrence of outliers. The same scenario happens to the χ^2 value of shape distribution. Therefore, the area and

volume computed from triangulation meshes are more robust against the varying of density and outliers than orientation and shape distribution.

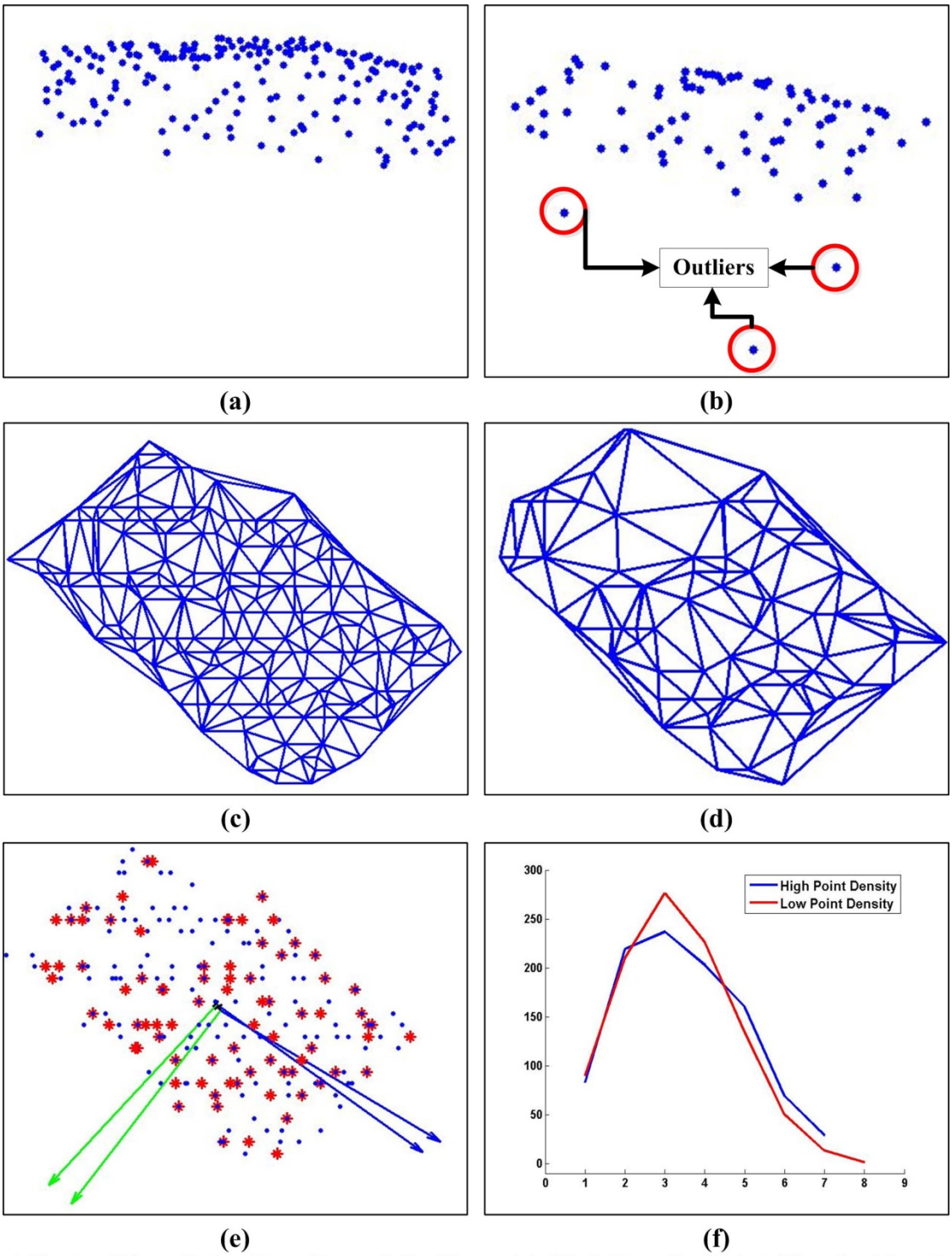

Affects of Low Point Density and Outliers: (a) High Density Point Cloud without Outliers; (b) Low Density Point Cloud with Outliers; (c) Delaunay Triangles of (a); (d) Delaunay Triangles of (b); (e) Orientation between (a) and (b); (f) Shape Distribution, dist_pt2pt, between (a) and (b)

Figure 6. Affects of Point Density and Outliers

EXPERIMENT AND RESULTS

A test is conducted using the data collected at Seaside Heights, pre- and post- hurricane Sandy. The data is was collected from an airborne LiDAR system and the area of the region was $1550(\text{meter}) \times 140(\text{meter})$. After the data pre-processing, the ground data and vegetation data are removed, the building data is remained as shown in Figure 7 (a), where the left strip is the pre-event data, and the right strip is the post-event data.

1. Result of Data Clustering

Due to the difference of point density (Figure 7 (b)), for this case, the point density of post-event is lower than that of pre-event data, different clustering parameters are used. For clustering the pre-event data, the two parameters are chosen as $K = 3, \varepsilon = 1$, and for post-event data, they are chosen as $K = 3, \varepsilon = 1.5$. For the results, each data cluster is assigned with a label, and a color map of clustering is shown in Figure 7 (c). As the result, 2074 clusters are obtained from pre-event data, and 5707 clusters are extracted from post-event data, this is partially because the point density of post- data is much lower. In addition, the number of post- cluster is more than that of pre-cluster is because some buildings damaged or splited during the hurricane.

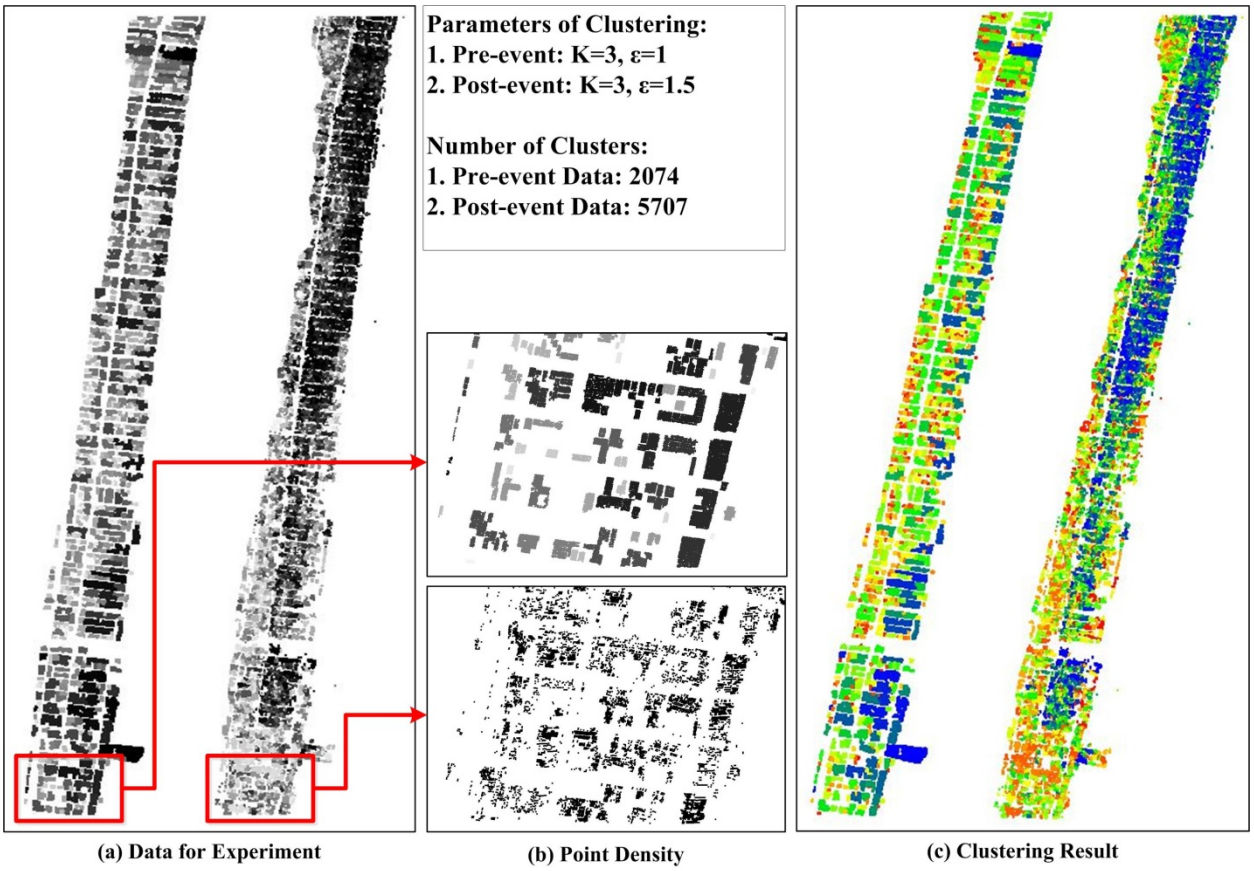

Figure 7. Result of Data Clustering

2. Result of Cluster Matching

In section 3 of Methodology, the authors proposed a novel cluster matching approach, which can robustly match splited clusters corresponding to the same building together. For what is shown in Figure 8 (a), the red points represent the one building cluster of pre-event data, and the red polygon is the footprint of this data cluster. In Figure 8 (b), the red asterisk is the centroid of this cluster, and the asterisks in other colors are the centroids of nearby post- clusters. It is noticed that these post- centroids are all within the region of pre- cluster, and therefore they are all matched with this pre- cluster. Although it is observed in Figure 8 (c) that part of the points from clusters colored in yellow and black are outside of the region of reference cluster, they are still considered as matching clusters, and are grouped as one cluster corresponding to the reference cluster.

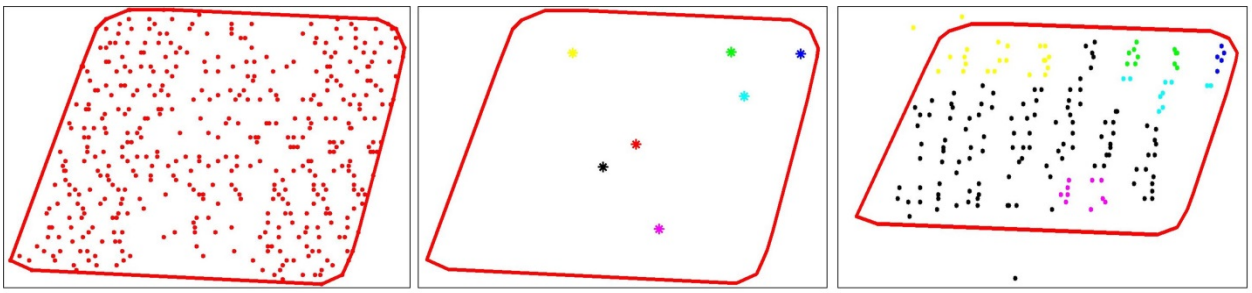

(a) (b) (c)

Result of Clusters Matching: (a) Reference cluster and footprint; (b) Centroid points of reference cluster and target clusters; (c) Matching clusters

Figure 8. Result of Cluster Matching

3. Damage due to Change of Area or Volume

By computing the area and volume of each pair of matching clusters, the change ratio of area and volume are obtained. For the test data, the threshold value of triangle edge length L_0 are chosen as $1.2192m$ for pre-event data and $2.4384m$ for post-event data. Figure 9 (a), (b) show the histograms of damage level determined from change ratio of area and volume. It is noticed from the figure that only 300 buildings are not damaged determined from the change of roof area, and approximately 1400 buildings are not damaged from the change of volume. From the union of rules 2, 5, 6, and 8, the number of damaged buildings due to loss of roof area or volume is 1763, which counts 85% of the total buildings in the test area.

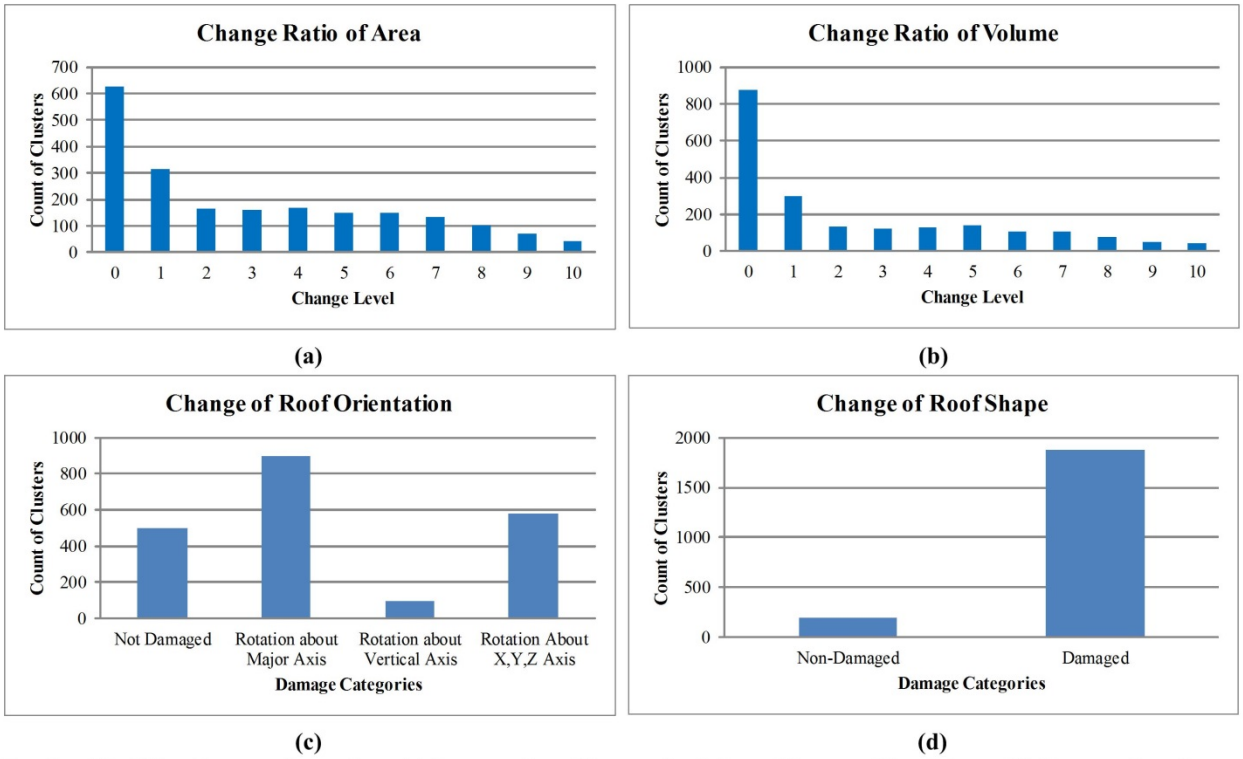

Result of Building Damage Detection: (a) Damage Level Determined from Change of Roof Area; (b) Damage Level Determined from Change of Volume; (c) Damage Level Determined from Change of Roof Orientation; (d) Damage Level Determined from Change of Roof Shape

Figure 9. Damage Level Determined

4. Damage due to Change Roof orientation

Figure 9 (c) shows the damage level determined from the orientation of roof, where the threshold value of θ_0 is set as 10°. It is noticed from the figure that most of the buildings have the issue of roof tilting and inclination, while only a few buildings, less than 100, have the issue of roof horizontal rotation. From rule 3, 5, 7 and rule 8, it is determined that the total number of damaged buildings due to change of roof orientation is 1575, which counts 75.9% of the total buildings.

5. Damage due to Change of Roof Shape

The damage determined from the change of roof shape is presented in Figure 8 (d). The threshold value, ξ, is chosen as 0.2 for this test data set. It is found that this damage indicator tends to categorize more buildings as damaged than other indicators. Based on the rule 4, 6, 7

and 8, around 90% of the buildings are determined as damaged, which is 1880 buildings in detail.

6. Final Damage Pattern

It is noticed from previous result that one single building might have multiple damage patterns and the priority of each damage pattern, according to the 8 rules proposed in section 7, is sorted in the order of $\text{Area/Volume} > \text{Orientation} > \text{Shape}$. For example, for the building shown in Figure 10 (a), the damage pattern is obviously categorized as loss of area or volume. Although one of the shape indicator, $\chi^2_{V_{tetra}} = 1.463786$, exceeds the threshold value, the damage pattern of this building is still categorized as DC_1. The building presented in Figure 10 (b), (c) is a good example of DC_2 damage. The ratio of area and volume for this building are $r_A = 1.02435$ and $r_V = 1.62314$, which implies no damage due to area or volume change. However, it is obvious that the roof rotates around the vertical axis. The damage category is therefore determined as DC_2 due to the higher priority of orientation indicator, though its $\chi^2_{V_{tetra}}$ exceeds the threshold. Figure 10 (d) (e) and (f) show the case of DC_3. The change ratio of this building are $r_A = 0.908$ and $r_V = 0.9312$, respectively, and the angles between corresponding eigenvectors are $\theta_1^{r,t} = 3.3814°\theta_2^{r,t} = 4.0238°$, and $\theta_3^{r,t} = 2.2805°$. Although these indicate no damage caused by change of area/ volume or orientation, the shape indicator, $\chi^2_{V_{tetra}} = 1.6915$ still suggests that the building has the issue of roof shape change. An visual inspection of Figure 10 (f) gives that the post-event roof points are slightly higher than that of pre-event, and the points jump up dramatically from the pre-event data at some local position, which implies partial roof tilting.

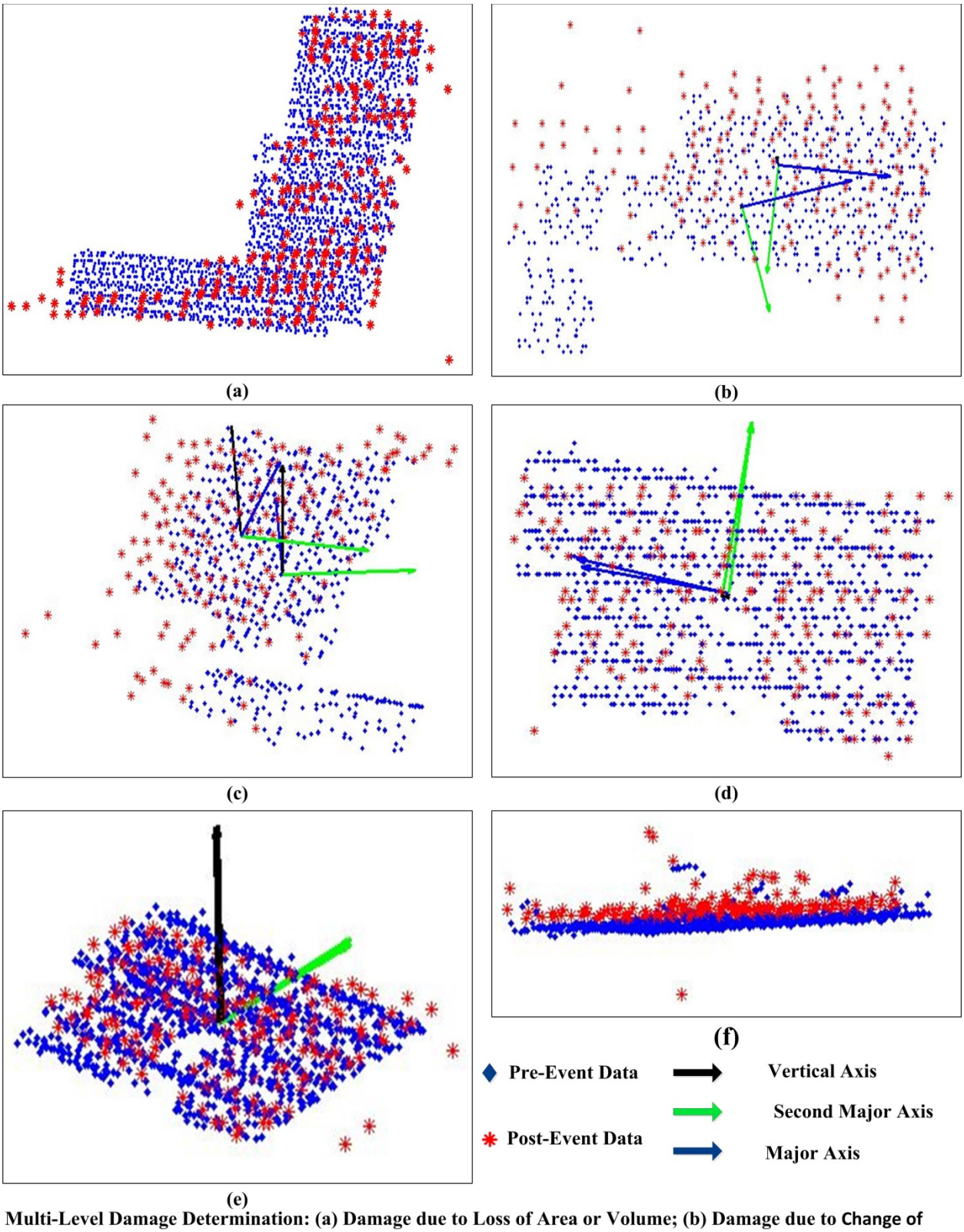

Multi-Level Damage Determination: (a) Damage due to Loss of Area or Volume; (b) Damage due to Change of Orientation (Top View); (c) Damage due to Change of Orientation (3D View); (d) Damage due to Change of Shape (Top View); (e) Damage due to Change of Shape (3D View); (f) Damage due to Change of Shape (Side View)

Figure 10. Multiple-Level Change Determination

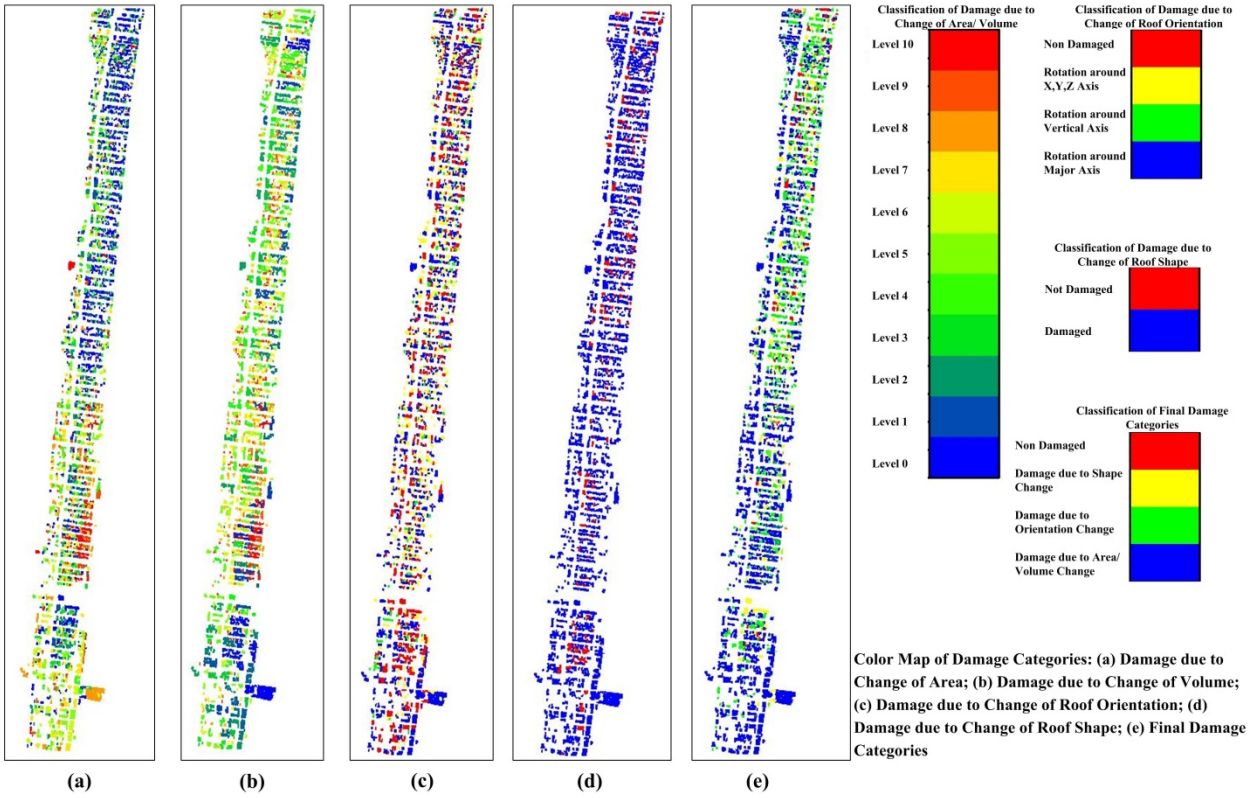

Color Map of Damage Categories: (a) Damage due to Change of Area; (b) Damage due to Change of Volume; (c) Damage due to Change of Roof Orientation; (d) Damage due to Change of Roof Shape; (e) Final Damage Categories

Figure 11. Color Map of Damage Classification

Figure 11 shows the color damage map of test data. It is observed from the figure that the buildings located at south part are mainly damaged due to change of area or volume, while the buildings at north part are mainly damaged due to change of roof orientation. Due to the affect of low point density of post-event airborne data, the damage condition tends to be amplified. This is because the building might be mis-determined as DC_1 if some part of the roof data is not collected. In addition, the clustering is also influenced if the density is low so that the density between building objects and non-building objects is similar. Therefore, non-building objects might be clustered as building objects, resulting in change of orientation and shape. Nevertheless, the damage condition of the buildings at south part is much severe than that at north part, which is of high value to rapid post-disaster damage assessment, rescue and recovery. The determination relies on three user defined threshold values, which are highly empirically selected. The higher the threshold is, the more conservative the determination process is.

7. Validation

To validate the accuracy of proposed method, the data gathered and analyzed by Federal Emergency Management Agency (FEMA) and a research group from Princeton University (Owensby, M, et al., 2013) is used as ground truth, since their investigation covered the same area. Figure 12 (a) and (b) show the area where the ground truth data was collected and the shape file created by Princeton group using ArcGIS. To validate the accuracy of building data clustering, the footprint of polygon shape of ground truth data is compared with each building cluster segmented from pre-event and post-event airborne LiDAR data sets. Figure 12 (c) - (f) show the comparison between experiment results and ground truth data. It is observed from the comparison between pre-event data and ground truth data that the building clusters match the polygons of shape file accurately for most of the buildings. Although the comparison between post-event data and ground truth data is worse, it makes sense because the post-event clusters are mostly damaged. An intuitive metric for assessing the accuracy of clustering is the area of each cluster. For the purpose of validation, the area of each building of ground truth data, A_g, and the area of each clusters of experiment data, A_e, are compared and the ratio of them, $r_{e\to g} = A_e/A_g$, is computed. Ideally, $r_{e\to g} = 1$ if the building clusters are perfectly extracted. Due to the errors in creating shape file and scanning airborne data, however, $r_{e\to g} = 1$ is hardly met for the clusters which are actually accurate enough. A buffer interval, therefore, is introduced to consider the errors. Figure 13 (a) shows the histogram of the area ratio $r_{e\to g}$. It is noticed that only 32.95% of the ratio very close to 1.0, which implies a very high accuracy of clustering. However, when choosing a buffer interval as $[0.8, 1.2]$, this percentage jumps up to 64.77%, when the interval is selected as $[0.7, 1.3]$, the percentage becomes 78.69%. Although the choose of buffer interval is affected by the parameters of clustering, ε and K, and the parameter L_0 in computing point cloud area, and the creation of ground truth shape file, it is still a subjective procedure. A large interval tends to increase the clustering accuracy, the accuracy is decreased if a small buffer interval is chosen.

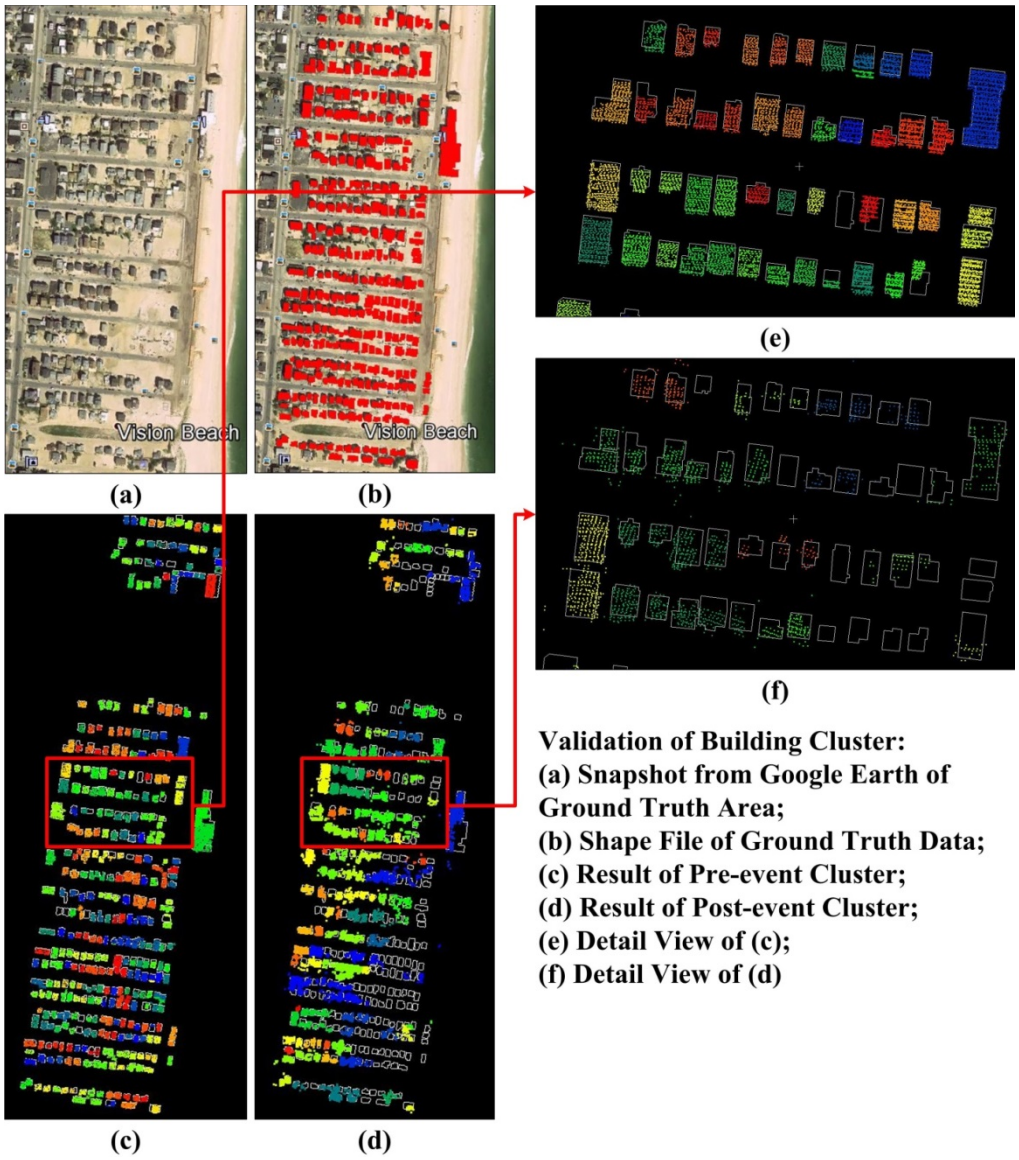

Figure 12. Validation of Building Cluster

In addition to the validation of building clustering, the accuracy of damage level determined by proposed method still needs be validated. Since different damage levels are used in experiment data and ground truth data set, unification is conducted first. In Princeton data, the building damage level is divided into 21 categories. They are denoted as $\mathfrak{D}_g = \{0, 0.5, 1, \dots, 9.5, 10\}$. This damage level is determined based on integration of multiple damage components, including wind damage, damage at each floor, roof sheat damage, roof cover damage, window damage, door damage, garage damage, etc. For experiment data, although roof orientation and roof shape are considered as damage indicators, the damage is mainly determined

by the loss of area and volume. For those buildings determined as DC_1, the damage level is labeled as 1, 2, …, 10, respectively. For those buildings determined as DC_2, the damage level is labeled as 1, and for buildings as DC_3, the damage level is labeled as 0.5, and the non-damaged buildings are labeled as 0. This is determined based on the sequence of priority of each damage pattern. Therefore, the overall damage level of experiment data is denoted as $\mathfrak{D}_e = \{0, 0.5, 1, 2, \dots, 10\}$. Denote a new value, $\mathfrak{D}_{e\to g} = \mathcal{D}_e - \mathcal{D}_g$, for each building, the accuracy of damage level determination can be evaluated from this value. Intuitively, $\mathfrak{D}_{e\to g} = 0$ implies that the damage level estimated by proposed approach matches ground truth exactly. If $\mathfrak{D}_{e\to g}$ is greater than 0, it implies the proposed method overestimates the damage level, and on the contrary, it is implied that underestimation occurs. The larger $|\mathfrak{D}_{e\to g}|$ is, the worse the estimation is. A histogram of $\mathfrak{D}_{e\to g}$ is presented in figure 13 (b). It is observed that the proposed method tends to overestimate the damage level, only 23.3% of the building matches ground truth damage level exactly. Considering the fact that the damage level of ground truth data is determined based on multiple criteria, which goes into detail of component level and story level, while the proposed approach only leverages the airborne LiDAR data, $\mathfrak{D}_{e\to g} = 0$ is too restrictive. If both $\mathfrak{D}_{e\to g} = 0$ and $\mathfrak{D}_{e\to g} = \pm 0.5$ are considered as acceptable, the percentage of accuracy ratio is 29.55%. If $\mathfrak{D}_{e\to g} = \pm 1.0$ is also considered, the percentage rises to 43.18%.

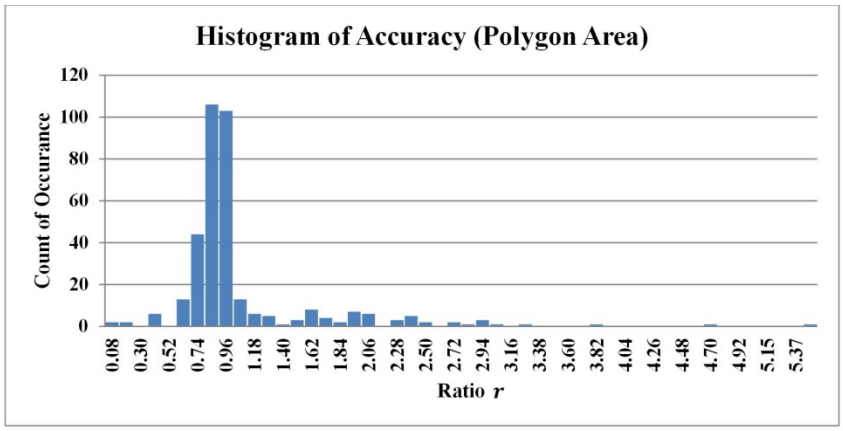

(a)

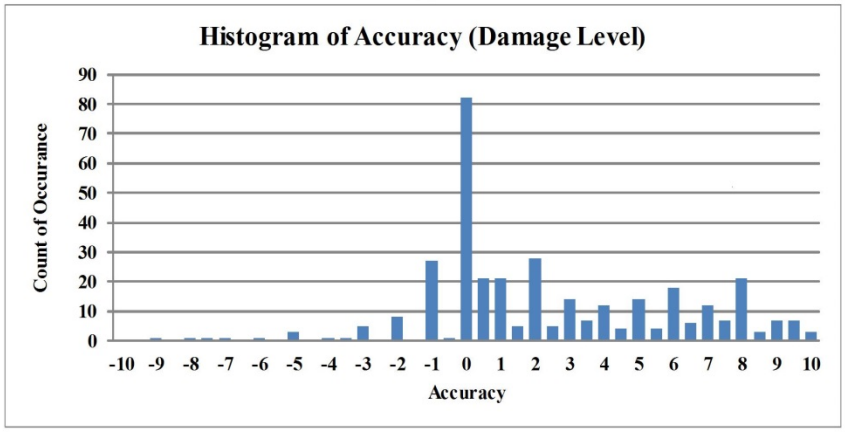

(b)

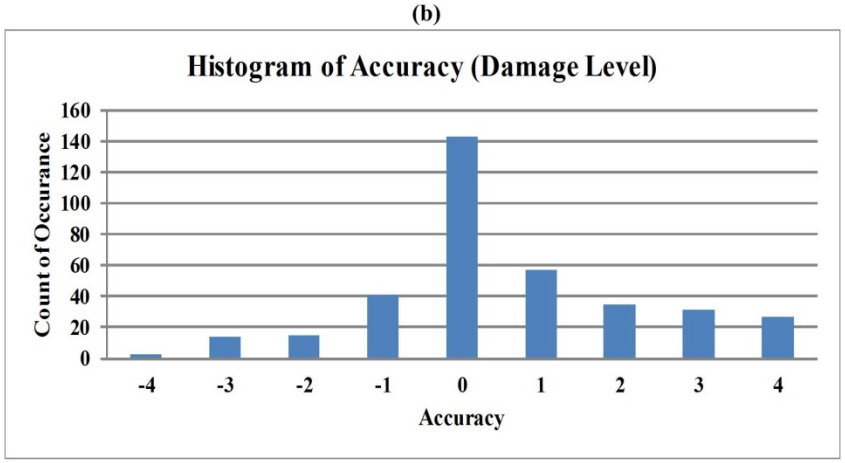

(c)

Histogram of Accuracy : (a) Accuracy of Polygon Area between Experiment Data and Princeton Ground Truth Data; (b) Accuracy of Damage Level between Experiment Data and Princeton Ground Truth Data; (c) Accuracy of Damage Leel between Experiment Data and FEMA Ground Truth Data

Figure 13. Histogram of Accuracy

Since Princeton data takes too many factors into consideration when scoring the overall damage, it affects the validation result. Since the proposed method estimates the damage level

mainly based on the loss of roof area and volume, it is ideal if it can be benchmarked using loss of roof area as ground truth. The FEMA MOFT data collected during Hurricane Sandy is used here as ground truth. The damage level is determined based on visible imagery based classification (FEMA). However, since different damage level are used for different data sets, they are unified at first. Table 4 shows the damage level used in FEMA data and the corresponding loss of roof area for experiment data. The same value, $\mathfrak{D}_{e\to g}$, is used here for the measurement of accuracy, and the histogram of accuracy is shown in Figure 13 (c). If only $\mathfrak{D}_{e\to g} = 0$ is considered, the accuracy rate is 39.07%. However, since the FEMA damage level of minor, major, and destroyed are mainly classified according to the condition of roof diaphragm, walls, and other considerations, only considering $\mathfrak{D}_{e\to g} = 0$ is, again, too restrictive. For this reason, the accuracy rate jumps to 65.85% when $\mathfrak{D}_{e\to g} = \pm 1$ is also considered, this, compared to the accuracy rate validated using Princeton data, is a huge increase.

Table 4. Damage Level Definition (FEMA Data)

Damage Level $\mathfrak{D}$	Ground Truth Data	Experiment Data
	Damage Classification	Loss of Roof Area
1	No Damage	0%
2	Affected	$(0\%, 20\%]$
3	Minor	$(20\%, 50\%]$
4	Major	$(50\%, 80\%]$
5	Destroyed	$(80\%, 100\%]$

Another metric measuring the accuracy is

$$\frac{\text{TurePositive} + \text{FalseNegative}}{\text{TurePositive} + \text{TrueNegative} + \text{FalsePositive} + \text{FalseNegative}}$$

where

True: the proposed method determines the building as Damaged;

False: the proposed method determines the building as No Damage;

Positive: the ground truth determines the building as Damaged;

Negative: the ground truth determines the building as No Damage

The confusion matrix for both Princeton and FEMA data are presented in Table 5. The diagonal elements are taken into consideration because they stand for the correct estimation of building damage condition. The accuracy ratio can be obtained as 87.78% for Princeton Data, and 67.76% for FEMA Data, respectively.

Table 5. Confusion Matrix

	Princeton Data		FEMA Data	
	Positive	Negative	Positive	Negative
True	307	26	214	34
False	17	2	84	34

CONCLUSION

This research presented a novel rapid post-hurricane damage assessment approach using both pre- and post-event airborne Data. The approach uses multiple indicators for damage determination. And a multi-level damage determination process is proposed to identify the building damage condition and damage pattern. By specifying the determination threshold value and clustering parameters, the approach then automatically extract the damage information and damage pattern. A color map of damage pattern is then generated to assist the rapid assessment and decision making. The comparison of the results between experiment data and ground truth data suggests that the proposed approach is capable of extracting building clusters from airborne LiDAR data in a good accuracy benchmarked by manually-created shape file.

REFERENCE:

Bovolo, F., Marin, C., & Bruzzone, L. (2012, November). A novel approach to building change detection in very high resolution SAR images. In SPIE Remote Sensing (pp. 85370Y-85370Y). International Society for Optics and Photonics.

Chen, Q., Gong, P., Baldocchi, D., & Xie, G. (2007). Filtering airborne laser scanning data with morphological methods. Photogrammetric Engineering & Remote Sensing, 73(2), 175-185.

Elberink, S. O., Shoko, M., Fathi, S. A., & Rutzinger, M. (2011). Detection of collapsed buildings by classifying segmented airborne laser scanner data. Proc. Int. Archives Photogramm., Remote Sens., Spatial Inf. Sci, 307-312.

Ester, M., Kriegel, H. P., Sander, J., & Xu, X. (1996, August). A density-based algorithm for discovering clusters in large spatial databases with noise. In Kdd (Vol. 96, No. 34, pp. 226-231).

Federal Emergency Management Agency. FEMA MOTF Hurricane Sandy Impact Analysis. http://fema.maps.arcgis.com/home/item.html?id=307dd522499d4a44a33d7296a5da5ea0.

Filin, S., & Pfeifer, N. (2006). Segmentation of airborne laser scanning data using a slope adaptive neighborhood. ISPRS journal of Photogrammetry and Remote Sensing, 60(2), 71-80.

Graham, R. L. (1972). An efficient algorith for determining the convex hull of a finite planar set. Information processing letters, 1(4), 132-133.

Hodgson, M. E., Jensen, J., Raber, G., Tullis, J., Davis, B. A., Thompson, G., & Schuckman, K. (2005). An evaluation of lidar-derived elevation and terrain slope in leaf-off conditions. Photogrammetric Engineering & Remote Sensing, 71(7), 817-823.

Huang, X., Zhang, L., & Zhu, T. (2014). Building change detection from multitemporal high-resolution remotely sensed images based on a morphological building index. Selected Topics in Applied Earth Observations and Remote Sensing, IEEE Journal of, 7(1), 105-115.

Kashani, A. G., & Graettinger, A. J. (2015). Cluster-Based Roof Covering Damage Detection in Ground-Based Lidar Data. Automation in Construction, 58, 19-27.

Khoshelham, K., & Oude Elberink, S. J. (2012, May). Role of dimensionality reduction in segment-based classification of damaged building roofs in airborne laser scanning data.

In Proceedings of the International Conference on Geographic Object Based Image Analysis (pp. 372-377).

Labiak, R. C., Van Aardt, J. A., Bespalov, D., Eychner, D., Wirch, E., & Bischof, H. P. (2011, May). Automated method for detection and quantification of building damage and debris using post-disaster LiDAR data. In SPIE Defense, Security, and Sensing (pp. 80370F-80370F). International Society for Optics and Photonics.

Lari, Z., & Habib, A. (2014). An adaptive approach for the segmentation and extraction of planar and linear/cylindrical features from laser scanning data. ISPRS Journal of Photogrammetry and Remote Sensing, 93, 192-212.

Lee, D. T., & Schachter, B. J. (1980). Two algorithms for constructing a Delaunay triangulation. International Journal of Computer & Information Sciences, 9(3), 219-242.

Li, M., Cheng, L., Gong, J., Liu, Y., Chen, Z., Li, F., ... & Song, X. (2008). Post-earthquake assessment of building damage degree using LiDAR data and imagery. Science in China Series E: Technological Sciences, 51(2), 133-143.

Meng, X. (2005). A slope-and elevation-based filter to remove non-ground measurements from airborne LIDAR data. UCGIS Summer Assembly, 28.

Meng, X., Wang, L., & Currit, N. (2009). Morphology-based building detection from airborne LIDAR data. Photogrammetric Engineering & Remote Sensing, 75(4), 437-442.

Meng, X., Wang, L., Silván-Cárdenas, J. L., & Currit, N. (2009). A multi-directional ground filtering algorithm for airborne LIDAR. ISPRS Journal of Photogrammetry and Remote Sensing, 64(1), 117-124.

Murakami, H., Nakagawa, K., Hasegawa, H., Shibata, T., & Iwanami, E. (1999). Change detection of buildings using an airborne laser scanner. ISPRS Journal of Photogrammetry and Remote Sensing, 54(2), 148-152.

Osada, R., Funkhouser, T., Chazelle, B., & Dobkin, D. (2002). Shape distributions. ACM Transactions on Graphics (TOG), 21(4), 807-832.

Owensby, M., N. Lin and A. Kennedy (2013). An assessment and analysis of Hurricane Sandy damage in Ortley Beach, New Jersey. Proceedings of 11th International Conference on Structural Safety & Reliability (ICOSSAR 2013), Columbia University, New York, June 16-20, 2013.

Pang, S., Hu, X., Wang, Z., & Lu, Y. (2014). Object-Based Analysis of Airborne LiDAR Data for Building Change Detection. Remote Sensing, 6(11), 10733-10749.

Sui, H., Tu, J., Song, Z., & Li, Q. (2014). A Novel 3D Building Damage Detection Method Using Multiple Overlapping UAV Images. ISPRS-International Archives of the Photogrammetry, Remote Sensing and Spatial Information Sciences, 1, 173-179.

Teo, T. A., & Shih, T. Y. (2013). Lidar-based change detection and change-type determination in urban areas. International journal of remote sensing, 34(3), 968-981.

Tian, J., Cui, S., & Reinartz, P. (2014). Building change detection based on satellite stereo imagery and digital surface models. Geoscience and Remote Sensing, IEEE Transactions on, 52(1), 406-417.

Tomljenovic, I., Höfle, B., Tiede, D., & Blaschke, T. (2015). Building Extraction from Airborne Laser Scanning Data: An Analysis of the State of the Art. Remote Sensing, 7(4), 3826-3862.

Tralli, D. M., Blom, R. G., Zlotnicki, V., Donnellan, A., & Evans, D. L. (2005). Satellite remote sensing of earthquake, volcano, flood, landslide and coastal inundation hazards. ISPRS Journal of Photogrammetry and Remote Sensing, 59(4), 185-198.

Tsai, F., Hwang, J. H., Chen, L. C., & Lin, T. H. (2010). Post-disaster assessment of landslides in southern Taiwan after 2009 Typhoon Morakot using remote sensing and spatial analysis. Natural Hazards and Earth System Sciences, 10(10), 2179.

Turner, D., Lucieer, A., & Watson, C. (2012). An automated technique for generating georectified mosaics from ultra-high resolution unmanned aerial vehicle (UAV) imagery, based on structure from motion (SfM) point clouds. Remote Sensing, 4(5), 1392-1410.

Van Aardt, J. A., McKeown, D., Faulring, J., Raqueño, N., Casterline, M., Renschler, C., ... & Gill, S. (2011). Geospatial disaster response during the Haiti earthquake: A case study spanning airborne deployment, data collection, transfer, processing, and dissemination. Photogrammetric engineering and remote sensing, 77(9), 943-952.

Vögtle, T., & Steinle, E. (2004). Detection and recognition of changes in building geometry derived from multitemporal laserscanning data. International Archives of the Photogrammetry, Remote Sensing and Spatial Information Sciences, 35(B2), 428-433.

Vu, T. T., Matsuoka, M., & Yamazaki, F. (2004, September). LIDAR-based change detection of buildings in dense urban areas. In Geoscience and Remote Sensing Symposium, 2004. IGARSS'04. Proceedings. 2004 IEEE International (Vol. 5, pp. 3413-3416). IEEE.

Yonglin, S., Lixin, W., & Zhi, W. (2010, June). Identification of inclined buildings from aerial LIDAR data for disaster management. In Geoinformatics, 2010 18th International Conference on (pp. 1-5). IEEE.

Zeng, C., Wang, J., Zhan, W., Shi, P., & Gambles, A. (2014). An elevation difference model for building height extraction from stereo-image-derived DSMs. International Journal of Remote Sensing, 35(22), 7614-7630.

Zhang, J., Lin, X., & Ning, X. (2013). SVM-based classification of segmented airborne LiDAR point clouds in urban areas. Remote Sensing, 5(8), 3749-3775.

Zhang, K., Chen, S. C., Whitman, D., Shyu, M. L., Yan, J., & Zhang, C. (2003). A progressive morphological filter for removing nonground measurements from airborne LIDAR data. Geoscience and Remote Sensing, IEEE Transactions on, 41(4), 872-882.

Data Efficiency of LiDAR Technologies for Supporting Post-Sandy Damage Assessment

Xuan Hu[1], Jie Gong[2], and Zheng Yi Wu[3]

[1]Ph.D. Candidate, Dept. of Civil & Environmental Engineering, Rutgers, the State University of New Jersey, cee.shawn@rutgers.edu

[2]Assistant Professor, Dept. of Civil & Environmental Engineering, Rutgers, the State University of New Jersey, Phone: 848-445-2881, Jg931@rci.rutgers.edu

[3]Bentley Fellow, Director Applied Research, Bentley Systems, Incorporated, Zheng.wu@bentley.com

Abstract

LiDAR (a portmanteau of "light" and "radar.") is a remote sensing technology that measures distance by illuminating a target with a laser and analyzing the reflected light. Among other applications, LIDAR is useful for detailed mapping of terrain, elevation, structures, and change detection in disaster management at several levels. The field is rapidly maturing in capabilities, applications, and utility. During large-scale natural disasters, various LiDAR systems, such as airborne and terrestrial LiDAR, can be deployed to collect time sensitive spatial data. However, there are often great challenges in synthesizing the collected LiDAR data sets and performing rapid integrative damage impact analysis as the collected data are often varied in resolution, accuracy, spatial completeness, and storage requirement and strategies. This paper presents a detailed analysis of various LiDAR data sets that have been collected before and after Hurricane Sandy according to these key data performance metrics. Resolution of LiDAR data from different carrier varies dramatically (0.35- 5 point/$m^2$for airborne system and 1750 point/m^2 for land based mobile system). The achievable relative vertical positon accuracies five locations are computed by the comparison of the airborne and mobile LiDAR datasets and it is within 0.10 ± 0.05 m (mean ± SD). The natural drawback of the airborne system in the loss of vertical information is complemented by the land based mobile system, which has an average coverage of 43.5%. The results of this study provide practical knowledge of the data efficiency of various LiDAR technologies, which can be leveraged by emergency response organizations to better plan data acquisition and maximize the benefit of such data acquisition effort.

Keywords: ***Lidar, resolution, accuracy, spatial completeness***

Introduction

In 2010, Hurricane Sandy, the biggest Atlantic storm in United States history, swept through the Caribbean and up the East Coast of the United States. The storm is estimated to have cost over $68 billion (2013 USD), and at least killed 286 people in the country. Hurricane often causes damage so widespread that it overwhelmed the capacity of traditional surveying methods. Typically for hurricane Sandy, LIDAR is widely utilized for documenting and assessing the damage along with this extreme event.

Airborne LiDAR is currently the most efficient tool for terrain mapping and federal agencies including FEMA, USGS etc. regularly released the public domain airborne data sets. These data sets are extremely valuable in constructing digital elevation models (DEMs) and providing topography information. Different agencies released their LIDAR data sets which provide unique opportunities to look into the details of pre and post hurricane sandy situations.

USGS Center for LIDAR Information Coordination and Knowledge (USGS CLICK) conduct a LIDAR survey in three New Jersey Countries (Ocean County included) on April 10 2010. Even though, it is five months before the occurrence of the hurricane Sandy, it remains the one of the most high resolution airborne data reference for these disastrous events.

US Army Corps of Engineers (USACE) Joint Airborne Lidar Bathymetry Technical Center of expertise (JALBTCX) performed a coastal survey along the Atlantic coast of NJ and New York (Rockaway) from August 28 to September 11 2010. The collection effort follows the coastline and extends 500m inland and 1000m offshore or to laser extinction, whichever comes first.

The USGS use by Experimental Advanced Airborne Research Lidar (EAARL) system to conduct two surveys targeted at hurricane Sandy on October 26 2012 and November 1 2012. The post and pre LIDAR data are compared to characterize the hurricane-induced coastal changes.

Airborne does not equally meritorious in providing the detail vertical information for the damage assessment of individual houses. Terrestrial system is restricted for their disability in mobility. Mobile LiDAR system fills the gap between the airborne LiDAR system and terrestrial system by bringing mobility to the terrestrial system without losing much of its resolution and accuracy. The use of mobile LiDAR in such a post-disaster scenario holds great potential. However,

despite this obvious potential, there have been few systematic studies (Ellum and N El-Sheimy 2002; Barber et al 2008; Haala et al 2008) on examining the types of damage data that can be collected via such a technology. A team led by Rutgers civil engineering professor Jie Gong, Ph.D., CAIT, teamed up with Ohio-based Woolpert Geospatial Mapping Co. collected the first hand mobile Light Detection and Ranging (LiDAR) data in the devastated coastal areas (Gong 2013). These areas include Staten Island, Rockaway in the New York City and Ortley Beach, Seaside Heights, Mantoloking on the New Jersey Shoreline. Our collected post-Sandy mobile LiDAR data set provides a unique opportunity to evaluate the strength and weakness of the mobile LiDAR technology as a field data collection method for hurricane damage assessment. To ensure the decision and assessment based on mobile LiDAR system, the validation of the data is extremely important.

Terrestrial LiDAR is with highest accuracy (2-5 mm) However, a single scan of the terrestrial LiDAR can take more than 10 minutes. Even though the ranging of the LiDAR can be as far as 300 meters, the laser light can be easily blocked by the houses and vegetation which make it even difficult to scan the objects a block away. Both the duration of scan time and the ranging of reflection laser lights make it impossible to be the ideal tool for the rapid data collection in the post disaster environment in wide range of areas..

Application of individual LIDAR system has been widely adopted by researchers and for practical usage. Airborne LIDAR have been used in building detection or feature extraction. (Awrangjeb et al 2010; Jochem et al 2012; Meng et al 2010; Sofia et al 2011). Other researchers conduct terrestrial LIDAR scan to detect details for structural damage assessment (Olsen et al 2009, 2012; Fewtrell et al 2008,2011;). Mobile LIDAR is utilized for data collection (Gong et al 2012; El-Halawany et al 2011).

Recent studies focus integration of these system and most commonly combination of terrestrial LIDAR with airborne LIDAR for modeling and mapping (Starek at al 2011; Hopkinson et al 2013; Lindberg et al 2012; Bremer et al 2012; Hilker et al 2010). More innovated approaches attempt to combine all Airborne, Mobile and Terrestrial LIDAR for measurements (Fowler and Kadatskiy 2011; Lin et al 2012; Holopainen et al 2013; Hyyppä et al 2013).

Literature Review

LIDAR has been widely applied in damage assessment for extreme events. Many papers have focus on error analysis. A thorough description of different type of accuracies can be viewed Baltsavias's research (1999). He derived formulas represent approximation of these accuracies. The derived result of each error scale is listed in the table 1.

Table 1 Derived error scale by Baltsavias (1999)

Accuracy Type	Description and influence factors	Possible Error Scale
Range accuracy	Most complicated, minimum among the error sources (necessary measures and precautions)	Around 1.5 cm
Position accuracy	Depends on DGPS, GPS hardware and satellite constellation	5 – 15 with DGPS and post processing
Attitude accuracy	Depends on the quality of the INS, INS frequency (i.e., interpolation error) ,	-
Time offsets	Dependent on major parameters like flying height, scan angle, terrain topography, and land cover	5–10 cm in good cases

Both mapping systems (airborne based systems and land based mobile systems) are composed of different components including GPS, Inertial Measurement Unit (IMU)/ Inertial Navigation System (INS), Distance Measurement Unit (DMI) and Sensors (LiDAR scanners). The vertical positioning accuracy of sensors is provided by the manufacture companies.

Table 2 Key features of major sensor provided by manufacture companies

Company	Type	Range	Accuracy	Data Rate
		10% Reflectivity	1 sigma	Up to
Velodyne	HDL-64E	50 m	20 mm	1.3 m
	HDL-32E	50 m	20 mm	700 k
Optech	Lynx	250 m	5 mm	600 k

RIEGL	VQ250	180 m	5 mm	300 k
FARO 3D	130	0.6-130 m	2 mm	976 k
	300	0.6-300 m	2 mm	976 k
Leica	Scan Station P20	120 m	3 mm	1 m

More researches have been focus on the accuracy induced by the integration system and their performance under practical environments. Airborne laser altimetry system was first proposed by NASA in 1980s and a pioneer study including changes monitoring in the Greenland ice sheets. In this study, Krabill indicated that the reliably accuracy of the airborne LiDAR system can be around 0.20 meters. During the late 1990s, the Airborne Laser Swath Mapping (ALSM) is available from commercial manufactures and more studies are focus on the vertical accuracy of the system under different environments.

Table 3 Smarmy of previous literatures on the vertical accuracy of airborne system in different environment

Studies	Environment	Reference	Vertical Accuracy
Krabill(1995)	Ice-surface elevations	Differential Global Positioning System	0.20m
Kraus and Pfeifer(1998)	wooded area	photogrammetry with reference to a big pilot project	0.25 m
Latypov(2002)	surface size and flatness	overlapping LIDAR datasets	0.21m

a Töyrä(2003)	wetlands, deltas, or other similar areas	in situ survey data	0.26 m
Reutebuch et al (2003)	heavily forested areas	Conventional ground survey methods	0.22 ± 0.24 m (mean ± SD)
Hodgson and Bresnahan(2004)	Pavement, Low Grass, High Grass, Brush/ Low Trees, Evergreen Forest, Deciduous Forest		0.17-0.19m
Hopkinson et al(2005)	Utikuma boreal wetland area	kinematic GPS surveys	0.15 ± 0.22 m (mean ± SD)
May and Toth(2007)	-	analytical derivation of error formulas	0.225m
Bowen and Waltermire(2007)	Western river coridor (variable terain and large topographic relief.)	ground GPS surveys	0.43 m

Other researchers evaluated the horizontal accuracy of the airborne LiDAR system. Kilian et al (1996) purposed the method of overlapping strips to calibrate the airborne LiDAR data and this method is adopted to exam and increase the airborne LiDAR horizontal accuracy in researches (Crombaghs et al 2000; Maas, 2000; Bretar et al 2004; Vosselman, 2002; Pfeifer et al 2005). The accuracy of the first operational land-based Mobile Mapping System (MMS) GPSVANTM developed by Ohio State University in 1991 was limited to 1-3 meters (C Ellum and N El-Sheimy, 2002). In mid 1980s, high precision IMU have dramatically increase potential of the MMS by providing high-accuracy orientation information and the accuracy can reach 0.06-0.20 meters when the speed of vehicle is less than 70 km/h (R Li 1997). Some recent studies purposed that the z position RMS error can be as around 0.5mm (Dix et al 2012; Jaakkola et al 2014).

There is little systematic study on the performance of the LIDAR in residential shoreline areas and combination of both mobile and airborne LIDAR for damage assessments. The purpose of this research is to explore the potential feasibility of mobile LiDAR integrated with current government agency released airborne LIDAR as a tool for the damage assessments. This paper starts by a description of the approach for our data management. The analysis will base on three aspects: (1) accuracy analysis; (2) resolution analysis; (3) completeness analysis. In accuracy analysis, an airborne LiDAR is utilized as a baseline data to the validation of the mobile LiDAR data collected. ANOVA analysis is conducted to determine whether the difference between mobile LiDAR and airborne LiDAR data is significant. The resolution analysis followed will demonstrate to what extend can the house components be represented by points in the mobile LiDAR data. Coverage analysis will focus on the limitation of the mobile LiDAR system on the components features extraction by illustrating what parts of information is missing in the data collection process. Finally, a discussion of the analysis results and some conclusions are given.

LiDAR Applications in Hurricane Sandy

Data Storage

Different from traditional data collection method, LIDAR data collection is a massive data generating process. According to the LAS specification by ASPRRS, each single LIDAR point should contain at least core 20 bytes. From the summary of the datasets we have, each point contains around 28 bytes. Given the fact that the data rate for the most common used sensor is from 300 thousands to 1.3 million points per second, when it is multiplied by 28 bytes, the data produced in a second is 8 to 35MB and accumulatively 0.5 to 2GB data is required for storage every minute. Even for the most powerful 64 bit personal computer which supports a maximum of 128GB memory, it is beyond its capacity to open 2 hour LiDAR data at a time. Thus, data storage management becomes critical and essential issue for the LiDAR survey. Two simple ways to discrete the data is dividing the data into smaller pieces by fixed duration of the time or fixed size. These methods are good for its simplicity in operation and maintaining the time continuity, but fail to reflect the spatial relation between points. The requirement for rapid assessment for such disaster scenario spurs a systematic way of data management.

Rather than simply discrete the data with fixed duration or file size, a multi-scale grid system is introduced to store the data. The tremendous data file is divided into three different sizes of

blocks. The file size is subtracted to megabyte scale, which is appropriate for the computation of current normal computers. Furthermore, each block is geo-referenced and has a corresponding boundary. A CAD file is linking the geo location to the data file. Compared to the ambiguity of the location in traditional data management, this approach save the trouble of remembering the file name to the corresponding location by automatically figure out which file the target location is belong to.

Table 4 Multi-scale grid system of damage assessment

Scale	Type	Grid Size	Data Resource	Total Size	Average Size	Purpose Addressed
Entire Shoreline	Airborne LiDAR	5km by 5km	NY USACE Rockaway	8.6 GB	500 MB	Airborne LiDAR storage, shoreline & municipality based change detection, DEM extraction
			NJ CLICK	20.5 GB	500 MB	
			NJ USACE	50.0GB	350 MB	
			Pre Eaarl-B	1.3 GB	30 MB	
			Post Eaarl-B:	1.2 GB	30 MB	
Municipality	Mobile LiDAR / Airborne	80m by 80m	Rutgers Survey	212GB	300 MB	Mobile LiDAR storage, municipality based change detection;
Individual Building	Mobile LiDAR	house outline polygons	Rutgers Survey	212GB	3 MB	Detail assessment for individual house, component based assessment, damage measurements,

From the approach above, the gigabytes data are subtracted into smaller blocks without losing the spatial relation and different size of blocks are targeted at different assessment purposes. This

data management method will potentially have two advantages: (1) improvement of the data processing efficiency; (2) preparation for future parallel computing for rapid response.

Data Resolution

The resolution of the datasets varies due to different data collection systems and the features of the system carrier, e.g. speed, distance to the objects etc. Even for the airborne system, the resolution can be dramatically different. The horizontal resolution for the NJ CLICK data is 10 times the resolution of the Eaarl-B Pre hurricane data sets. This low resolution does not mean these data is no use for damage assessment, but do have some limitation in the accuracy of component measurement. Even for the NJ CLICK airborne data sets, there are only around 4 points per square meter horizontally, which means, any objects within 30 cm might be ignored.

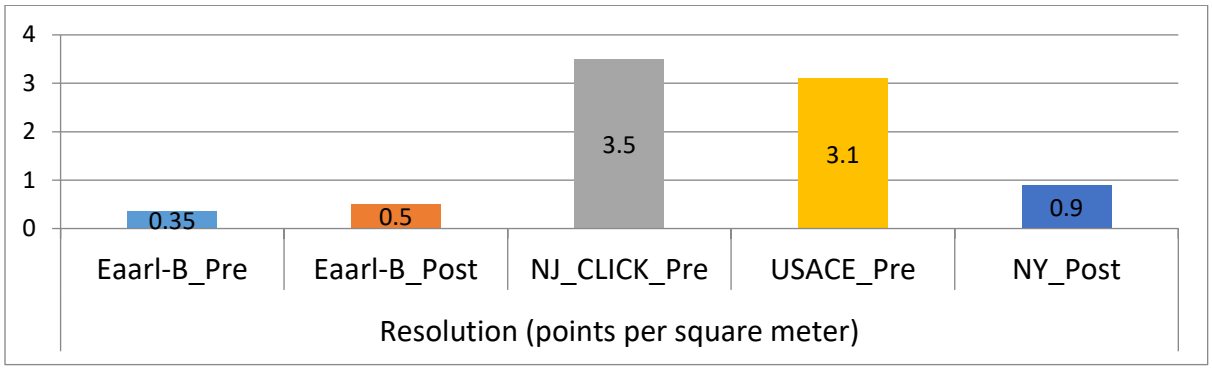

Figure 1 Resolution of different airborne LiDAR data sets

This limitation can be implemented by the mobile LIDAR data sets. Typically, the horizontal resolution of the mobile system can reach an average of 1750 points per square meter compared to a maximum of 3.5 points per square meter for the airborne LiDAR system. The surface resolution of mobile LIDAR can be even higher with 6300 points per square meter. This high resolution makes it possible for the capture of very tiny objects, which is curtail important for the detail assessment.

Results of the data resolution:

Table 5 Summary of solution of airborne and mobile LiDAR data sets

	Horizontal	Surface Resolution
Airborne	0.35 - 5 points/m2	N.A
Rutgers Mobile	1750 points/m2	6300 points/m2

Data Accuracy

Reference is required to evaluate the precision and accuracy of the mobile LiDAR data. A true reference requires an accuracy at least one magnitude higher that the data to be assessed. High accuracy checkpoint is beyond the resource of current study. Instead, different published airborne LiDAR datasets are utilized as baseline to compare the performance of the LiDAR data collected by Rutgers mobile LiDAR systems.

The comparison is conducted in various environment conditions including urban environment (New Brunswick downtown), shoreline residential communities (Normandy Beach and Ortley Beach) and important infrastructures (Rockaway Bridge), which are representative for the dense population area. Due to the limitation of the coverage of mobile LiDAR data collected, the comparison analysis does not extend to mountains and other low population density areas.

Three possible resources for the errors (Hodgson and Bresnahan (2004)) including elevation error, horizontal error form the sensor measurements and the error in the labeling process from different returns. This analysis will focus on the elevation error of the data set of the pre airborne LIDAR to the post mobile LIDAR.

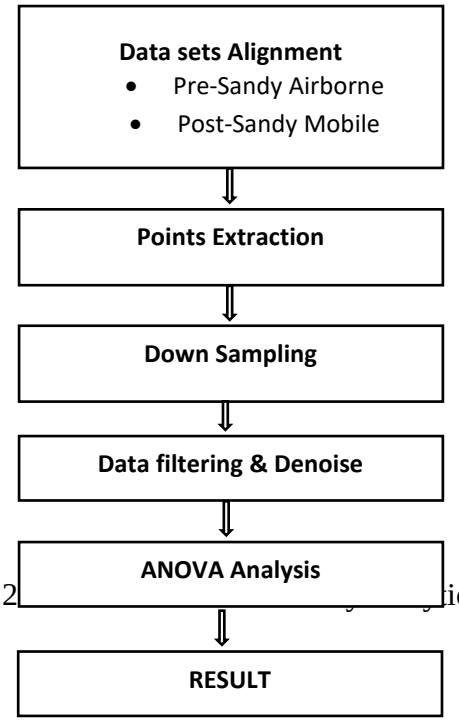

Figure 2 ics

Data filtering and Denoise

In order to conduct the analysis of variance (ANOVA), significant noise is removed. This noise includes: a) Missing data gap of the airborne data sets due to the low resolution; b) Sudden elevation jump due to the unexpected objects above road (e.g. rock, vegetation).

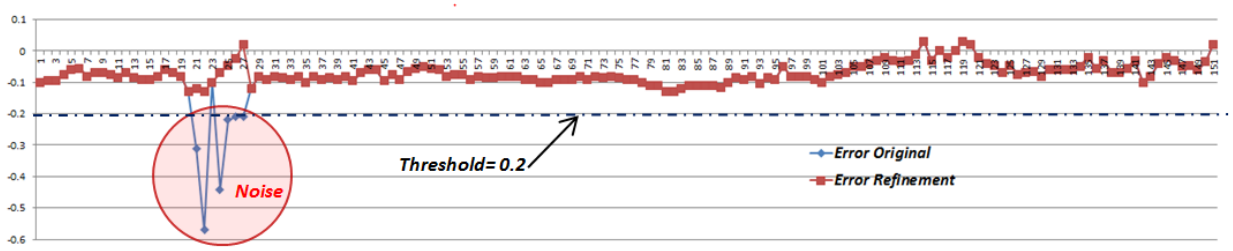

Figure 3 Comparison of airborne and mobile LiDAR in Normandy Beach (w/o denoise)

These noises are addressed to by the slope continuity of the road profile. A conservative threshold of 0.2 meters is selected to remove the noise in the comparison. The accuracy of airborne system is around 0.1 meter and the accuracy of the mobile LiDAR system is around 0.05 meter. Thus any difference greater than the combination of the maximum error of both systems (0.15 meter) are defined as noise.

Table 6 Summary of accuracy analytical results in different environments

Environment	Locations	Airborne Data	Mean (m)	Standard Deviation (m)
Urban& Residential	New Brunswick Downtown	USGS NJ	-0.073	0.051
Urban& Schools	Rutgers Busch Campus	USGS NJ	-0.123	0.021
Shoreline & Residential	Normandy Beach	USGS NJ	-0.069	0.037
Shoreline & Residential	Ortley Beach	USGS NJ	-0.103	0.020
Urban & Infrastructure	Rockaway Bridge	USGS NY	0.023	0.044

Spatial Completeness

The completeness of the LIDAR is another critical issue for the assessments based on LIDAR. With its nature limitation of airplane as a LIDAR system carrier, airborne LIDAR system inherently perfect at capture at capture top view projection of communities, but disable in obtaining vertical information. Thus the application for airborne LIDAR focus on feature outline extraction, digital elevation map (DEM), change detection.

Mobile LIDAR implemented airborne LIDAR not only in the way of higher resolution but most importantly envision the vertical information. However, compared to airplane, the mobile LIDAR system carrier, the mobile vehicles are dramatically impacted by the trajectory and obstructive objects in the middle of the lesser emitted. In the post-disaster situations, especially for hurricane damage which combines wind damage with flood damage, the access to the severe damage area could be blocked by the collaborate damage caused by the disasters. To specify, the sand brought from the eroded sand dune and the debris of the collapsed houses brought by both flood and wind stop the mobile vehicles from assessing. Besides, time emergency and the limitation of accessibility of mobile vehicle itself make it impossible to conduct a 360-degree scan of the all damaged houses.

Another influence is the scan angel. Theoretically, in optics, Lambert's cosine law says that the radiant intensity or luminous intensity observed from an ideal diffusely reflecting surface or ideal diffuse radiator is directly proportional to the cosine of the angle θ between the observer's line of sight and the surface normal. Ideally, when the angle between the scanner and the wall is less than certain threshold θ, the diffusely reflecting laser lights are not strong enough to bounce back to the scanner resulting in losing of the data.

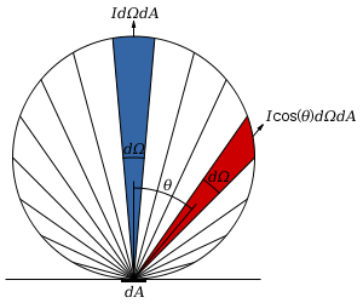

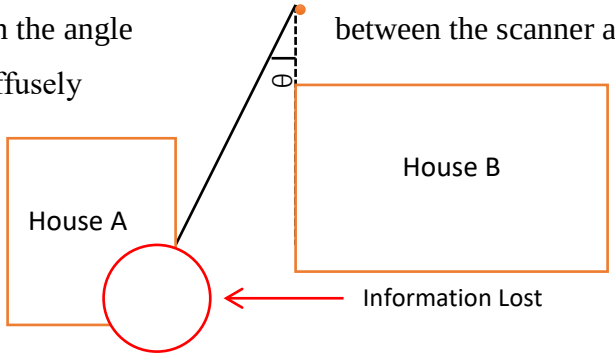

Figure 4a Lambert's Lar for diffusely reflection; 4b Information missing in the practical survey

Practically, our mobile survey data collected from the Ortley Beach after hurricane Sandy provides us a unique way to validate what exactly percentage of data can be captured in the real survey environment.

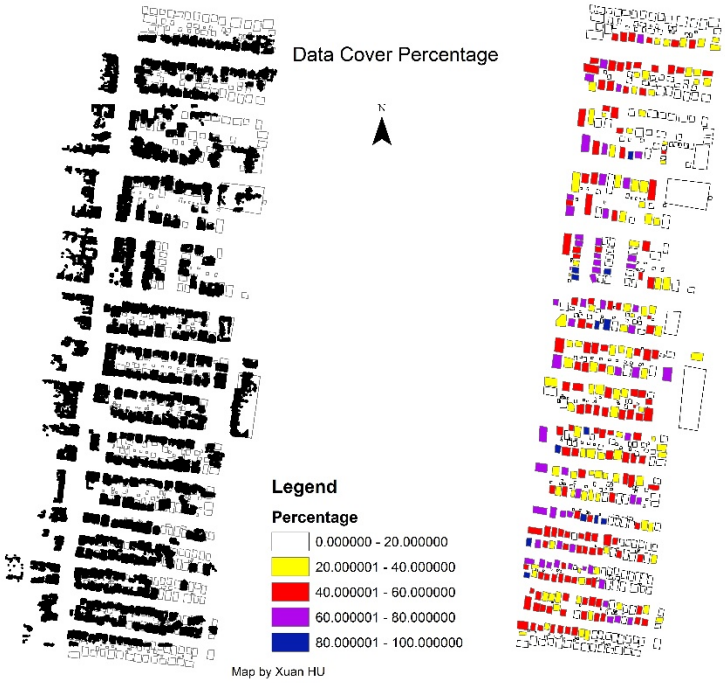

Figure 5 Horizontal data coverage for mobile LiDAR

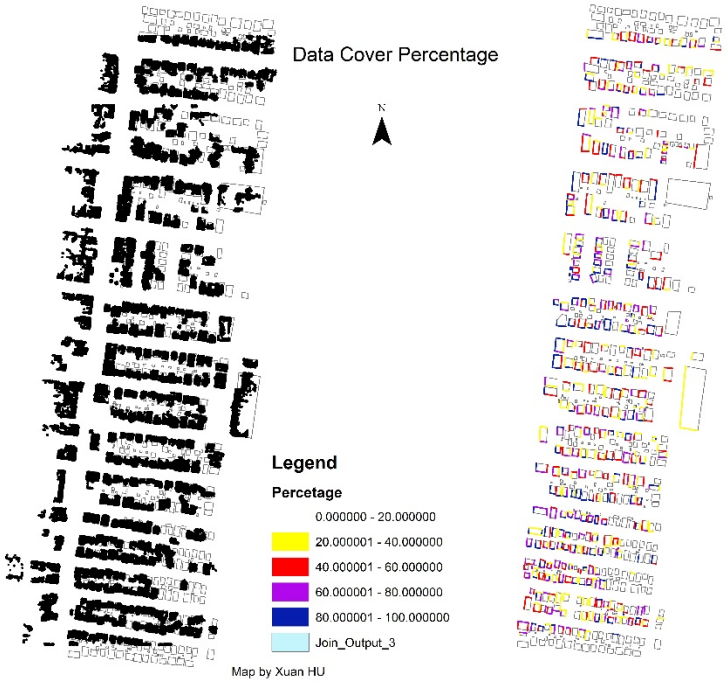

Figure 6 Wall coverage for mobile LiDAR

Conclusion of coverage analysis

A coverage analysis of all houses in Ortley Beach is conducted in this study. An average of 43.57% of the building is captured by mobile LiDAR systems with a standard deviation of 19.67%.

Table 7. Accuracy Analysis

	Horizontal Coverage		Vertical Coverage	
	MEAN	STD	MEAN	STD
Airborne	~100%	N.A	~0%	N.A
Rutgers Mobile	43.57%	19.67%	47.44%	29.26%

With the limitation of the scan angle and accessibility, mobile LiDAR system is not 100% coverage all the scan area and there is no way to fill in the missing information especially when mobile LiDAR data serve as a historic documentation. Thus the future UAV LiDAR system should be significantly necessary for the 360-degree information collection and documentation.

Results and Discussion

This paper presents a systematic study of performance of the current collected LIDAR data sets and addresses to four frequently ask questions: How can this gigabyte data be storage for future computation? What is the resolution of the LIDAR data? How accurate can the LIDAR be? What part of communities is missing when using LIDAR?

The multi-scale grid data management method provides an innovated approach for data storage and future analysis. This approach will inevitably speed up the processing speed of the massive data sets, which enable rapid response for urgent tasks in such disastrous scenario. Quantitative analysis of the resolution and completeness give a detail description of to what extent can be objects be represented by different LIDAR and what part of information is missing. From ANOVA analysis, our result shows that the post hurricane mobile LIDAR aligned correspondingly to the pre hurricane airborne data sets published by government agencies. However, one of the drawbacks of this paper is failing to validate the accuracy of the mobile LIDAR data with a higher accuracy reference points. Future work will likely be focused on optimization of the grid size for the data management system. And the datasets from the new grid system are extracted for the damage assessment. It would be instructive to apply the LIDAR data to rapid computation and response for such hazard event.

Reference

Awrangjeb, Mohammad, Mehdi Ravanbakhsh, and Clive S. Fraser. "Automatic detection of residential buildings using LIDAR data and multispectral imagery."*ISPRS Journal of Photogrammetry and Remote Sensing* 65.5 (2010): 457-467.

Barber, David, Jon Mills, and Sarah Smith-Voysey. "Geometric validation of a ground-based mobile laser scanning system." *ISPRS Journal of Photogrammetry and Remote Sensing* 63.1 (2008): 128-141.

Bowen, Zachary H., and Robert G. Waltermire. "Evaluation Of Light Detection And Ranging (LIDAR) For Measuring River Corridor Topography1." (2002): 33-41.

Bremer, Magnus, and Oliver Sass. "Combining airborne and terrestrial laser scanning for quantifying erosion and deposition by a debris flow event."*Geomorphology* 138.1 (2012): 49-60.

Bretar, Frédéric, Marc Pierrot-Deseilligny, and Michel Roux. "Solving the strip adjustment problem of 3D airborne lidar data." *Geoscience and Remote Sensing Symposium, 2004. IGARSS'04. Proceedings. 2004 IEEE International*. Vol. 7. IEEE, 2004.

Crombaghs, M., R. Brügelmann, and E. J. De Min. "On the adjustment of overlapping strips of laseraltimeter height data." *International Archives of Photogrammetry and Remote Sensing* 33.B3/1 (2000): 230-237.

Dix, Michael, et al. "Accuracy Evaluation of Terrestrial LIDAR and Multibeam Sonar Systems Mounted on a Survey Vessel." *Journal of Surveying Engineering* 138.4 (2011): 203-213.

El-Halawany, Sherif Ibrahim, and Derek D. Lichti. "Detection of road poles from mobile terrestrial laser scanner point cloud." *Multi-Platform/Multi-Sensor Remote Sensing and Mapping (M2RSM), 2011 International Workshop on*. IEEE, 2011.

Ellum, Cameron, and Nasser El-Sheimy. "Land-based mobile mapping systems." *Photogrametric Engineering & Remote Sensing* 68.1 (2002): 13-28.

Fewtrell, T. J., et al. "Evaluating the effect of scale in flood inundation modelling in urban environments." *Hydrological Processes* 22.26 (2008): 5107-5118.

Fewtrell, Timothy J., et al. "Benchmarking urban flood models of varying complexity and scale using high resolution terrestrial LiDAR data." *Physics and Chemistry of the Earth, Parts A/B/C* 36.7 (2011): 281-291.

Filin, Sagi. "Recovery of systematic biases in laser altimetry data using natural surfaces." *Photogrammetric Engineering & Remote Sensing* 69.11 (2003): 1235-1242.

Filin, Sagi. *Calibration of airborne and spaceborne laser altimeters using natural surfaces*. Diss. The Ohio State University, 2001.

Fowler, A., and V. Kadatskiy. "Accuracy and error assessment of terrestrial, mobile and airborne lidar." *Proceedings of American Society of Photogrammetry and Remote Sensing Conference (ASPRP 2011), 1–5 May 2011, Milwaukee, Wisconsin*. 2011.

Gong, J., et al. "Mobile terrestrial laser scanning for highway inventory data collection." *Proceedings of International Conference on Computing in Civil Engineering, Clearwater Beach, FL, USA*. 2012.

Gong, Jie. "Mobile LiDAR Data Collection and Analysis for Post-Sandy Disaster Recovery." *2013 International Workshop of Computing in Civil Engineering, Los Angeles, CA*. 2013.

Goulden, Tristan, and Chris Hopkinson. "The forward propagation of integrated system component errors within airborne lidar data." *Photogrammetric Engineering & Remote Sensing* 76.5 (2010): 589-601.
Haala, N., et al. "Mobile lidar mapping for urban data capture." *Proceedings of the 14th International Conference on Virtual Systems and Multimedia, Limassol, Cyprus*. 2008.
Hilker, Thomas, et al. "Comparing canopy metrics derived from terrestrial and airborne laser scanning in a Douglas-fir dominated forest stand." *Trees* 24.5 (2010): 819-832.
Holopainen, Markus, et al. "Tree mapping using airborne, terrestrial and mobile laser scanning–A case study in a heterogeneous urban forest." *Urban Forestry & Urban Greening* 12.4 (2013): 546-553.
Hopkinson, Chris, et al. "Integrating terrestrial and airborne lidar to calibrate a 3D canopy model of effective leaf area index." *Remote Sensing of Environment*136 (2013): 301-314.
Hopkinson, Chris, et al. "Vegetation class dependent errors in lidar ground elevation and canopy height estimates in a boreal wetland environment."*Canadian Journal of Remote Sensing* 31.2 (2005): 191-206.
Hyyppä, J. U. H. A., et al. "Unconventional LIDAR mapping from air, terrestrial and mobile." *Proceedings of the Photogrammetric Week*. 2013.
Jaakkola, Anttoni, Juha Hyyppa, and Eetu Puttonen. "Measurement of Snow Depth Using a Low-Cost Mobile Laser Scanner." (2014): 1-5.
Jochem, Andreas, et al. "Area-wide roof plane segmentation in airborne LiDAR point clouds." *Computers, Environment and Urban Systems* 36.1 (2012): 54-64.
Kilian, Johannes, Norbert Haala, and Markus Englich. "Capture and evaluation of airborne laser scanner data." *International Archives of Photogrammetry and Remote Sensing* 31 (1996): 383-388.
Krabill, W. B., et al. "Accuracy of airborne laser altimetry over the Greenland ice sheet." *International Journal of Remote Sensing* 16.7 (1995): 1211-1222.
Kraus, Karl, and Norbert Pfeifer. "Determination of terrain models in wooded areas with airborne laser scanner data." *ISPRS Journal of Photogrammetry and remote Sensing* 53.4 (1998): 193-203.
Latypov, Damir. "Effects of laser beam alignment tolerance on lidar accuracy."*ISPRS journal of photogrammetry and remote sensing* 59.6 (2005): 361-368.

Latypov, Damir. "Estimating relative lidar accuracy information from overlapping flight lines." *ISPRS Journal of Photogrammetry and Remote Sensing* 56.4 (2002): 236-245.
Li, Rongxing. "Mobile mapping: An emerging technology for spatial data acquisition." *Photogrammetric Engineering and Remote Sensing* 63.9 (1997): 1085-1092.
Lin, Yi, Juha Hyyppä, and Anttoni Jaakkola. "Combining mobile and static terrestrial laser scanners to investigate individual crown attributes during foliation." *Canadian Journal of Remote Sensing* 37.4 (2012): 359-375.
Lindberg, Eva, et al. "Estimation of stem attributes using a combination of terrestrial and airborne laser scanning." *European Journal of Forest Research*131.6 (2012): 1917-1931.
Maas, Hans-Gerd. "Least-Squares Matching with airborne laserscanning data in a TIN structure." *International Archives of Photogrammetry and Remote Sensing* 33.B3/1; PART 3 (2000): 548-555.
May¹, Nora Csanyi, and Charles K. Toth. "Point positioning accuracy of airborne LiDAR systems: A rigorous analysis." (2007).
Meng, Xuelian, Nate Currit, and Kaiguang Zhao. "Ground filtering algorithms for airborne LiDAR data: A review of critical issues." *Remote Sensing* 2.3 (2010): 833-860.
Olsen, Michael J., et al. "Damage assessment of the 2010 Chile earthquake and tsunami using terrestrial laser scanning." *Earthquake Spectra* 28.S1 (2012): S179-S197.
Olsen, Michael J., et al. "Terrestrial laser scanning-based structural damage assessment." *Journal of Computing in Civil Engineering* 24.3 (2009): 264-272.
Pfeifer, Norbert, S. Oude Elberink, and Sagi Filin. "Automatic tie elements detection for laser scanner strip adjustment." *International Archives of Photogrammetry and Remote Sensing* 36.3/W3 (2005): 1682-1750.
Reutebuch, Stephen E., et al. "Accuracy of a high-resolution lidar terrain model under a conifer forest canopy." *Canadian Journal of Remote Sensing* 29.5 (2003): 527-535.
Schenk, T. "Modeling and analyzing systematic errors in airborne laser scanners." *Technical Notes in Photogrammetry* 19 (2001): 46.
Sofia, G., et al. "An objective approach for feature extraction: distribution analysis and statistical descriptors for scale choice and channel network identification." *Hydrology and Earth System Sciences* 15.5 (2011): 1387-1402.

Starek, Michael J., et al. "Modeling and analysis of landscape evolution using airborne, terrestrial, and laboratory laser scanning." *Geosphere* 7.6 (2011): 1340-1356.
Töyrä, Jessika, et al. "Assessment of airborne scanning laser altimetry (lidar) in a deltaic wetland environment." *Canadian Journal of Remote Sensing* 29.6 (2003): 718-728.
Vaughn, C. R., et al. "Georeferencing of airborne laser altimeter measurements." *International Journal of Remote Sensing* 17.11 (1996): 2185-2200.
Vosselman, George. "On the estimation of planimetric offsets in laser altimetry data." *International Archives of Photogrammetry Remote Sensing and Spatial Information Sciences* 34.3/A (2002): 375-380.

Fusion of Geo-Tagged Post-Storm Damage Photos with Mobile LiDAR Data for Storm Surge Height Measurement

Jie Gong[1], Mengyang Guo[1], Zixiang Zhou[1], Ning Lin[2], and Andrew Kennedy[3]

[1]The State University of New Jersey, Department of Civil & Environmental Engineering, Piscataway, NJ, USA

[2]Princeton University, Department of Civil & Environmental Engineering, NJ, USA

[3]University of Notre Dame, Department of Civil & Environmental Engineering & Earth Science, IN, USA

ABSTRACT

Storm surge generated by tropical storms is a severe threat to coastal communities. During a hurricane event, it is essential to collect data on storm surge height as it helps researchers understand the process that triggered the event, provides insights about localized flooding patterns, and forms the bases for forecasting future vulnerabilities. Tide stations, high water marks, and pressure sensors are commonly used methods for observing and measuring storm surge. Among these methods, high water marks is the best method for measuring the highest storm surge for an event, but it relies on trained survey crews to measure high water marks with GPS equipment. In this research, we proposed a new method for precise and rapid measurement of high water marks by fusing geo-tagged post-storm damage photos with mobile LiDAR data. As our data collection capability quickly expands with the proliferation of mobile devices and the rapid rise of mobile LiDAR mapping technologies, we are poised to tap into the potential of internet-scale storm surge height measurement with our proposed storm surge measurement method. Specifically, this paper describes the development of such a new method, and the validation of the proposed method using several spatial and imagery data sets collected during Hurricane Sandy. Challenges encountered during the research are discussed to highlight future research needs.

INTRODUCTION

Storm surge height is one of the critical hazard parameters to be collected during post-hurricane data assessment. Storm tide, defined by the National Oceanic and Atmospheric Administration (NOAA), is the water level rise due to the combination of storm surge, the

abnormal rise of water level due to the storm, and the astronomical tide, the normal rise and fall of the water due to the gravitational pull of moon and sun. In reality, storm surge or even storm tide only make up a part of what causes water level to rise along the coast during a hurricane.

In the United States, storm surge height information is generally provided by USGS and FEMA though water-level sensors, tide stations and field teams. In some cases, though, this information is not very precise due to the limited number of data. For example, the water-level and wave-height sensors were used for storm height characterization during the Hurricane Sandy by USGS. However, the number of these sensors is limited. For example, only 23 sensors were used in New Jersey and 58 in New York to monitor Hurricane Sandy storm tide. This contrasts sharply with the rest of the storm damage data which are often complied for individual housing properties. The lack of detailed and fine-scale storm surge height information could lead to the difficulty in developing accurate storm surge damage models as there is an apparent mismatch between the resolutions of storms surge data and building damage data. Wave and surge models have been shown to result in increasing errors as they move overland arising from two major factors: (A) Increased dissipation overland is not fully accounted for in standard models, particularly for water waves; and (B) Overland wind stress will be partially absorbed by canopy elements like trees and houses and will not entirely reach the water surface, with strong implications for surge and waves (Kennedy et al., 2011). Therefore, knowledge of storm surge heights, in particular at locations further away from the shoreline, is valuable information for calibrating storm surge models.

Field teams are a good source of storm surge height information as one of their tasks is to find high water marks. High water marks, formed by dirt and debris in the water that deposited on wall surfaces, can provide the best estimate of the storm surge level. Generally, the still water level was found in a room that was not breached by wave action. The high water mark is often caused by the conjunction of storm surge, tides, wave, and freshwater input. Traditionally, high water mark is the best method for capturing the highest surge from a storm, though it relies on trained survey crews and can be subjective.

In this paper, we introduce a new data fusion method that fuses disaster photos from a variety of sources (field teams, volunteers, and Internet) with mobile lidar data for accurately obtaining high water mark information without performing field measurement. Because of the pervasive use of mobile devices, disaster photos are now often widely shared and available on the Internet. Many of these photos provide first-hand information on the extent of disaster, some of

them way before the arrival of field teams. The new method will promote a crowd source-based approach for collecting critical hurricane impact parameters. The approach will greatly reduce field data collection time and improve the safety of field teams as it eliminates the need of performing measurement on damaged structures, some of them may be too dangerous to approach. Also since the high water mark data is calculated and estimated though a well built and scientific process, the error caused by personal bias could be diminished.

RESEARCH BACKGROUND

Post-disaster field data collection is a documentation procedure that provides perishable damage data for damage assessment. A variety of methods can be used for this purpose. These methods include, but are not limited to, paper and pen (Chiu & wadia- Fascetti 1999), Electronic (Crandell & Kochkin 2005), Photo/Video log (Curtis & Mills 2012), VGI (Volunteered Geographic Information) (ASCE Indonesia Study 2014), Aerial/Satellite imagery (Adams et al. 2004, Yamazaki et al. 2005, Klemas 2009), static terrestrial lidar (Olsen and Kayen 2013; Chock et al. 2013, Gupta et al., 2012), airborne lidar (Ferrucci et al. 2007), and mobile lidar (Gong and Maher 2014). Most of these approaches rely on data remotely sensed from air- or ground-based platforms. Recently, with the ubiquitous use of mobile devices, an increasing number of images have been shared through the internet. Such VGI information makes it possible for researchers to assess damage data remotely or provide crowdsourced damage data to the public. For example, the Philippines Hurricane Yolanda Structural Analysis team (PHYSA 2014)) created a new open-forum project model for post-disaster inspection. In the project, the investigators not only shared their week-long, post-disaster damage assessment of the impacted regions, but also invited other team input data on Philippines Hurricane post-disaster investigation. This provides a way to all ASCE members to participate in the Indonesia Study simultaneously and remotely, which can accelerate the speed of Philippines Hurricane damage evaluation and analysis. One of the usages of this kind of data is to measure storm surge height. This is accomplished through a comparison between the height of tree bark removal and the height of people in some of the photographs (Needham 2013). Albeit this is a simple and feasible method, the outcome is likely only accurate to certain degree as it involves a subjective estimation process.

The rising of Internet/crowdsourced damage data and the increasing availability of high resolution and high accuracy 3D disaster data, such as terrestrial scan and mobile lidar data,

provides a unique opportunity to rethink how damage assessment and field data collection can be done with these new methods. One of the intriguing applications is to remotely measure high water marks and recover accurate and finer scale storm surge height information in the impacted communities. During mobile lidar data collection, street-view photos are often collected, geo-referenced, and projected onto point cloud data for point cloud colorization. The lidar data provides detailed 3D information of the buildings, from which we can easily measure the dimension of the buildings in various aspects. However, since the lidar point clouds have very coarse color information, often from the street view imagery, this leads to the difficulty to tell the surge line from the mobile lidar data only. This is mainly because the lidar scans and photos are taken from a mobile vehicle driving on the road and positioned at a relatively large distance from the damaged housing properties. On the other hand, images taken by damage survey teams and property owners tend to narrowly focus on certain damage features and often have higher resolution. However, it is difficult to recover 3D information from these photos, especially geo-referenced 3D information. The advantages and disadvantages of these two sources limit the employment of them individually. But a combination of two overcomes the disadvantages.

In this paper, we introduce a method that leverages both types of data and exacts each other's strength to accomplish the task of storm surge height estimation. More specifically, we formulated a computational approach that fuses geo-tagged post-storm damage photos with mobile LiDAR data to extract high water mark information in a common geospatial coordinate system. We explored the use of local image feature-based 3D alignment and user assisted 3D alignment to support storm surge height calculation. The lesson learned in this storm surge height data processing will provide the foundation for future improvement of this technology to better support post-disaster recovery process.

PROPOSED STORM SURGE HEIGHT ESTIMATION METHOD

The technical rationale behind our proposed approach is local feature-based image matching and 3D alignment of point clouds with photos from heterogeneous sources, such as disaster assessment teams, social media, and etc.. We assume the photos taken from sources other than the mobile lidar system itself are geo-tagged as the pervasive use of GPS capable mobile devices. Figure 1 outlines the detailed workflow in our proposed approach. The major components are GPS based screening, image matching, and VGI and lidar data fusion. To develop and validate

all the methods involved in this workflow model, we used several data sets acquired during Hurricane Sandy. In the following, we give an overview of the data sets, explain each of the components in our proposed approach, and discuss the results of our proposed approach.

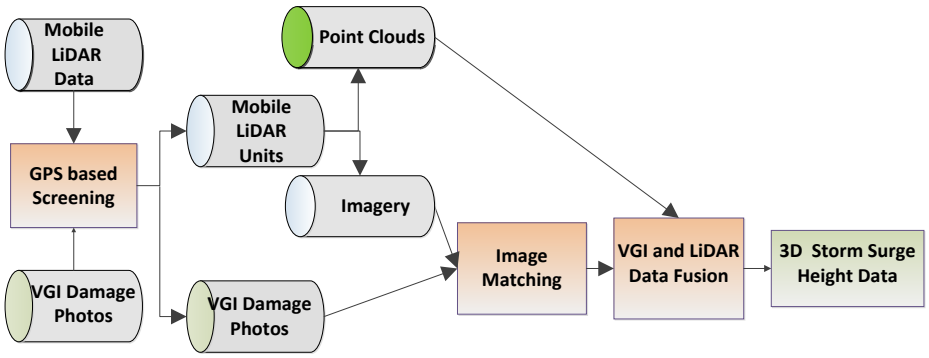

Figure 1. Proposed Surge Height Estimation Approach

The data sets used in this research include a post-Sandy mobile lidar data set collected by Rutgers University and a damage photo data set collected by several other post-disaster damage assessment teams. Mobile lidar offers an opportunity to scan residential buildings at ground level and simultaneously capture street-view imagery. The system used for mobile lidar data collection is an Optech LYNX Mobile Mapper M1 system. The LYNX system relies on two 500 kHz LiDAR sensors to collect a million points per second while maintaining survey grade quality precision. Without ground control points but with a mobile base station, the Optech system is capable of obtaining LiDAR data sufficient for feature extraction of planimetric and topographic features typically at an absolute accuracy of +/-10cm @ 1 σ in good GPS coverage areas and an relative accuracies of +/- 5cm @ 1 σ anywhere within the project area.

In the aftermath of Hurricane Sandy, several academic research teams also entered into the disaster impacted area to collect perishable storm damage data with the tradition field survey methods. As a part of their trips, they often took geo-tagged post-storm damage photos. In this research, we used a set of geo-referenced photos from a joint Princeton University and University of Notre Dame damage assessment team. Hereby, we refer this set of photos as VGI photos. The team surveyed the severed damaged communities along the New Jersey coastline during their week-long damage assessment activity.

Mobile lidar data usually consists of geo-referenced point clouds and street-view imagery. The point cloud data can be projected onto the imagery data by treating the laser scanners and high-definition cameras as classical stereo-pairs. The mobile lidar imagery are often taken at larger

distance from damaged structures when compared to the VGI photos taken by foot-on-ground damage assessment teams. Therefore, it is often difficult to identify high water marks directly from mobile lidar imagery. For example, Figure 2 shows that high water marks can be clearly identified in VGI photos while it is not the case with the mobile lidar imagery.

(a) (b)

Figure 2. (a) Mobile lidar imagery; (b) A photo taken by the field survey team

GPS-based Screening

Running local feature-based image matching between the entire set of mobile lidar imagery and survey photos is prohibitively expensive, even if it is only for individual communities. Considering both mobile lidar imagery and survey photos have embedded GPS information, albeit at different positional accuracies, one logic step is to group them into subsets - a step we referred to as GPS-based screening. Another motivation behind the screening is that it is well-known that building structures often have similar local features that tend to confuse the local feature based image matching methods. By dividing the photo sets into smaller subsets, this source of confusion can be greatly reduced.

The mobile lidar imagery in this research is organized according to the vehicle trajectories. Thus, the trajectory information was used as one source of information to pair with field survey photos. The detailed steps for GPS screening are shown in Figure 3. An essential step in this approach is projecting the GPS traces of VGI and mobile lidar photos onto one map frame which has grid sizes spanning 0.002 latitude and 0.001 longitude. The subsequent photo matching will be only carried out within each grid. In this way, computational effort and complexity can be greatly reduced.

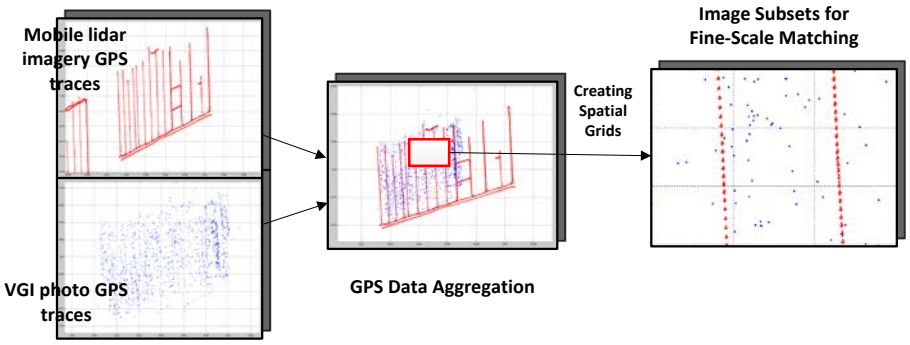

Figure 3. GPS-based Screening of Images from Different Sources

Image Matching

This step involves registration or alignment of VGI photos with mobile lidar imagery. The mobile lidar imagery has known projection properties to lidar point clouds. Therefore, once the relationship between mobile lidar imagery and VGI photos can be derived, 3D information of water marks in a common chosen coordinate system can be calculated. However, manually finding the paired mobile lidar imagery for each VGI photo is not an easy work. To automatically detect images which captured damages of the same structures, a SIFT (Scale-invariant feature transform) based method for automated image matching was employed (Figure 4). This method is capable of finding images which display similar scenes based on local image features. Figure 4 shows some example matching of damage images from two different data sets used in this research. It can be seen that the method is robust to view angle and illumination variances.

Figure 4. SIFT-based Matching between VGI photos and Mobile Lidar Imagery

VGI and Lidar Data Fusion

This step involves 3D alignment of VGI images with mobile lidar imagery. Once pairs of mobile lidar imagery and VGI images are identified, it is straightforward to relate VGI photos to point cloud data since there is known correspondence between mobile lidar imagery and lidar point clouds. Once this is accomplished, there are three steps involved in recovering the coordinates of high water marks.

The first step is to compute the Projection Matrix $\boldsymbol{P}$ between each point in a lidar point cloud $\boldsymbol{Pw}$ and each pixel in a VGI image $\boldsymbol{Pc}$. Currently, this projection is solved with the assistance of manual inputs of several correspondences between VGI image pixels and lidar point clouds. We used the camera calibration with 3D objects method developed by Zhang (2004). More specifically, the feature points of the building in both lidar point cloud and images are manually detected in exactly the same order as shown in Figure 5, and are saved *Pc* and *Pw*. The 2D pixel is denoted by $P_c = [x, y]^T$, and 3D point is denoted by $P_w = [X, Y, Z]^T$. Write the point coordinate as homogeneous coordinate format as $P_c = [x, y, 1]^T$ and $P_w = [X, Y, Z, 1]^T$. The relationship between *Pw* and *Pc* could be expressed as

$$sP_s = \boldsymbol{A}[\boldsymbol{R}\ \boldsymbol{t}]P_w \qquad (1)$$

where

$$\boldsymbol{A} = \begin{bmatrix} \alpha & \gamma & u_0 \\ 0 & \beta & v_0 \\ 0 & 0 & 1 \end{bmatrix}$$

is the intrinsic matrix and $\boldsymbol{P} = \boldsymbol{A}[\boldsymbol{R}\ \boldsymbol{t}]$ is the projection Matrix. Based on (1), the correspondence between P_w and P_c could be written as:

$$\begin{bmatrix} X_i & Y_i & Z_i & 1 & 0 & 0 & 0 & 0 & x_iX_i & x_iY_i & x_iZ_i & x_i \\ 0 & 0 & 0 & 0 & X_i & Y_i & Z_i & 1 & y_iX_i & y_iY_i & y_iZ_i & y_i \end{bmatrix} \boldsymbol{P} = \boldsymbol{0}$$

where

$$\boldsymbol{P} = [p_{11}, p_{12}, \dots, p_{34}]^{\boldsymbol{T}}$$

For the *n* selected feature points, stack all equations as:

$$\boldsymbol{GP} = \boldsymbol{0}$$

$$\boldsymbol{G} = [\boldsymbol{G}_1^T, \dots, \boldsymbol{G}_n^T]^T$$

The Projection Matrix $\boldsymbol{P}$ is the eigenvector of $\boldsymbol{G}^T\boldsymbol{G}$ associated with the smallest eigenvalue.

The next step is to obtain the correspondence between LiDAR Point Cloud and Image. Since the Projection Matrix is a 3 by 4 matrix, which is non-invertible, the image cannot be projected onto the LiDAR directly. Instead, the LiDAR Point Cloud is projected onto the image

using the computed Projection Matrix $\boldsymbol{P}$. For each point of the LiDAR Point Cloud Pw_i, we find out where it is projected in the image Pc_j and construct the correspondence between i to j. The correspondence is illustrated in Figure 6.

The last step is to assign each point Pw_i a RGB value from the image Pc_j. The lidar point clouds then have information on which points are projected onto the high water marks shown in the VGI images. These water marks can be directly measured in the lidar point clouds (Figure 7).

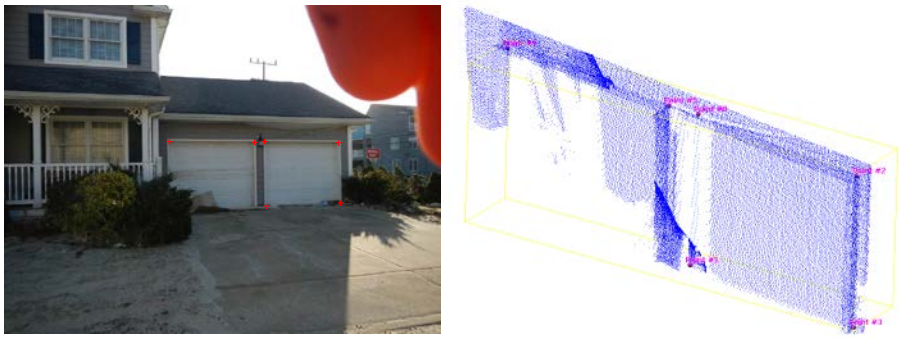

Figure 5. Establishing Correspondence Between Point Clouds and VIG Images

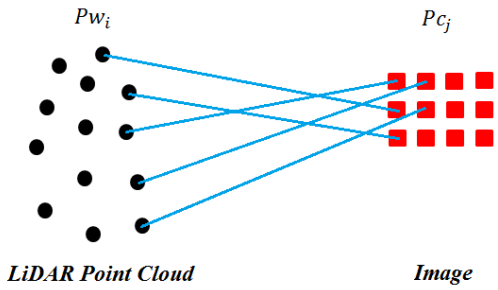

Figure 6. The correspondence between Lidar Point Clouds and VGI Images

Figure 7. High Water Mark Measurement from VGI Images and Point Cloud Data

RESULTS

The proposed method was applied on the Hurricane Sandy mobile lidar and Princeton-Notre Dame data sets. The focused community of interest is Ortley Beach,New Jersey. The analyses showed that thirteen VGI images that have high water mark information can be matched to mobile lidar data. The matching results and recovered high water mark information are shown in Table 1. The locations of these water marks are plotted in Figure 8. Knowing the elevation of these high water marks contributes to better understanding of the extent and distribution of storm surge in this particular community.

Table 1. Estimated High Water Mark Elevations

Building ID	Name	x(longitude)	y(latitude)	Storm Surge Height(m)
A55	DSCN0241.JPG	39.96	74.07	3.19
A37	DSCN0151.JPG	39.96	74.07	3.21
A310	Camera 3 1350.JPG	39.95	74.07	2.62
A274	Camera 3 1345.JPG	39.95	74.07	2.84
A236	Camera 3 1155.JPG	39.95	74.07	2.84
A227	DSCN0602.JPG	39.95	74.07	2.42
A21	DSCN0048.JPG	39.96	74.07	2.80
A20	DSCN0039.JPG	39.96	74.07	2.43
A196	DSCN0561.JPG	39.95	74.07	2.92
A194	DSCN0549.JPG	39.95	74.07	3.05
A17	DSCN0020.JPG	39.96	74.07	1.96
A165	Camera 3 628.JPG	39.95	74.07	3.22
A159	DSCN0424.JPG	39.95	74.07	2.90

Figure 8. Locations of High Water Marks

CONCLUSIONS

In this paper, we presented a novel method for estimating the elevations of high water marks using images collected from diverse sources. The proposed method eliminated the need of measuring high water marks in the field. Instead, it relies on computer vision techniques to fuse VGI images, which can be crowdsourced data, with high resolution mobile lidar data to recover the geospatial locations of high water marks. Mobile lidar data alone cannot provide adequate details about high water marks. However, when they are fused with close range VGI images, the strengths of both data sources can be harvested. While this research has focused on a limited set of data, it does provide an overall framework for combining heterogeneous geospatial data set for more efficient post-disaster data collection and damage assessment.

REFERENCES

Adams, B. (2005) “Collection of satellite-referenced building damage information in the aftermath of Hurricane Charley” Natural Hazards Center, 2005.

Chiu, G. L. F., & Wadia-Fascetti, S. J. (1999). “Assessment and quantification of hurricane induced damage to houses.” International Journal Wind and Structures, 2(3), 133-150.

Chock, G., Carden, L., Robertson, I., Olsen, M., and Yu, G. (2013). "Tohoku tsunami-induced building failure analysis with implications for US tsunami and seismic design codes." Earthquake Spectra, 29(s1), S99-S126.

Crandell, J. H., & Kochkin, V. (2005). “Scientific damage assessment methodology and practical applications.” Paper presented at the Structures Congress 2005, New York, NY.

Curtis, A., & Mills, J. W. (2012). “Spatial video data collection in a post-disaster landscape: The Tuscaloosa tornado of April 27th 2011.” Applied Geography, 32(2), 393-400. doi: 10.1016/j.apgeog.2011.06.002

Ferruccci, F., Rocca, F., Calabretta, G., and Savio, G. (2007) “3-D Tsunami Coastal Hazard Mapping in Sri Lanka by Very-High Resolution, Airborne and Spaceborne Remote-Sensing “ IEEE Geoscience and Remote Sensing Symposium, 2007.

Gong, J. and Maher, A. (2014) “Mobile LiDAR-based Approaches for Assessing Hurricane Damages and Visualizing Resiliency Rebuilding Needs” Journal of Transportation Research Board, TRB, 2014.

Gupta, R. & Grau, D. (2012). “Building Damage Observations and EF Classifications from the Tuscaloosa, AL, and Joplin, MO, Tornadoes.” Structures Congress 2012, ASCE, Chicago, IL.

Kennedy, A.B., Rogers, S., Sallenger, A., Gravois, U., Zachry, B., Dosa, M., and Zarama, F. (2011). “Building Destruction from Waves and Surge on the Bolivar Peninsula during Hurricane Ike," J. Waterway, Port, Coastal and Ocean Eng.-ASCE, 137(3), 132-141.

Needham, H. (2013) “Researcher Estimates Philippines Storm Surge Height from Denmark” Hurricane Hal’s Storm Surge Blog.

Olsen and Kayen (2013) “Post-earthquake and tsunami 3D laser scanning forensic investigation” ASCE Forensic Engineering.

PHYSA (2014) “ASCE Indonesia Study” URL: http://physa.uncc.edu/

Zhang, Z. (2004) "Camera Calibration", in G. Medioni and S.B. Kang, eds., Emerging Topics in Computer Vision, Chapter 2, pages 4-43, Prentice Hall Professional Technical Reference, 2004.

LiDAR assisted Transportation Routing Decision Making to Improve Critical Asset Accessibility during Major Natural Disasters

Xuan Hu, Ph.D. Candidate, Department of Civil & Environmental Engineering

Rutgers, The State University of New Jersey

96 Frelinghuysen Road

Piscataway, NJ 08854

Phone: 732-668-9780

Cee.shawn@rutgers.edu

Jie Gong, Ph.D., CM-BIM, Department of Civil & Environmental Engineering

Rutgers, The State University of New Jersey

96 Frelinghuysen Road

Piscataway, NJ 08854

Phone: 848-445-2881

jg931@rci.rutgers.edu

Zhixiang Zhou, Ph.D. Candidate, Department of Civil & Environmental Engineering

Rutgers, The State University of New Jersey

96 Frelinghuysen Road

Piscataway, NJ 08854

Phone: 732-853-2747

zx_zhou@hotmail.com

Document Word Count: 5572

No. of Figures: 7

No. of Tables: 5

Total Word Count: 7372

Date: July 30, 2016

ABSTRACT

When a disaster strikes, disaster response operation is very critical to the human lives and assets. Meanwhile, transportation infrastructure system plays a major role in Search and Rescue (SAR) or evacuation effort. Roadblock of debris would hinder the trapped people from being rescued in "Golden 72 hours". Information gathering, data analyze and decision making are three key process for the disaster response. While these three elements are extensively investigated in literatures independently, the study on how to integrated them together as a whole is rare. In the light of this, the compatibility among them remains a big challenge, and naturally limiting overall performance of disaster response especially in time constrained and highly uncertain environment. In addressing to the abovementioned problem, this study proposed a conceptual framework based on the level of complexity (LOD) aiming at clarify the roles of each elements and identify how they can be connected together for rapid processing. This framework defined a 5 LODs data management system and for each level, the data types, task assignments, processing need, data Analytics and decision making need are described. The proposed framework is targeted at providing decision makers a well-organized mapping system that explore the capacity of each LODs and their corresponding needs. This framework is also beneficial for data storage management. Finally, an empirical study based on hurricane sandy is conducted to illustrucute the performance framework.

Keywords: LiDAR, Decision Making, Disaster Response, Disaster Management, Visualization Analysis

INTRODUCTION

With the frequency and intensity of natural hazards on the rise, communities have become increasingly vulnerable. Transportation infrastructure systems are critical elements of communities as they transport people and goods which are blood in the vein of a modern society. To keep communities running during extreme events, it is imperative to make transportation systems more resilience. However, this has been compounded by two challenges: 1) the transportation systems are becoming larger and more complex increasingly complex; and 2) the existing transportation systems are rapidly aging. For example, in New Jersey, the average age of bridges is 55-years old. Collectively, these issues have become critical concerns and created remarkable challenges to the transportation professions [1]. Situational awareness centered on the extent of damages to transportation infrastructure systems is a critical piece of information sought by many stakeholders immediately after an extreme event. This is because after a hazard strikes the failure of transportation infrastructure systems would quickly paralyze a community in many ways. For example, blockage in the transportation network can impede rescue and life supporting resources reaching survivors. In another example, failures of critical transportation facilities can potentially cause secondary hazards.

Given the emergency of disaster scenarios, every second counts. Traditional embed sensor systems or manually site survey method might not adequately address to reliable and timely issues of the data collection in cases of mass destruction. Geospatial remote sensing technique, especially LiDAR, is complementing traditional embed sensor systems or manually site survey by adequately address to reliable and timely issues of the data collection in cases of mass destruction. These techniques are quickly filling the gap between the spatial and timely requirements for information gathering in the disaster response phase. Gigabytes of data are generated every minute. At the meantime, in the field of operation research, the state of art algorithms is purposed to solve the disaster search and rescue problems. However, the deployment of LiDAR in emergency situation is still rare less than 1%, as reported in NCHRP Report 748 [2]. While these three elements are extensively investigated in literatures independently, the study on how to integrated them together as a whole is rare. In the light of this, the compatibility among them remains a big challenge, and naturally limiting overall performance of disaster response especially in time constrained and highly uncertain environment. While researchers had exploit the capacity of the state of art technology such as LiDAR or satellite imagery, how to apply it into specific cases remains rare. As a result, decision makers are often stuck into a dilemma that even the data are tools are rich – the returns are diminishing rapidly, because after a certain point the more information and algorithms exist, the harder it becomes to select a proper tool for the data. Ironically, if without proper extraction method, an excess of information resists analysis and comprehension in much the same way a lack of it does. As a result, as the remote sensing data is flooding the world and there exists a variety of algorithm, the more is calling for a proper framework, one that can extract meaning from the chaos data and feed the algorithm with sufficient information.

The purpose of this study is developing a LOD conceptual framework aiming at improve the efficiency of disaster decision making. First, an introduction is given to identify the need of such a framework. Next, a review of literature is conducted on the exiting data collection method, data

analysis tools and decision making methods. Third, a conceptual framework is introduced based on the LOD. This system explores the capacity of the system by connecting the available remote sensing data to corresponding data analysis tools and decision making method. Then an empirical study of Hurricane sandy using LiDAR is presented to illustrate how the big data collected can be transfer into critical input parameters for the Dijkstra's Shortest path algorithm. Last, a Monte Carlo simulation is then presented to show how this integrated workflow can help to improve the accuracy of the performance of decision making.

LITERATURE REVIEW

Disaster response is a decision making process with a short time window. Different from the traditional decision making, the emergency operations performance would largely depend on the time efficiency. For instance, in Search and Rescue (SAR), survival rate is heavily dependent on the speed of rescue. When rescue time exceeds the golden times of 72 hours, it is as low as 5% [3]. Moreover, a dilatory operation would expose children and adolescents to trauma and results in post-traumatic stress as well as other psychological disorders [4]. In the current practice, disaster response is often consisting of three major process: information gathering, data analytics and decision making.

In order to achieve an effective disaster response, information gathering is a key element in any phase of disaster management. Information gathering requires both baseline information and post-impact information. Baseline information can be quickly obtained based on the history data in normal circumstance. On the other hand, the challenge research question is how to obtain the post-impact information quickly and sensitively [5]. Remote sensing technology provides a good fit in addressing to the abovementioned question. Extensively investigation have been conducted in deploying new techniques in disaster response such as satellite imagery [6][7]; Aerial imagery [8][9], LiDAR [10]. While imagery was a key basemap for positioning other features on cartographic products through visual analysis [8], the further quantitative the disaster scenario remains difficult. LiDAR, it has great potential to precisely identify and quantify morphological change [11]. Based on this, Lu et al [12] developed methods for prompt identification of transportation infrastructure using LiDAR in coastal flooding area. On the other hand, measurements of debris and potholes volume [13] and distribution [14] are also critical in terms of search and rescue operation planning. Bull et al [15] pointed out that LIDAR data have significant advantage in revealing the clast size, thickness and volume of debris, which is a precise and powerful tool for disaster management. This also aligned with another study [16]. Based on the precise volume and location of the derbies, Kwan and Ransberger [10] developed algorithm to improve the speed by helping responder to find the quickest route available instead of re-routing each time they encounter a blockage. Mikes and Fleck [17] applied LIDAR to identify the inaccessible transportation network in post disaster and need to establish pre-plans for routes of ingress to these areas.

Data analysis tools or models are another key component in the disaster response. These tools are studied from different prospective such as logistic models, geography information systems (GIS), and etc. Traditionally, the disaster response logistics is studied in the field of operation

research. Özdamar et al [18] integrated a planning model into a natural disaster logistics Decision Support System. Yi and Kuma [19] solved the logistics problem arising in disaster relief activities using ant colony optimization. Golden and Raghavan [20] discussed the challenges for using Vehicle Routing Problem for disaster relief. GIS is another analysis tool for natural disaster management. Kwan and Lee [21] examine the potential of implementation of GIS-based intelligent emergency response systems. Conventional geospatial response to disasters has professional geospatial provide support to decision-makers on the ground [22]. The recent development of web based system encourage more information from crowdsourcing or Volunteered geographic information (VGI) for disaster response-support [23]. Other tools such as data mining from social media also contributed to the better inform of disaster situation [24].

Decision making is the core component in disaster response. Conventionally, decision making are made based on the experience based judgments or heuristic. Researchers have long been making this gut feeling more rational, scientific and efficiency. One attempt is eliminating the bias of the judgment by accumulation preference from different experts such as average analytic hierarchy process (AHP) [25]. Other researchers proposed methods to patch the incomplete information [26]. Gigerenzer and Gaissmaier [27] explore the core capacities of heuristics decision making from psychology prospective.

Conceptualization of remote sensing data framework for disaster response

Decision making process in disaster response phase is a timely issue. Information gathering, data analyze and decision making are three key elements for the disaster response. Extensive investigations have been conducted in all the three process. However, these study are conducted with the lab environment with in-situ data, abundant time. However, when it comes to disaster, most of the process should be finished in a narrow time window, data arriving too late for the data analyze or analyze result arriving too late for experts would result in the chaos of existing workflow. This chaos in information resist the decision makers from a comprehensive understanding of the real disaster situation. A flood in this data for decision makers would act much the same way as lacking of it.

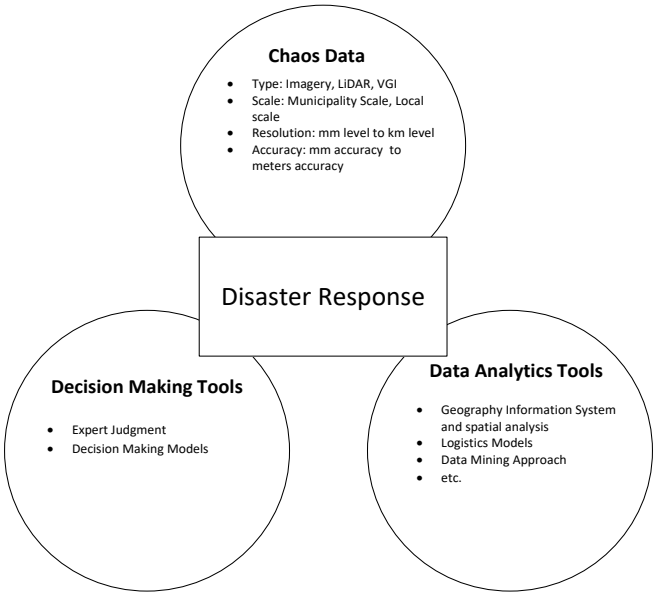

Figure 1 Key Component for Disaster Response

This part, the conceptualized framework for adopting remote sensing data for disaster response is defined as shown in figure 2. This framework aimed at prioritizing the remote sensing information based on the level of detail (LOD). For each LOD, the task assignment, the data management characters, the assignment goals, data processing, data analyze and decision making need are clarified. This framework would help decision makers to envision the capability of different LOD of remote sensing information in terms of disaster response. A five LODs systems is proposed in this conceptualized framework. LOD 0 simply indicates the existing of remote sensing data. The availability of information is the prior step for any further analytics and decision making. After envisioning the availability of the data, LOD 1 provides a global picture about the disaster situation. This picture would help decision makers to set focus and objectives for their further response. For this LOD, the scale is suggested to be segmented into municipality scale with 5km by 5km blocks. In this level of detail of data, coarse scale and relatively low accuracy data are required for the data inputs. This is useful for the experts to have a general recognition of the disaster scenarios based on effort saving methods such as visual analysis. Subsequently, when the focus and objectives are defined, LOD 2 provides information to identify the hard-hit locations and set the search and rescue priorities. Data are suggested to save in 500m by 500 meter blocks. In this level, intermediately (30 to 100 pts/m2) density and medium accuracy (0.05m to 0.20m) are required for the analysis. Rapid computation such as terrain change detection are necessary to incorporate with the visual inspection. For most of the disaster response phase, there is only enough time and computation resource budget for processing data with LOD 0 to LOD 2. However, more advanced computation efforts are necessary for detail assessment of critical infrastructure. This is extremely important in preventing secondary hazard cost by the failure of this critical infrastructures such as unclear power plants or bridges. LOD 3 and LOD 4 are targeted for disaster recovery phase which both time and resource are abundant. LOD 3 looks into details of individual infrastructure with require fine (100 to 1000 pts/m2) density and medium accuracy (0.05m to 0.20m). The purpose

for this level is to extract parameter of details for accessing and analyzing the risk of infrastructures. LOD 4 is a component level scale that utilize extra fine density (> 1000 pts/m2) and high accuracy (<0.05 m) of data to find the micro level of damage details such as cracks. The details of each LOD are summarized in table 1 and table 2.

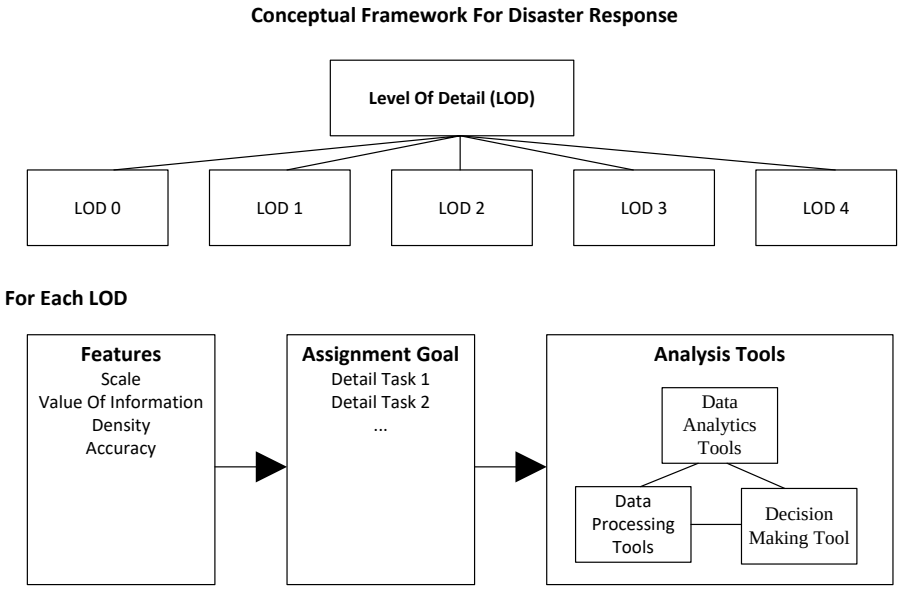

Figure 2 structure of conceptual framework for disaster response

Data management

Managing remote sensing is becoming a growing problem. In disaster response, large collections of different remote sensing or geospatial data are accumulated by different organizations, but how to keep track of what they are and what kind of information they can be provided to decision makers is a big challenge. This challenge largely limit the decision experts are other users from adopting them in their application. Especially for LiDAR, according to ASPRS [28] standard, each of the points occupied around 28 bits. Gigabytes or even Terabytes of data can be obtained. This huge amount of data is computation exhaustive if save in one file. A proper data structure index or file management system is necessary to reveal the content of the data without the effort of loading the datasets. The suggested scale for each LOD is tantamount to the datasets. This framework enables accessibility to the data without exhaustive computation effort. The data are segmented into different scale blocks for the storage and each storage file has a location index that enable the function of query. From the conceptual framework, each LOD are segmented into small blocks. This size has a maximize data size of 1 gigabyte, which can be processed using the normal computers.

LiDAR Data Collection Case Study: Hurricane Sandy

LOD 0 Envision the availability of geospatial data

In 2010, Hurricane Sandy, the biggest Atlantic storm in United States history, swept through the Caribbean and up the East Coast of the United States. The storm is estimated to have cost over

$68 billion (2013 USD), and at least killed 286 people in the country. This study utilized the data collected pre and after this catastrophic disaster to validate the workflow mentioned in the previously.

This study utilized both Airborne LiDAR and Mobile LiDAR system to investigate into the feasibility of rapid transportation network accessibility identification in disaster response phase based on hurricane Sandy. The LiDAR data include both baseline data and event data based on hurricane Sandy along the Atlantic coast.

Targeted at hurricane Sandy, USGS conducted two survey surveys right before (Oct 26) and after (Nov 1-5) its occurrence using the Experimental Advanced Airborne Research Lidar (EAARL) system. Another survey attempts are also conducted in 2010. From August 28 to September 11 2010, US Army Corps of Engineers (USACE) Joint Airborne Lidar Bathymetry Technical Center of expertise (JALBTCX) performed another coastal survey along the Atlantic coast of NJ and New York (Rockaway).

LOD 1 Gaining knowledge of disaster situation and set focus and objectives for disaster response

In disaster situation decision making, the best way to extract meaning from the data is to make it visible for the experts. General visual inspection is a step that decision makers are presented with a LiDAR based triangulated irregular network (TIN) map. This map contains the terrain information of the affected area that can assist experts to understand overall damage pattern of the disaster area and give them a sense of real damage situation. By glancning through the map, some input features for disaster operations can be obtained.

1. Identification of decision making units (DMUs). In the Search and Rescue (SAR) decision making (DM) process, DMUs are referred to the vulnerable locations that require Search and Rescue (SAR) operations. Quick identification of how many decision making units and how vulnerable they are, is the pre-step prior to any Search and Rescue effort can be made.
2. Identify the resource allocation site. Whenever disasters strike, the critical need for effective and efficient emergency response urges for a rapid deployment of resources (e.g. medical resources, food, clothing, shelter, etc.). It includes activities such as implementing relief plans and providing all necessary emergency services. Thus rapidly identifying the potential site for the resource allocation is also a necessary step.
3. Quick identification of accessible transportation network. Road obstruction by debris can disrupt the Search and Rescue (SAR) operations. LiDAR based terrain map have the potential probability to visualize the debris on the road which provides a sense of debris blockage distribution in the Search and Rescue (SAR) path selection.

From the visualization analysis result, the whole shoreline area along New Jersey and New York City, most severe damage is identified including Rockaway Park, NYC, Normandy Beach, New Jersey, Seaside heights New Jersey, Ortley Beach, New Jersey. Figure 1 shows the triangulated irregular network (TIN) map converted by airborne LiDAR data for the rockaway, NYC. This map is colored by the elevation. From the map, it shows that most of the damage occurs along

the shoreline area, as highlighted in the bottom of the map. These houses are situated in the relatively less dense residential area. In the north of the most affected area, there is some recreation area, which might be useful for temporary evacuation in case of emergency. In the northeast of the severe damage area, a bridge is connecting the far roackaway area to the inland. This bridge serves as a channel for resource transportation and SAR operation. Thus to prevent the potential secondary hazard caused by the failure of the bridge, further inspections are necessary to validate whether this piece of critical transportation facilities are safe to use.In the left side of the map, there is a large area of empty space, which might be used as the temporary debris piling site.

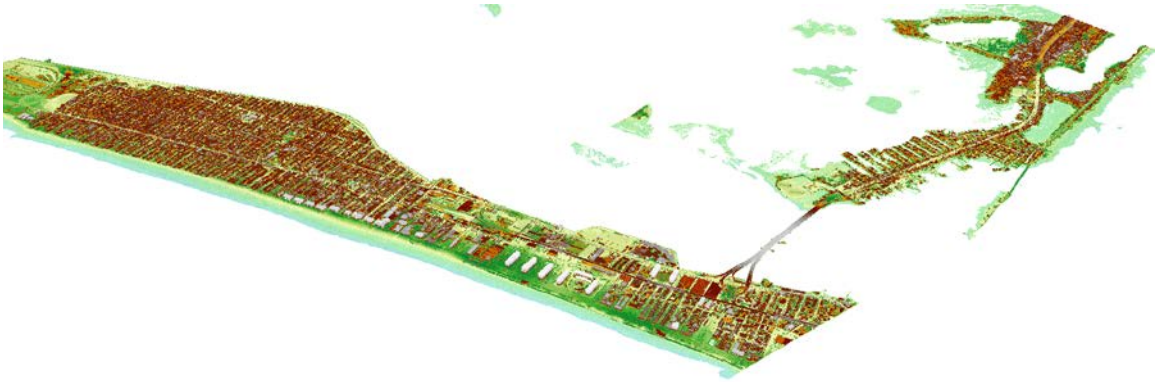

Figure 3 TIN Map for Rockaway NYC

Figure 4 TIN Map for Ortley Beach, NJ

LOD 2 Identify the hard-hit locations and set search and rescue priorities

Table 3 Bridge Damage states visual inspection Guideline by INDOT

Items	RED TAG
Movement at Expansion Joints	> 6 in. offset in vertical or horizontal alignment

Seats at Expansion Joints	unseating
Columns, Cross-Beams and Piers	bar buckling in RC beams, columns and piers local buckling in steel columns
Approach/ Abutment interface	> 6 in. settlement
Roadway	Impassible

Some agencies including INDOT [29], and FEMA HAZUS [30] provides some guidance to rapidly identify the unsafe bridges and other critical transportation infrastructures by visual inspection. Even though, the stress and strain or failure mechanism cannot be directed obtained by LiDAR systems, the significant failure of the bridges can be reflected in shape and deformation measurements. Indicators of failure of the bridges can be discovered in Damage classification tables for bridges. Both approaches provide guidance to the visual inspection based on the LiDAR data.

Table 4 Qualitative Damage State Descriptions Defined by Amending HAZUS for Typical Hurricane-Induced Bridge Damage (FEMA HAZUS [30])

Damage state	**Description**
Slight	**Minor cracking and spalling to the abutment, cracks in shear keys at abutments, minor spalling and cracks at hinges, minor spalling at the column damage requires no more than cosmetic repair, minor cracking to the deck, or slight damage to operator house.**
Moderate	**Any column experiencing moderate shear cracks cracking and spalling column structurally still sound, moderate movement of the abutment 2 in., extensive cracking and spalling of shear keys, any connection having cracked shear keys or bent bolts, keeper bar failure without unseating, rocker bearing failure, moderate settlement of the approach, moderate scour of the abutment or approach, damage to guardrails, wind and/or water damage to operator house resulting in switchboard or content damage.**
Extensive	**Any column degrading without collapse—shear failure column structurally unsafe, significant residual movement at connections, or major settlement approach, vertical offset of the abutment, differential settlement at connections, shear key failure at abutments, extensive scour of abutments, or submerged electrical or mechanical equipment.**
Complete	**Any column collapsing or connection losing all bearing support, which may lead to imminent deck collapse, tilting of substructure due to foundation failure.**

While the general visual inspection allows the decision makers to have a big picture of the affected area, detail visual inspection enables them to zoom in on details for more attentive

assessments. Special attention must be made on the critical infrastructures, which is a guarantee of societal functionality and safety [31]. Without properly taken care of, these critical facilities can generate a second hazard to the local community. For example, in August 1 2007, the collapse of I-35W Mississippi River Bridge killed 13 people and injures 145. Thus, a rapid inspection of whether this acute transportation facility can maintain its normal performance is essential and timely after the occurrence.

a) Debris Volume Quantification

As concluded in the visual inspection stage, one of the most severe damage areas is in Orltey beach along the shoreline area. However, emergency vehicles might be impassable to this vulnerable area due to the obstruction of debris. In the previous stage, it is focused only on the post disaster data, which provide no baseline for the comparison. Thus to what extent is the debris piling above the ground and how much cleaning effort is required to get access to the damage locations are uncertain. To address to this fact, not only the event data, but also the baseline data is needed in this stage to quantify and locate the debris. Change detection is conducted in ArcGIS to identify the volume and the location of the road blockage.

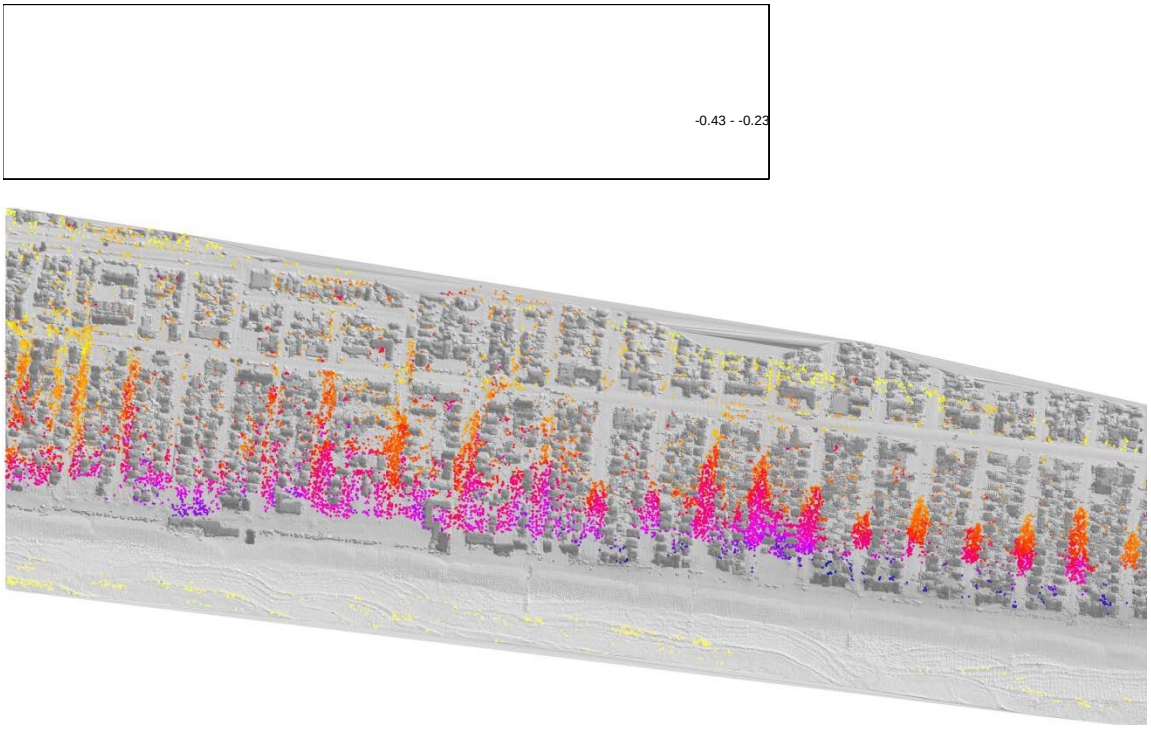

Figure 5 Quantification of the Debris and Identification of Accessible Route

Disaster can generate large amount of debris and the accumulation of debris will in turn impede rescuer, emergencies and lifetime support reaching researching survivors. The importance of measuring the volume and location of debris is pointed out by [10] [15]. The purpose of this stage is to quantify the volume of debris and locate their distribution for the SAR operations. The

identification of road blockage process is implemented in ArcGIS and the Pseudo code is provided as below:

```
PSEUDO CODE FOR DEBRIS VOLUME QUANTIFICATION
#INPUT:
  PRE (PRE-DISASTER AIRBORNE LIDAR RASTER FILE)
  POST (POST-DISASTER AIRBORNE LIDAR RASTER FILE)
#CALCULATE DEBRIS VOLUME
  DEBRIS_VOLUME = POST - PRE
    IF (DEBRIS_ELEVATION > ELEVETION.THRESHOLD):
      IF (ADJACENT.DISTANCE < DISTANCE.THRESHOLD):
        CLASSIFIED AS THE SAME CLUSTER OF DEBRIS
      ELSE:
        NEW CLUSTER OF DEBRIS_VOLUME
    ELSE:
    RETURN 0
#IDENTIFIED ROAD BLOCKAGE
    IF (CLUSTER.AREA > AREA.THRESHOLD):
      ROAD BLOCKAGE
    ELSE:
      RETURN 0 (NOT ROAD BLOCKAGE)
```

Figure 6 Pseudo code for debris QUANTIFIATION

b) Detail Visual Analysis

In some locations, there exist some critical infrastructures that will tremendously impact the SAR operation. For instance, Rockaway Bridge is the life channel for the SAR operations. Thus, the potential failure of this bridge can be a tremendous threat to societal functionality and safety of the local community. Thus detail inspection is required. From guidelines by the FEMA HAZUS [30] and INDOT [29], they suggest as an inspection based on the deformation of some critical components including damage at column, cross beam, movements at joints and abutment interface etc. Inspection of the bridge superstructure includes:

- Collapse of bridge span
- Significant displacement in Approach/ Abutment interface
- Lateral displacement of the superstructure (caused by Movement at Expansion Joints)
- Steep slope (collapse of columns, failure of bridge decks etc.)
- Significant pothole or debris piling
- Fallen of light and traffic signals

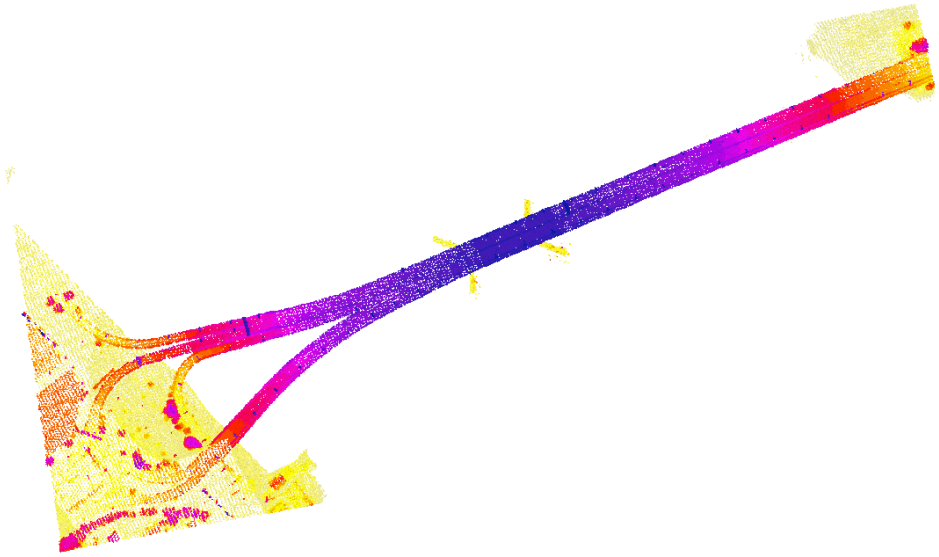

Figure 7 Top view of Rockaway Bridge

From the observation, there is no significant vertical, horizontal or lateral displacement which exceeds the 6 inch (15.24cm) threshold suggested by INDOT. Thus based on the inspection, this bridge is safe to use**.**

Simulation

The estimated routing time between two nodes is simplified and defined as:

$$t_{rou} = t_{tra} + t_{deb,r} \quad (1)$$

Where, $_{tral,}$ time required traveling between two nodes;

$t_{deb,}$ time required clearing off the debris between two nodes

The time from the start to each node is calculated as the shortest path from the start to each node using the Dijkstra shortest path algorithm. To simulate the uncertainty and the error of debris volume measured by the LiDAR information and the experience of the experts, the t_{est} is defined as:

$$t_{deb} = t_{deb,r} + \varepsilon \quad (2)$$

where,

$t_{deb,r}$ is true debris clearing off time;

ε is total error in the measurement,

$$\varepsilon \sim N(\mu, \sigma^2) \quad (3)$$

The time from the start to each node is calculated as the shortest path from the start to each node using the Dijkstra shortest path algorithm.

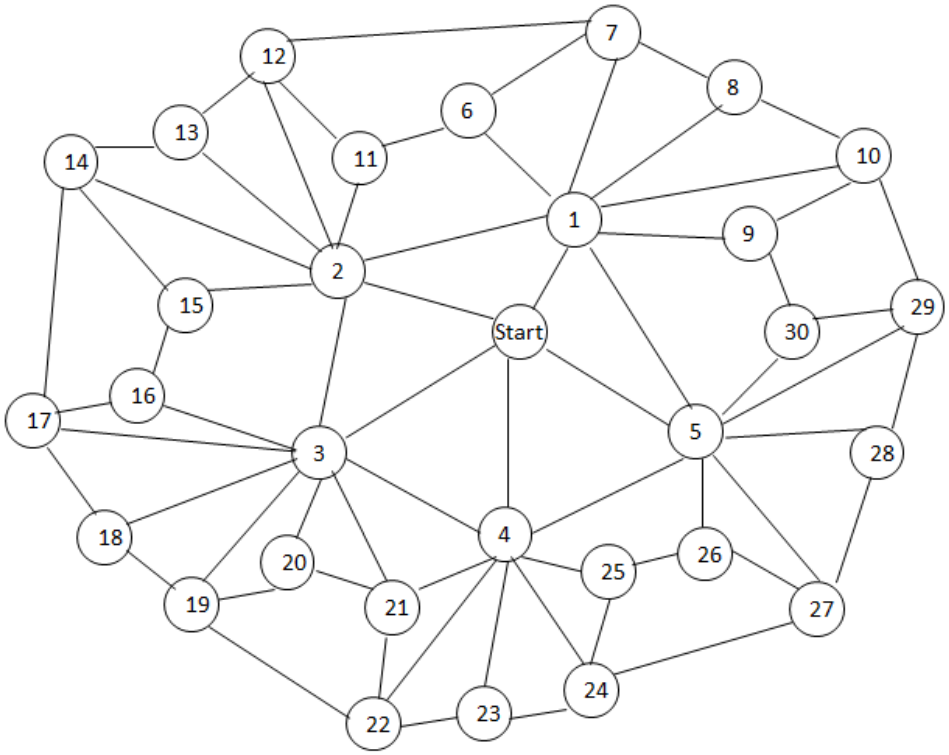

Figure 7 Diagram of transportation network

for the debris measured by LiDAR information, μ=20% x $t_{deb,r;}$, σ=0;

for the debris measured by expert experience, μ=100% x $t_{deb,r}$, σ=50% x $t_{deb,r;}$

Table 5 Simulation result

(In minutes)

Nodes	**Travel Time & Real Debris** $t_{tra} + t_{deb,r}$	**Travel Time & Debris Estimated by Experts** $t_{tra} + t_{deb,r} + \varepsilon_e$		**Travel Time & Debris Estimated by LiDAR** $t_{tra} + t_{deb,r} + \varepsilon_L$		**Nodes**	**Travel Time & Real Debris** $t_{tra} + t_{deb,r}$	**Travel Time & Debris Estimated by Experts** $t_{tra} + t_{deb,r} + \varepsilon_e$		**Travel Time & Debris Estimated by LiDAR** $t_{tra} + t_{deb,r} + \varepsilon_L$	
	T_{Real}	T_{Expert}	$\Delta t(\%)$	T_{LiDAR}	$\Delta t(\%)$		T_{Real}	T_{Expert}	$\Delta t(\%)$	T_{LiDAR}	$\Delta t(\%)$
1	182	279	53.04%	201	10.66%	**16**	298	443	48.60%	332	11.28%
2	210	326	55.10%	238	13.43%	**17**	403	588	45.98%	448	11.07%

3	204	300	46.93%	228	11.67%	**18**	401	616	53.55%	451	12.57%
4	97	108	11.35%	99	2.27%	**19**	410	613	49.54%	455	11.02%
5	204	252	23.55%	214	4.90%	**20**	417	677	62.26%	477	14.34%
6	352	531	50.72%	394	12.05%	**21**	253	386	52.50%	282	11.38%
7	405	611	50.90%	447	10.47%	**22**	250	310	23.89%	264	5.44%
8	358	568	58.74%	400	11.84%	**23**	142	171	20.52%	148	4.08%
9	321	446	39.04%	346	7.85%	**24**	166	183	10.27%	169	2.05%
10	271	395	45.58%	296	9.15%	**25**	347	473	36.25%	385	11.01%
11	303	426	40.51%	333	9.77%	**26**	392	580	48.00%	431	10.00%
12	351	550	56.76%	396	12.76%	**27**	422	602	42.72%	463	9.72%
13	356	527	48.03%	395	11.01%	**28**	414	634	53.22%	460	11.06%
14	392	646	64.73%	448	14.23%	**29**	418	600	43.48%	460	10.00%
15	441	750	70.11%	509	15.33%	**30**	376	516	37.25%	407	8.35%
Total	9556	14105	47.61%	10576	10.68%						

The result from the Monte Carlo simulation shows that the routing time has a significant decreased as the input parameters directly come from the objective extraction from LiDAR data than from expert's subjective input. The change amount is from 47.61 to 10.68%. This reduction indicates that LiDAR assist in quantifying the debris volume does help to improve the algorithm performance.

Since the error of the input is defined as a normal distribution with two variables: mean and variance. Another simulation is conducted to see how the method purposed will perform as these variables changes. The results indicate objective input from resources such as LiDAR would have low mean error (systematic error) and zero standard deviation, which would likely to results in few increase percentage (10%). On the other hand, subjective input from the experts, both high error in mean and standard deviation are likely to results in large increment percentage.

Conclusion

Disaster response is time sensitive which requires better coordination between data, processing tools and decision making tools. In this paper, a disaster response level of complexity (LOD) is developed. The remote sensing data are classified into 5 levels according to the LOD. For each LOD, the purpose, suggested accuracy and density, data processing, data analytics and decision making needs are described. Subsequently, the framework was evaluated using an empirical case of hurricane sandy.

The empirical study shows that the conceptualized framework is well-structure, which can help the experts to map the objectives of their decision making need to more specific tools such as processing tools, data analytics tool and decision making tools. LOD 0 provides information that help the users to envision the availability of remote sensing data. LOD 1 enhance the disaster

situation awareness and help to set the focus and objectives of disaster response. After LOD 1, further information is provided by LOD 2 make the response plan and set focus and priorities. In additional, LOD 3 and LOD 4 are complemented as a way for accessing the risk of critical infrastructures such as power plant or bridges, which prevents the happening of secondary hazard. The proposed LODs conceptual framework is well structured, which can also benefit the data management needs. The suggested scale for data management makes data storage more tangible for data query. In additional, this conceptual framework can be extended for building and other utilities.

An empirical study on hurricane sandy was conducted in this study, the result shows that the use of remote sensing typically LiDAR in this case, using the proposed framework largely improve the accuracy and time for the decision models. Compared to other cases that cannot keep track of the content of the remote sensing data, the proposed work help experts to not only visualized analysis (LOD 1) the disaster area after hurricane sandy strike, but extract debris volume (LOD 1) and rapidly access the transportation structures (LOD2).

It is important to note that this conceptual framework is tested with Monte Carlo Simulation rather than the hurricane sandy real case. The detail time and resource leveraging effort are not quantified in this research. For future researches. Real response data and surveys from the decision makers are necessary to implemented in evaluate the practical value of the proposed framework.

References

[1] Meyer, M., Amekudzi, A., & O'Har, J. (2010). Transportation asset management systems and climate change: adaptive systems management approach. Transportation Research Record: Journal of the Transportation Research Board, (2160), 12–20.

[2] Meyer, M., Amekudzi, A., & O'Har, J. (2010). Transportation asset management systems and climate change: adaptive systems management approach. *Transportation Research Record: Journal of the Transportation Research Board*, (2160), 12-20.

[3] Huang, J.-S., & Lien, Y.-N. (2012). Challenges of emergency communication network for disaster response. In Communication Systems (ICCS), 2012 IEEE International Conference on (pp. 528–532). IEEE.

[4] Bolton, D., O'Ryan, D., Udwin, O., Boyle, S., & Yule, W. (2000). The long-term psychological effects of a disaster experienced in adolescence: II: General psychopathology. Journal of Child Psychology and Psychiatry, 41(04), 513–523.

[5] Guha-Sapir, D., & Lechat, M. F. (1986). Information systems and needs assessment in natural disasters: an approach for better disaster relief management. Disasters, 10(3), 232-237.

[6] Voigt, S., Kemper, T., Riedlinger, T., Kiefl, R., Scholte, K., & Mehl, H. (2007). Satellite image analysis for disaster and crisis-management support. IEEE Transactions on Geoscience and Remote Sensing, 45(6), 1520–1528.

[7] Liu, S., & Hodgson, M. E. (2016). Satellite image collection modeling for large area hazard emergency response. ISPRS Journal of Photogrammetry and Remote Sensing, 118, 13-21.

[8] Hodgson, M. E., Battersby, S. E., Davis, B. A., Liu, S., & Sulewski, L. (2014). Geospatial data collection/use in disaster response: a united states nationwide survey of state agencies. In Cartography from pole to pole (pp. 407-419). Springer Berlin Heidelberg.

[9] Adams, S. M., & Friedland, C. J. (2011). A survey of unmanned aerial vehicle (UAV) usage for imagery collection in disaster research and management. publisher not identified.

[10] Kwan, M.-P., & Ransberger, D. M. (2010). LiDAR assisted emergency response: Detection of transport network obstructions caused by major disasters. Computers, Environment and Urban Systems, 34(3), 179–188.

[11] Van Aardt, J. A., McKeown, D., Faulring, J., Raqueño, N., Casterline, M., Renschler, C., … others. (2011). Geospatial disaster response during the Haiti earthquake: A case study spanning airborne deployment, data collection, transfer, processing, and dissemination. Photogrammetric Engineering and Remote Sensing, 77(9), 943–952.

[12] Lu, Q.-C., Peng, Z.-R., & Zhang, J. (2013). Critical Transportation Infrastructure Identification and Prioritization Under Flooding Risks. In Transportation Research Board 92nd Annual Meeting.

[13] Rickenmann, D. (1999). Empirical relationships for debris flows. Natural Hazards, 19(1), 47–77.

[14] Bilby, R. E., & Ward, J. W. (1989). Changes in characteristics and function of woody debris with increasing size of streams in western Washington. Transactions of the American Fisheries Society, 118(4), 368–378.

[15] Bull, J. M., Miller, H., Gravley, D. M., Costello, D., Hikuroa, D. C. H., & Dix, J. K. (2010). Assessing debris flows using LIDAR differencing: 18 May 2005 Matata event, New Zealand. Geomorphology, 124(1), 75–84.

[16] Haas, F., Heckmann, T., Hilger, L., & Becht, M. (2012). Quantification and modelling of debris flows in the proglacial area of the Gepatschferner, Austria, using ground-based LiDAR. IAHS-AISH Publication, 293–302.

[17] Mikes, C., & Fleck, D. (n.d.). Earthquake and Infrastructure Damage Analysis in Multnomah and Clackamas Counties: The Application of LiDAR In The Development of an Emergency Response Plan

[18] Özdamar, L., Ekinci, E., & Küçükyazici, B. (2004). Emergency logistics planning in natural disasters. Annals of operations research, 129(1-4), 217-245.

[19] Yi, W., & Kumar, A. (2007). Ant colony optimization for disaster relief operations. Transportation Research Part E: Logistics and Transportation Review, 43(6), 660-672.

[20] Golden, B. L., Raghavan, S., & Wasil, E. A. (Eds.). (2008). The vehicle routing problem: latest advances and new challenges (Vol. 43). Springer Science & Business Media.

[21] Kwan, M. P., & Lee, J. (2005). Emergency response after 9/11: the potential of real-time 3D GIS for quick emergency response in micro-spatial environments. Computers, Environment and Urban Systems, 29(2), 93-113.

[22] Kawasaki, A., Berman, M. L., & Guan, W. (2012). The growing role of web-based geospatial technology in disaster response and support.

[23] Zook, M., Graham, M., Shelton, T., & Gorman, S. (2010). Volunteered geographic information and crowdsourcing disaster relief: a case study of the Haitian earthquake. World Medical & Health Policy, 2(2), 7-33.

[24] Ashktorab, Z., Brown, C., Nandi, M., & Culotta, A. (2014). Tweedr: Mining twitter to inform disaster response. Proc. of ISCRAM.

[25] Saaty, T. L. (1990). How to make a decision: the analytic hierarchy process.European journal of operational research, 48(1), 9-26.

[26] Weber, M. (1987). Decision making with incomplete information. European Journal of Operational Research, 28(1), 44-57.

[27] Gigerenzer, G., & Gaissmaier, W. (2011). Heuristic decision making. Annual review of psychology, 62, 451-482.

[28] Flood, M. (2004). ASPRS Guidelines: Vertical accuracy reporting for LiDAR data.

[29] Ramirez, J. A., Frosch, R. J., Sozen, M. A., & Turk, A. M. (2000). Handbook for the Post-Earthquake Safety Evaluation of Bridges and Roads.

[30] HAZUS-MH, F. E. M. A. (2003). Flood Model: Technical Manual. Federal Emergency Management Agency.

[31] Hellström, T. (2007). Critical infrastructure and systemic vulnerability: Towards a planning framework. Safety Science, 45(3), 415–430.

Table 1 Summary of Level of Detail (LOD) and corresponding goals and processing need

	Scale	Value of timely information	Density	Accuracy	Goals	Data Processing	Data Analytics	Decision Making
LOD 0	**Full-Scale**	**$$$$**	**-**	**Low (>0.2 m)**	**Envision the availability of geospatial data**	**Basic**	**-**	**Judgment**
LOD 1	**Municipality (5km x 5km)**	**$$$$**	**Coarse Scale (0 to 30 pts/m2)**	**Low (>0.2 m)**	**Gaining knowledge of disaster situation and set focus and objectives for disaster response**	**Basic**	**Simple models**	**Judgment to decision making models**
LOD 2	**Building Block/ critical infrastructures (500m x 500m)**	**$$$**	**Intermediate (30 to 100 pts/m2)**	**Medium (0.05m to 0.20 m)**	**Identify the hard-hit locations and set search and rescue priorities**	**Basic to Advanced**	**Simple to advanced models**	**Judgement to decision making models**
LOD 3	**Individual infrastructure (50m x 50m)**	**$**	**Fine (100 to 100 pts/m2)**	**Medium (0.05m to 0.20 m)**	**Extraction of parameter details for access and analyze Risks of infrastructure**	**Advanced**	**advanced models**	**-**
LOD 4	**Component Details (1m x 1m)**	**$**	**Extra Fine (> 1000 pts/m2)**	**High (< 0.05 m)**	**Micro level component detail damage assessment for failure mechanism studies**	**Advanced**	**advanced models**	**-**

Legend: $$$$ extremely need in initial disaster response phase (a few hours). $$$ need in the early disaster response phase (within a day); $ potential useful in disaster response phase (a week or more).

Table 2 dETAIL DESCRIPTION FOR LOD0 TO LOD 2 FOR DISASTER RESPONSE

	Tasks assignment	Example Question	Data Processing	Data Analytics	Decision Making
LOD 0	**Envision the availability of geospatial data**				
	Identify the existing of data	**Is the data available in X?**	**-**	**-**	**Judgement**
LOD 1	**Have a** synoptic view of **disaster area and set focus and objectives for disaster response**				
	Quickly assess the severity impact of damage;	**How severity is the impact of the disaster X, can it declare a major Disaster?**	**Visual Representation , Change detection and etc.**	**-**	**Judgement**
	Identify the accessibility of transportation network for escape routes, ambulances services and search and rescue teams to reach;	**Is routine evacuation transportation free of obstruction?** **Is location X accessible by ambulance? of critical infrastructure;**	**Visual Representation , Change detection and etc.**	**-**	**Judgement**
	Analyze Critical Infrastructure dependencies, interdependencies, and associated cascading effects;	**What is the impact area if critical infrastructure X fail?**	**Visual Representation**	**Spatial analysis**	**Judgement**
	Set focus and objective.	**What is the potential candidate locations for sending search and rescue crews?**	**Visual Representation , Change detection and etc.**	**Spatial analysis**	**Judgement or Decision making models**
LOD 2	**Identify the hard-hit locations and set search and rescue priorities**				
	Quick identification infrastructure damage status based on the terrain change?	**How many percentage of the infrastructure will be at high risk if given a terrain change threshold of x?**	**Visual Representation , Change detection and etc.**	**Probability based model**	**Judgement**

	Calculation of the potential demand for the evacuation and shelters based on the damage of residential buildings	**How many people need to evacuated from the potential disaster zone?**	**Visual Representation , Change detection and etc.**	**Spatial analysis**	**Judgement**
	Analyze building dependencies, interdependencies, and associated cascading effects;	**What is** cascading effects of the sea front buildings in terms of debris flow during hurricane sandy?	**Visual Representation , Change detection and etc.**	**Spatial analysis**	**Judgement**
	Analysis the condition (safe or unsafe) of critical infrastructure;	**Based on the elevation change and visual inspection, is it the critical infrastructure X safe to use?**	**Detail Visual Representation**	**-**	**Judgment**
	Roughly quantification of debris volume;	**What is the volume of the debris if we would like to clear the obstruction in Highway X from location A to B?**	**Visual Representation , Change detection and etc.**	**-**	**Judgement**
	Set focus on the hotspot for search and rescue are	**What is the priority sequential for the search and rescue teams?**	**Visual Representation , Change detection and etc.**	**Operation research models, spatial analysis**	**Judgement or Decision making models**

[END OF DOCUMENT]